MAX-PLANCK-INSTITUT
FÜR METEOROLOGIE

AMOC Impacts on Surface Temperatures Across Changing CO_2 Concentrations

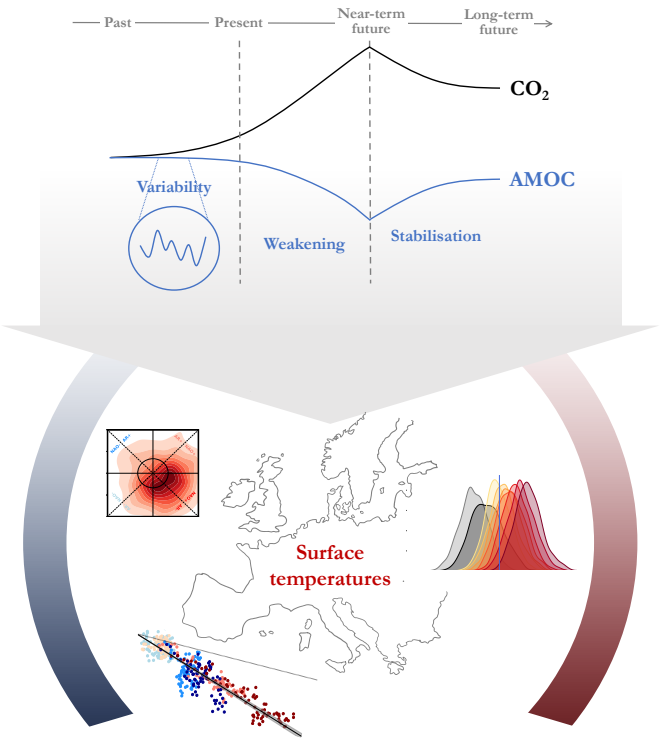

Eduardo Alastrué de Asenjo

Hamburg 2026

Berichte zur Erdsystemforschung 302
Reports on Earth System Science 2026

Hinweis

Die Berichte zur Erdsystemforschung werden vom Max-Planck-Institut für Meteorologie in Hamburg in unregelmäßiger Abfolge herausgegeben.

Sie enthalten wissenschaftliche und technische Beiträge, inklusive Dissertationen.

Die Beiträge geben nicht notwendigerweise die Auffassung des Instituts wieder.

Die "Berichte zur Erdsystemforschung" führen die vorherigen Reihen "Reports" und "Examensarbeiten" weiter.

Anschrift / Address

Max-Planck-Institut für Meteorologie
Bundesstrasse 53
20146 Hamburg
Deutschland

Tel./Phone: +49 (0)40 4 11 73 - 0
Fax: +49 (0)40 4 11 73 - 298

name.surname@mpimet.mpg.de
www.mpimet.mpg.de

Notice

The Reports on Earth System Science are published by the Max Planck Institute for Meteorology in Hamburg. They appear in irregular intervals.

They contain scientific and technical contributions, including PhD theses.

The Reports do not necessarily reflect the opinion of the Institute.

The "Reports on Earth System Science" continue the former "Reports" and "Examensarbeiten" of the Max Planck Institute.

Layout

Bettina Diallo and Norbert P. Noreiks
Communication

Copyright

AMOC Impacts on Surface Temperatures Across Changing CO_2 Concentrations

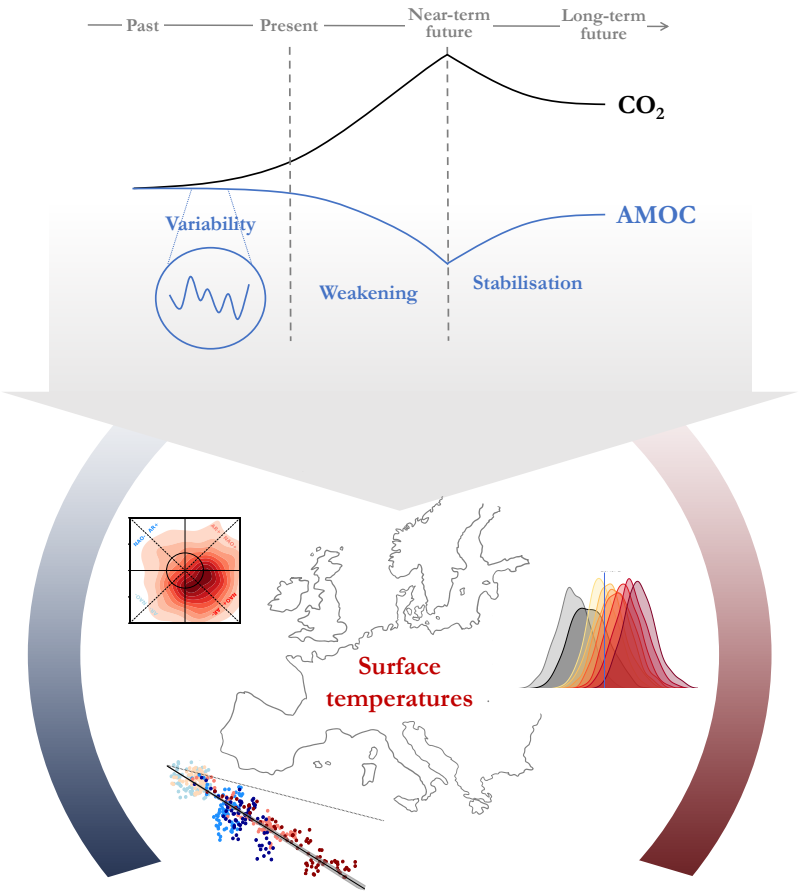

Eduardo Alastrué de Asenjo

Hamburg 2026

Eduardo Alastrué de Asenjo
aus Madrid, Spanien

Max-Planck-Institut für Meteorologie
The International Max Planck Research School on Earth System Modelling
(IMPRS-ESM)

Universität Hamburg
Fachbereich Erdsystemwissenschaften
Institut für Meereskunde

Bundesstrasse 53
20146 Hamburg

Tag der Disputation: 10. April 2026

Folgende Gutachter empfehlen die Annahme der Dissertation:
Prof. Dr. Johanna Baehr
Prof. Dr. Jana Sillmann

Vorsitzender des Promotionsausschusses:
Prof. Dr. Hermann Held

Dekan der MIN-Fakultät:
Prof. Dr.-Ing. Norbert Ritter

ISSN 1614-1199 - doi: 10.17617/2.3713149

This document was typeset using the typographical look-and-feel `classicthesis` developed by André Miede. The `classicthesis` template is available at https://bitbucket.org/amiede/classicthesis/

Eduardo Alastrué de Asenjo: *AMOC Impacts on Surface Temperatures Across Changing CO_2 Concentrations*, PhD thesis, © September 2025

Para Mila
1935 – 2022

ABSTRACT

As human emissions alter atmospheric CO_2 concentrations, surface temperatures and other major climate components are changing. In this thesis, I focus on one of these systems, the Atlantic Meridional Overturning Circulation (AMOC), to investigate the concurrent impacts this circulation may have on surface temperatures. Using an Earth system modelling approach, I jointly consider plausible CO_2 and AMOC changes (past, upcoming, and long-term) and address diverse impacts on surface temperatures that have been overlooked thus far.

In a first study, I investigate the past influence of the AMOC interannual variability on European winter cold extremes. I use a single-model large ensemble approach to analyse the changes in such extremes and the physical mechanisms involved. I find that AMOC interannual variations can shift the distributions of cold extremes. However, this shift is much less evident in the recent period compared to a preindustrial climate. I explain the early shift and the contrast in the late period by changes in sea surface temperatures, sea ice, heat fluxes, and Euro-Atlantic winter circulation regimes.

Second, I focus on the AMOC carbon feedback, not only to quantify it, but also to project its economic impact until the end of the century. The approach is to first design Earth system model simulations (which combine carbon cycle feedback and freshwater hosing experiments), and later incorporate the assessed feedback into an integrated assessment model. The results indicate that an AMOC weakening linearly leads to reduced ocean carbon uptake. This reduction in uptake would give rise to economic damages, possibly turning AMOC weakening into a net cost to society.

Third, I inspect the long-term evolution of European heat extremes in the context of net-zero emissions and a recovering and stabilising AMOC. This analysis is carried out in a set of net-zero emissions simulations that extend for 1000 years and allow for evaluating the effect of delays in emissions cessation. The findings suggest that the intensity and frequency of these extreme heat events might remain constant for many centuries, and that any delay in emissions cessation will bring significantly more intense extremes.

Ultimately, I argue that combining such interdisciplinary approaches across timescales is essential for mitigating climate change and adapting to its uncertain impacts in the context of a changing AMOC.

ZUSAMMENFASSUNG

Da menschliche Emissionen die atmosphärischen CO_2-Konzentrationen verändern, werden sich die Oberflächentemperaturen und andere wichtige Klimakomponenten voraussichtlich verändern. In dieser Arbeit konzentriere ich mich auf eine dieser Komponenten, die Atlantische Umwälzströmung (Atlantic Meridional Overturning Circulation, AMOC), um zu untersuchen, welche zusammenwirkenden Auswirkungen diese Strömung auf Oberflächentemperaturen haben kann. Unter Verwendung eines Erdsystemmodellierungsansatzes betrachte ich plausible CO_2- und AMOC-Änderungen in der Vergangenheit, in der nahen Zukunft und auf längeren Zeitskalen und gehe auf verschiedene Auswirkungen auf die Oberflächentemperaturen ein, die bisher übersehen wurden.

In einer ersten Studie untersuche ich, welchen Einfluss die interannuelle Variabilität der AMOC in der Vergangenheit auf winterliche Kälteextreme in Europa haben konnte. Ich verwende einen großen Ensemble-Ansatz mit einem einzigen Klimamodell, um die Veränderungen der Extrema und die beteiligten physikalischen Mechanismen zu analysieren. Ich stelle fest, dass die zwischenjährlichen AMOC-Variationen die Verteilung der Kälteextreme verschieben können. Diese Verschiebung ist jedoch in der jüngeren Vergangenheit im Vergleich zu einem vorindustriellen Klima viel weniger deutlich. Ich erkläre diese Unterschiede durch Veränderungen der Meeresoberflächentemperaturen, des Meereises, der Wärmeflüsse und der nordatlantischen Winterzirkulationsregime.

Zweitens konzentriere ich mich auf die AMOC-Kohlenstoffrückkopplung, nicht nur um sie zu quantifizieren, sondern auch um ihre wirtschaftlichen Auswirkungen bis zum Ende des Jahrhunderts zu projizieren. Die Methodik umfasst zunächst Erdsystemmodellsimulationen (die Experimente mit Kohlenstoffkreislauf-Rückkopplung und mit künstlichem Süßwassereintrag kombinieren). In einem zweiten Schritt wird die untersuchte Rückkopplung in ein integriertes Bewertungsmodell (integrated assessment model) mit einbezogen. Die Ergebnisse zeigen, dass eine Abschwächung der AMOC linear zu einer geringeren Kohlenstoffaufnahme im Ozean führt. Ein plausibles wirtschaftliches Maß für diese Auswirkung deutet darauf hin, dass diese verringerte Aufnahme zu wirtschaftlichen Schäden führen würde, wodurch sich der Nettobeitrag der AMOC-Abschwächung möglicherweise in Nettokosten für die Gesellschaft umkehrt.

Drittens untersuche ich die langfristige Entwicklung europäischer Hitzeextreme im Kontext von Netto-Null-Emissionen und einer sich potenziell erholenden und stabilisierenden AMOC. Diese Analyse wird in einer Reihe von Netto-Null-Emissionssimulationen durchge-

führt, die sich über einen Zeitraum von 1000 Jahren erstrecken und es ermöglichen, die Auswirkungen von Verzögerungen bei der Beendigung der Emissionen zu bewerten. Die Ergebnisse deuten darauf hin, dass Intensität und Häufigkeit dieser Ereignisse über viele Jahrhunderte hinweg konstant bleiben könnten und dass jede Verzögerung bei der Beendigung der Emissionen zu deutlich intensiveren Extremen führen wird.

Letztlich ist die Kombination solcher interdisziplinären und zeitskalenübergreifenden Ansätze unerlässlich, um die ungewissen Auswirkungen einer sich verändernden AMOC in einem sich wandelnden Klima abzumildern und sich an sie anzupassen.

PUBLICATIONS

The following publications are part of this dissertation and are included as appendices after the unifying essay:

Alastrué de Asenjo, E., Borchert, L. F., Sillmann, J., & Baehr, J. (in preparation). Changing past influence of interannual AMOC variability on European cold extremes.

Schaumann, F., & **Alastrué de Asenjo, E.** (2025). Weakening AMOC reduces ocean carbon uptake and increases the social cost of carbon. *Proceedings of the National Academy of Sciences*, *122*(9), e2419543122. https://doi.org/10.1073/pnas.2419543122

Alastrué de Asenjo, E., King, A. D., & Ziehn, T. (2025). European heat extremes under net-zero emissions. *Environmental Research Letters*, *20*(7), 074029. https://doi.org/10.1088/1748-9326/addee4

In addition, I have further contributed to the following submitted (preprint accessible) or published articles during my PhD:

Clark, S. P., King, A. D., Brown, J. R., Cassidy, L., **Alastrué de Asenjo, E.**, & Ziehn, T. (in review, *Earth's Future*). The reversibility of monthly local and regional temperature extremes in CDRMIP. https://doi.org/10.22541/essoar.176556040.07127388/v1

Diamond, R., Sime, L. C., Schroeder, D., Jackson, L. C., Holland, P. R., **Alastrué de Asenjo, E.**, Bellomo, K., Danabasoglu, G., Hu, A., Jungclaus, J., Montoya, M., Meccia, V. L., Saenko, O. A., & Swingedouw, D. (2025). A Weakened AMOC Could Cause Southern Ocean Temperature and Sea-Ice Change on Multidecadal Timescales. *Journal of Geophysical Research: Oceans*, *130*(7), e2024JC022027. https://doi.org/10.1029/2024JC022027

Jackson, L. C., **Alastrué de Asenjo, E.**, Bellomo, K., Danabasoglu, G., Haak, H., Hu, A., Jungclaus, J., Lee, W., Meccia, V. L., Saenko, O., Shao, A., & Swingedouw, D. (2023). Understanding AMOC stability: The North Atlantic Hosing Model Intercomparison Project. *Geoscientific Model Development*, *16*(7), 1975–1995. https://doi.org/10.5194/gmd-16-1975-2023

Jackson, L. C., **Alastrué de Asenjo, E.**, Bellomo, K., Danabasoglu, G., Haak, H., Hu, A., Jungclaus, J., Lee, W., Meccia, V. L., Saenko, O., Shao, A., & Swingedouw, D. (in review, *Climate Dynamics*). Processes and feedbacks for AMOC stability following freshwater-induced weakening. https://doi.org/10.21203/rs.3.rs-8742476/v1

King, A. D., Abram, N. J., **Alastrué de Asenjo, E.**, & Ziehn, T. (2025a). ESD Ideas: Extended net zero simulations are critical for informed decision making. *Earth System Dynamics*, *16*(5), 1605–1609. https://doi.org/10.5194/esd-16-1605-2025

King, A. D., **Alastrué de Asenjo, E.**, Maycock, A., Ziehn, T., Borowiak, A. R., Clark, S., & Maher, N. (2025b). Detectability of Post-Net Zero Climate Changes and the Effects of Delay in Emissions Cessation. *Earth's Future*, *13*(12), e2025EF006918. https://doi.org/10.1029/2025EF006918

ACKNOWLEDGMENTS

How ironic is it to write this thesis in the first-person singular, when every page reflects the support of so many people? I try here to amend this stylistic "injustice" by thanking some of you (and possibly forgetting many others!) and acknowledging how indispensable you all were in my PhD journey.

First, a huge thanks to my two PhD supervisors, Johanna and Jana. Your appreciation, encouragement, and feedback lifted me in the toughest days of my PhD. Without your willingness to both provide scientific guidance and allow freedom to explore other topics, my PhD would not have materialised. To Johanna, thanks for your enduring empathy, fairness, and pragmatism over all these years. I am still perplexed by how all challenges seem manageable just by knowing that I can count on your support! To Jana, thank you for your optimism and for genuinely making me feel like a true member of your group. Thanks as well to Eleanor for volunteering to oversee my PhD progress and doing such a great job!

I am grateful to Andrew for warmly hosting me in Melbourne for my research stay. My months in Melbourne were the most productive of my academic life, and that was possible thanks to your mentoring, generosity, enthusiasm, and kindness. Thanks as well to the University of Melbourne and the MIN Graduate Center for financing part of the stay.

I want to show my gratitude to all my other scientific collaborators. In particular, I want to thank Felix: working and discussing with you has been, without a doubt, the most fun part of my PhD. I am really proud to be able to call you both my collaborator and friend. I must also show appreciation for all the people providing technical (e.g. the DKRZ support team) and modelling help (especially Helmuth and Kalle), whose indispensable work often goes unnoticed.

My sincere thanks also go to all the present and past members of the Climate Modelling and Climate Extremes groups. I highly valued the predominant approachability and sincerity among all members in both groups, and I will cherish the memory of our group meetings, lunches, and retreats. Among everyone, I want to give a special shout out to Goratz, David, Marlene, Maite, Sebastian, Kaja, Leo, Ben, and all my accompanying PhD peers.

I am deeply grateful to have been a member of the IMPRS-ESM graduate school, surrounded by many awesome people and enduring principles. I cannot thank the IMPRS-ESM Office enough for their support. Antje, Florian, Connie, and Michaela: you are not simply so

great and professional at your roles, but you add a touch of kindness that can make German bureaucracy seem gentle.

Thanks to my friends, and even more to my family, for your unconditional and limitless support. For many of you, these three demanding years have meant less time and moments together, but your affection and confidence in me never weakened. I regard this thesis as a reflection of your effort and sacrifice, and I am forever and wholeheartedly indebted.

Finally, there are not enough pages in this thesis to thank Lena, my partner. You have been my lighthouse in this adventure, journeying alongside me with love, compassion, and happiness. You give purpose to this thesis and the exciting future that awaits us beyond it.

CONTENTS

LIST OF FIGURES

LIST OF TABLES

ACRONYMS

ACCESS-ESM Australian Community Climate and Earth System Simulator - Earth System Model

AMOC Atlantic Meridional Overturning Circulation

AR Atlantic Ridge

BGC-only biogeochemically-only coupled

BLO Scandinavian Blocking

CMIP6 Coupled Model Intercomparison Project Phase 6

ERA5 Fifth generation of the European Centre for Medium-Range Weather Forecasts Retrospective Analysis

EOF Empirical Orthogonal Function

FARs fractions of attributable risk

GWL global warming level

IAMs integrated assessment models

IPCC Intergovernmental Panel on Climate Change

IPCC AR6 Sixth Assessment Report of the Intergovernmental Panel on Climate Change

META Model for Economic Tipping Analysis

MPI-GE Max Planck Institute Grand Ensemble

MPI-ESM Max Planck Institute Earth System Model

NAHosMIP North Atlantic Hosing Model Intercomparison Project

NAO North Atlantic Oscillation

PDFs probability distribution functions

RRs risk ratios

SCC social cost of carbon

SSTs sea surface temperatures

SMILE single model initial-condition large ensemble

ZEC Zero Emissions Commitment

ZECMIP Zero Emissions Commitment Model Intercomparison Project

Part I

UNIFYING ESSAY

1 INTRODUCTION

"In nature nothing exists alone."

— Rachel Carson (1962)

Climate science has conclusively identified acute and multifaceted impacts of anthropogenic climate change. These impacts are prominent for the North Atlantic region, which drives and endures changes across multiple timescales and processes. However, some physical, biogeochemical, and economic impact dimensions related to the most prominent Atlantic circulation system have been overlooked. Specifically, previous research has ignored or failed to quantify certain variability, weakening, and stabilisation effects of this circulation on surface temperatures. These temperature impacts are uncertain and modulated by the background climate state, and therefore require an integrated framework that accounts for past and future plausible CO_2 and circulation changes.

1.1 A CHANGING CLIMATE

Global warming with increasing CO_2

Human emissions have increased atmospheric CO_2 concentrations by more than 50% since 1750 (from 278 to 419 parts per million, Friedlingstein et al., 2025). This drastic increase in CO_2 and other greenhouse gases, along with additional anthropogenic forcings such as aerosols, has warmed the Earth by 1.2°C (this decade relative to 1850–1900, Forster et al., 2025). Projecting societal and climatic changes to the end of the century yields a very likely probability of an additional 0.2-1.0°C warming under low emissions (SSP1-1.9 scenario, compared to 1995–2014) and 2.4–4.8°C under high emissions (SSP5-8.5, Lee et al., 2021). Yet, these past and future global temperature changes emerge from a very complex interplay between external anthropogenic forcings and internal processes at many temporal and spatial scales (Ghil & Lucarini, 2020). While mean temperature shifts are the most evident result of forced disequilibrium, climate change is also manifested in more subtle but crucial interactions.

Internal variability affected by increasing CO_2

First, forced climate change is concurrent with internal climate variability (Mitchell, 1976). Internal variability originates from the uneven distribution of energy in Earth's climate (e.g Lehner & Deser, 2023), arising from non-linear and chaotic (Lorenz, 1963) as well as stochastic (Hasselmann, 1976) interactions. Despite being in part predictable, internal variability is considered an irreducible uncertainty

(e.g. Hawkins & Sutton, 2009; Hawkins et al., 2016). Still, climate science has developed tools, such as large ensembles of model simulations (e.g Deser et al., 2020), to separate internal variability from the forced response and quantify its relative relevance (e.g. Deser et al., 2012; Marotzke & Forster, 2015; Thompson et al., 2015). Moreover, internal variability can be modulated by external forcings, and thus change in a warming climate (e.g. Huntingford et al., 2013; Brown et al., 2017). Examples of internal variability changes are already observed and projected for Arctic sea ice variability (e.g. Deser et al., 2000; Olonscheck et al., 2019), interannual atmospheric modes such as the El Niño Southern Oscillation (e.g. Latif & Keenlyside, 2009; Callahan et al., 2021), or the seasonal cycle of land ecosystems (Rodgers et al., 2021). Such variability changes with changing forcing must be considered to comprehensively represent climate change impacts (Schwarzwald & Lenssen, 2022).

CO_2-induced mean changes can trigger feedbacks

Second, forced changes induce mean changes in other climatic variables that can result in amplifying or dampening feedbacks with mean surface temperatures. Systems exhibit feedback responses when initial perturbations (e.g. changes in CO_2 concentrations) are at a later stage enhanced or diminished by the internal dynamics of the system (e.g. Goosse et al., 2018). Destabilising feedbacks are known as "positive feedbacks" (e.g. the sea ice-albedo feedback, Budyko, 1969; Curry et al., 1995), while stabilising feedbacks are termed "negative feedbacks" (e.g. the Planck temperature feedback, Forster et al., 2021). Some notable Earth system components with potential positive feedback mechanisms include ice sheet disintegration (Fyke et al., 2018), permafrost thawing (Schuur et al., 2015), and Amazon forest dieback (Gatti et al., 2021). As with internal variability, these feedbacks are increasingly being investigated and characterised, but are still insufficiently incorporated in models and impact studies (e.g. Schädel et al., 2024).

Stabilisation after CO_2 emissions cessation

Third, delayed responses to forced climate change can lead to persistent impacts even after forcings cease. While global temperature deviations may be small after net-zero emissions (e.g. Borowiak et al., 2024), significant regional temperature changes are projected over land and at high latitudes (MacDougall et al., 2022). Besides, the climate will continue evolving on long-term timescales, influencing the impacts associated with global temperature targets (e.g. Schaeffer et al., 2012). These post-net-zero and long-term impacts are poorly understood, with a lack of appropriate experiments to address them (King et al., 2021b, 2025a).

Altogether, these variability, feedback, and stabilisation effects are integral to understanding climate impacts of CO_2 changes. In this thesis, I focus on how these effects of varying CO_2 concentrations impact surface temperatures in relation to North Atlantic processes.

1.2 A CHANGING NORTH ATLANTIC

Why is the Atlantic relevant?

The Atlantic Ocean's prominent role in climate science stems mainly from two unique features. Typically, the surface ocean redistributes excess heat from the tropics towards the poles. However, meridional heat transport is different in the Atlantic Ocean, where the net heat transport is northward in both hemispheres (e.g. Trenberth & Caron, 2001). Furthermore, the North Atlantic has the largest concentration of anthropogenic carbon of any ocean region (e.g. Khatiwala et al., 2013; Brown et al., 2021). Both characteristics, the unique heat and carbon transports, largely result from a complex system of currents, the Atlantic Meridional Overturning Circulation (AMOC).

What is the AMOC?

The AMOC is a large-scale system encapsulating thermohaline and wind-driven water transports in the Atlantic, characterised by balancing northward warm surface flow with cold southward flow at depth (Buckley & Marshall, 2016). Aside from other driving mechanisms, this circulation is "pushed" (Visbeck et al., 2001) by deep convection of polar dense surface waters. The AMOC strength is often measured as the maximum integrated water volume transport for all depths at a given latitude (e.g. Frajka-Williams et al., 2019). This concept of strength, often measured in Sverdrups (Sv, one million cubic meters per second), gauges both the northward flow intensity and the rate of deep water formation. The northward transport of warm and salty waters brings heat to northern high latitudes, while the sinking of waters efficiently sequesters surface carbon. Thus, these two key North Atlantic heat and carbon transports would be influenced if the AMOC strength changes.

AMOC under climate change

The AMOC strength is *very likely*[1] to weaken this century as climate change warms and freshens subpolar waters, but there is *low confidence*[2] regarding its exact evolution (Fox-Kemper et al., 2021). In the most extreme scenarios, based on the system's multiple stable equilibria first described by Stommel, 1961, several recent studies warn of a potential AMOC collapse this century (e.g. Boers, 2021; Ditlevsen & Ditlevsen, 2023; van Westen et al., 2024b). Nevertheless, Earth system models from the Coupled Model Intercomparison Project Phase 6 (CMIP6) project a more gradual weakening this century, on average between 24% in lower emissions scenarios and 39% under higher emissions (Weijer et al., 2020). While Earth system models are often criticised as too stable to capture abrupt transitions (e.g. Valdes, 2011; Liu et al., 2017; Swingedouw et al., 2022), recent studies suggest that overturning circulations in other basins may help stabilise the AMOC

1 According to the Intergovernmental Panel on Climate Change (IPCC) calibrated language, which expresses the likelihood of an outcome and its uncertainty, *very likely* corresponds to 90-100% probability (Mastrandrea et al., 2010).

2 Again in the IPCC guidance language, and in contrast to probabilistic measures of uncertainty, confidence in a finding reflects a qualitative assessment of the "type, amount, quality, and consistency of evidence".

(Baker et al., 2025; Årthun et al., 2025). In fact, whether the AMOC has already weakened is still an open scientific debate (e.g. Caesar et al., 2018; Latif et al., 2022; Volkov et al., 2024; Terhaar et al., 2025). This conundrum arises in part from the short length of direct observational records (only 20 years for the RAPID project, Hirschi et al., 2003), added to the substantial internal variability in the AMOC strength (Hirschi et al., 2007; Mecking et al., 2015). Likewise, AMOC variability at multiple timescales is expected to change in a warmer climate (Drijfhout et al., 2008; Cheng et al., 2016; Ferster et al., 2025). Collectively, all these elemental uncertainties in the AMOC evolution underscore how impact studies must consider a collection of plausible past and future AMOC changes.

1.3 AMOC VARIABILITY IMPACTS

AMOC strength and variability affect surface variability

The AMOC strength and its atmospheric impacts interact across multiple timescales. AMOC strength affects surface variability in the Atlantic and Europe from seasonal (Gastineau & Frankignoul, 2012; Frankignoul et al., 2013; Carvalho-Oliveira et al., 2021) and interannual (Pohlmann et al., 2006; Svendsen et al., 2014; Borchert et al., 2018), to decadal (Robson et al., 2014; Zhang & Zhang, 2015) and multidecadal (Zhang & Wang, 2013; Tandon & Kushner, 2015; Zhang et al., 2019) timescales. The ensuing impacts on surface variability stretch further by affecting variability, for instance, of Arctic sea ice (Mahajan et al., 2011), or Pacific temperatures and circulations (Zhang & Delworth, 2005; Williamson et al., 2018; Orihuela-Pinto et al., 2022; Liu et al., 2023a). The AMOC does not simply modulate changes in short-term variability through its mean state, but AMOC observations also show strong interannual variability (e.g. Srokosz & Bryden, 2015; Frajka-Williams et al., 2019) that can have substantial repercussions. For instance, observed AMOC interannual changes, such as the strong negative anomaly in 2009/2010, resulted in a record negative winter North Atlantic Oscillation (NAO) and a strong summer hurricane season (Bryden et al., 2014). Importantly, such anomalies are also driven by strong atmospheric variations (McCarthy et al., 2012; Polo et al., 2014), highlighting the difficulties of decoupling ocean-atmosphere interactions. Yet, the effect of short-term AMOC variability on North Atlantic and European surface climate is apparent and needs to be analysed in the particular context of variability in this region.

A distinctive North Atlantic atmospheric variability

The North Atlantic region exhibits prominent atmospheric variability and circulation patterns. Due to the relative relevance of the eddy-driven jet in comparison to the subtropical jet, North Atlantic variability is less constrained than in similar regions (Woollings, 2010). Variability across many temporal scales is largely attributed to the NAO, its dominant variability mode (Hurrell et al., 2003). Its dipolar

atmospheric pressure gradient accounts for more variance in winter, when the flow is strongest and atmospheric anomalies are largest (e.g. Hurrell & Deser, 2010). The phase and characteristics of the NAO have clear connections with winter climate over Europe (e.g. Hurrell, 1995; Marshall et al., 2001b). Also, the NAO and other relevant circulation modes such as the Scandinavian Blocking directly impact climate extremes (e.g. Marshall et al., 2001a; Scaife et al., 2008; Sillmann et al., 2011). Ultimately, these modes of variability are not independent of forcings, and have been shown to respond to climate change (e.g. Corti et al., 1999; Mitevski et al., 2025; Liu et al., 2025). Therefore, these forced changes and interactions with other major North Atlantic components, such as the AMOC, determine the eventual imprint on European climate.

European temperatures and extremes

Europe is the fastest-warming continent, warming twice as fast as the global average in the last 30 years, (0.53°C/decade compared to 0.26°C/decade, Copernicus Climate Change Service (C3S) & World Meteorological Organization (WMO), 2025). This additional warming on top of the global warming signal is caused by local forcings (such as aerosol emissions reductions, Acosta Navarro et al., 2016), feedbacks (e.g. Arctic amplification, England et al., 2021; Rantanen et al., 2022), and atmospheric circulation pattern changes (Corti et al., 1999; Faranda et al., 2023). Beyond the mean temperature shift, the distribution shapes of European extreme temperature events are also affected. On the one hand, heat extremes have also increased, notably over some European regions (Patterson, 2023; Vautard et al., 2023), and already resulted in high-impact events (Stott et al., 2004; Barriopedro et al., 2011; Sun et al., 2025). Heat extremes are projected to continue to increase rapidly (Suarez-Gutierrez et al., 2023) and proportionally for higher levels of global warming (King & Karoly, 2017; Tebaldi & Wehner, 2018; Li et al., 2021). On the other hand, cold extremes have decreased in frequency and intensity in the last decades (Blackport et al., 2024). Despite global warming, these extremes, although reduced in frequency, are projected to persist in intensity and duration in future climates for many European regions (Kodra et al., 2011; Quesada et al., 2023). Taken together, the distinctive features of European temperatures and extremes highlight the critical importance of considering multiple perspectives and interactions when analysing their climate change impacts.

AMOC and European cold extremes

The AMOC effect on extreme events in a changing climate has been recently researched from a large AMOC weakening perspective. Such weakening would impact cold extremes over Europe (Meccia et al., 2024; van Westen & Baatsen, 2025), North (Yin & Zhao, 2021) and South (Meccia & Blázquez, 2025) America, and Siberia/Asia (Wang et al., 2022), as well as European heat (Meccia et al., 2025; Duarte et al., 2025) and precipitation extremes (Ma et al., 2024). In particular, cold extremes would be overall colder, due to the reduced meridional

heat transport (Meccia et al., 2024). They would also be less likely, as the increased meridional temperature gradient produces less persistent atmospheric blocking systems. However, this large weakening is uncertain, and the observed AMOC does change on shorter timescales, such as interannually, with associated atmospheric impacts (e.g. Bryden et al., 2014). Interannual variations have also been shown to potentially affect seasonal and mean temperatures over Europe (Pohlmann et al., 2006). However, the past AMOC interannual variability effect on European extremes has not been addressed yet. Particularly, whether this potential AMOC variability impact changes in the context of recent forced climate change is still unknown.

1st research question

In short, I have identified a notably neglected aspect of AMOC influence on European temperatures, where short-term AMOC variability, Atlantic circulation modes, and extreme cold events meet. Specifically, the gap pertains to past and present-day climates, where the AMOC strength has not yet distinctly weakened, but where the variables mediating the surface impacts have already responded to increased CO_2 concentrations. Therefore, the first research question of this thesis is:

Q1: What is the past AMOC interannual variability influence on European extreme cold temperatures?

Before answering this research question on AMOC variability impacts, I first derive the two other research gaps related to impacts from a weakening and a stabilising AMOC. By doing so, I construct a framework that better contextualises the challenges and implications of each research question, as well as their joint significance.

1.4 AMOC WEAKENING IMPACTS

Physical impacts of AMOC weakening

Considerably more than past variability impacts, AMOC impacts have been predominantly studied for large and often idealised future weakenings. An overall AMOC weakening would result in widespread effects across the climate system, as impacts in precipitation (Jacob et al., 2005; Bellomo et al., 2023) and monsoon patterns (Parsons et al., 2014; Sandeep et al., 2020; Ben-Yami et al., 2024b), Arctic and Antarctic sea ice (Mahajan et al., 2011; Liu et al., 2020; Diamond et al., 2025), terrestrial and marine ecosystems (Kuhlbrodt et al., 2009; Ritchie et al., 2020; Boot et al., 2025), or sea level rise (Levermann et al., 2005; Chen et al., 2019; Little et al., 2019), among many others. Among all, the most widely studied impact is regional cooling from reduced northward surface heat transport, particularly over Europe and much of the Northern Hemisphere (e.g. Vellinga & Wood, 2002; Stouffer et al., 2006; Laurian et al., 2010; Jackson et al.,

2015; Bellomo et al., 2021). All these AMOC impacts contribute to the broad consequences of climate change on socioeconomic systems.

Economic impacts of climate change

Beyond the physical impacts of anthropogenic climate change, economic impacts have also been extensively studied (Stern, 2006). Economic impact is generally measured through the social cost of carbon (SCC) and quantified using integrated assessment models (IAMs). IAMs combine natural and economic modules to calculate the SCC, conventionally as the present (discounted) value of future damages from an additionally emitted ton of CO_2. While SCC estimates are actually used in decision-making, studies and experts believe that these estimates are often too low (e.g. Rennert et al., 2022; Moore et al., 2024). Beyond the difficulties, uncertainties, and normative choices of modelling humans and markets, SCC estimates are also largely limited by the representation of physical processes beyond mean temperature changes.

Economic impacts of climate feedbacks

One clear deficiency in IAMs is that they largely omit climate feedbacks (e.g. Moore et al., 2024). This behaviour, often related to climate tipping elements (Lenton et al., 2009; Armstrong McKay et al., 2022), is characteristic in the North Atlantic for the AMOC, presenting several potential feedbacks (e.g. Swingedouw et al., 2007a; Zickfeld et al., 2008; van Westen et al., 2024b). Recently, climate feedbacks have started to be included in economic quantifications of climate change damages (Cai et al., 2015, 2016; Dietz et al., 2021; Dietz & Koninx, 2022), but their AMOC representation has been controversial.

Oversimplified economic impact of AMOC weakening

Despite the numerous AMOC impacts already identified, they have mostly not been incorporated into economic modelling. The impact of a weakening AMOC has only been accounted for by its direct cooling effect on the Northern Hemisphere (Anthoff et al., 2016; Dietz et al., 2021). This effect is considered favourable for the economy as it would counteract some of the surface warming from increased greenhouse gas concentrations. Besides, this effect is modelled without an explicit temporal dependence of AMOC strength on temperatures, but rather with an idealised stochastic tipping behaviour that does not reflect future AMOC projections. This limited representation has caused stark criticism (Keen et al., 2022; Dietz et al., 2022), but AMOC economic assessments have surprisingly not yet been extended to include other AMOC impacts.

AMOC weakening and ocean carbon

One evident effect to be added to economic assessments is the impact of the AMOC carbon feedback. If CO_2 concentrations increase, global warming increases and the AMOC weakens. Then, reduced deep water formation leads to a decrease in carbon uptake, and more carbon stays in the atmosphere. The additional carbon produces more surface warming, weakening AMOC further (Figure 1). Therefore, a positive feedback between AMOC strength and ocean carbon uptake is possible. Many studies have addressed the connection between the AMOC and ocean carbon storage (Obata, 2007; Swingedouw et al.,

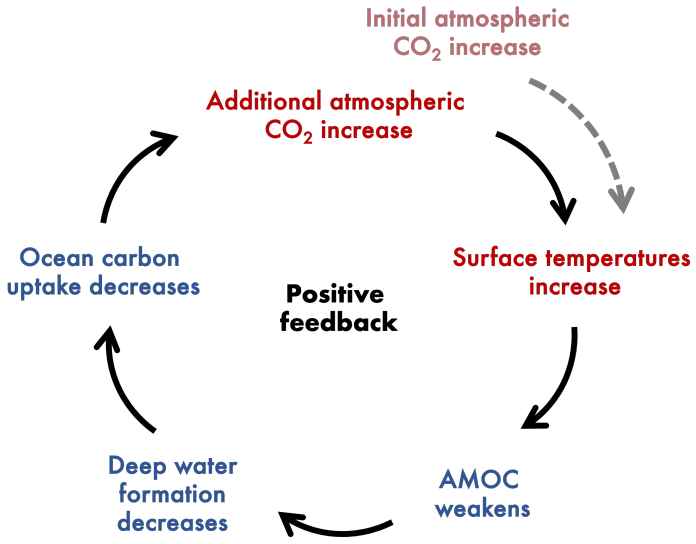

Figure 1: Sketch of the positive AMOC carbon feedback.

2007a; Zickfeld et al., 2008; Pérez et al., 2013; Gruber et al., 2019; Nielsen et al., 2019; Brown et al., 2021; Katavouta & Williams, 2021; Liu et al., 2023b; Boot et al., 2024), but the exact year-to-year relationship between the AMOC strength and ocean carbon uptake is unknown. This relationship, across different estimations of future AMOC weakening, is needed for incorporating the AMOC carbon feedback effect into economic estimates.

2nd research question

AMOC weakening impacts on surface temperatures, except for the direct Northern Hemisphere cooling, have been overlooked in economic assessments. Economic assessments of climate feedbacks must, among other impacts, also include a precise quantification of the AMOC strength and ocean carbon uptake relationship. Therefore, the second research question of this thesis is:

Q2: What is the projected economic impact of the AMOC carbon feedback?

1.5 AMOC STABILISATION IMPACTS

Committed changes of net-zero emissions

Alongside conventional emissions scenarios, projecting climate evolution in high-mitigation futures is equally relevant for understanding the climatic consequences of policy decisions. A key associated concept is achieving net-zero emissions, where anthropogenic greenhouse gas emissions are balanced by anthropogenic removals. A fundamental response to net zero is the Zero Emissions Commitment (ZEC), defined as the global temperature change after emissions cessation (usually of CO_2, Palazzo Corner et al., 2023). The Zero Emissions Commitment Model Intercomparison Project (ZECMIP) designed the most extensive modelling framework to date to identify the ZEC

in idealised experiments (MacDougall et al., 2020), finding ZEC to be small but significant (Borowiak et al., 2024, 2025). Post-net-zero changes in regional temperatures have also been identified, and some of the largest inter-model variance occurs over the North Atlantic (MacDougall et al., 2022).

AMOC under net-zero emissions

One of the most prominent mechanisms contributing to these variable post-net-zero North Atlantic responses is the AMOC evolution. The AMOC strength is expected to at least partly recover under net zero (Sigmond et al., 2020; Schwinger et al., 2022a; MacDougall et al., 2022; Lee et al., 2025). However, different models show diverging responses both in the timing and magnitude of recovery. Some initial experiments showed a continued decline 10 years after net zero, followed by a 150-year recovery, all independent of the emissions scenario (Sigmond et al., 2020). Other models show longer recovery times (Schwinger et al., 2022a), with large disagreements even between ensemble members within the same model (Lee et al., 2025). But, generally, models show a weaker final recovered state compared to preindustrial strength. Simulations of climate overshoot under net-negative emissions show similar disagreement in responses, with potential final states stronger than preindustrial (An et al., 2021; Schwinger et al., 2022a, 2022b; Lee et al., 2025). In any case, the AMOC weakening and its magnitude and pace of recovery, despite the wide range of possible responses, have a direct impact on post-net-zero North Atlantic surface temperatures. While regional changes in mean temperatures have been more systematically analysed, many of the net-zero responses of extreme temperatures are still poorly characterised.

European heat extremes under emissions mitigation

Due to the disproportionate recent increase in European heat extremes (e.g. Rousi et al., 2022), studies have analysed the impacts of climate mitigation in reducing the intensity of such events. European heat extremes have been characterised at different global warming levels in transient climates, finding clear benefits from limited warming (e.g. Sillmann & Roeckner, 2008; King & Karoly, 2017; Suarez-Gutierrez et al., 2018). Particularly for net-zero emissions, a recent global study based on the ZECMIP found monthly maximum temperatures to be reduced up to 40% in some regions (Cassidy et al., 2024). However, there is no study yet with a regional focus on Europe and with more realistic net-zero simulations than the ZECMIP experiments, so that they can be put in context with 21st-century scenarios. Also, regional temperatures and seasonal extremes have been found to differ between transient and equilibrium warming levels following certain emissions scenarios (King et al., 2020, 2021a), suggesting that a long-term perspective might be relevant in the characterisation of net-zero emissions futures.

Long-term stabilisation

The timescales considered in end-of-century scenario projections or in ZECMIP, 50-100 years after net-zero emissions, are too short to

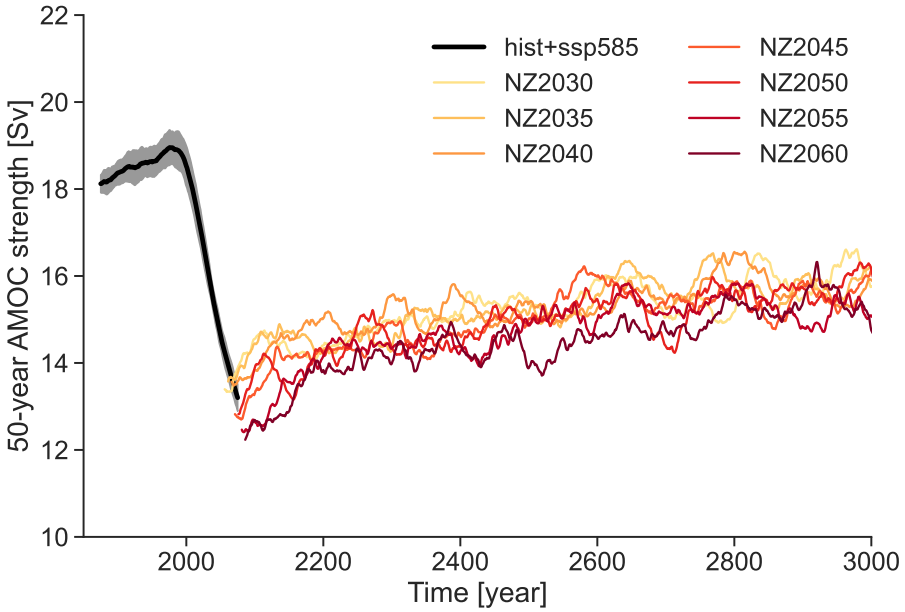

Figure 2: AMOC stabilisation under net-zero emissions in ACCESS-ESM-1.5 1000-year simulations.

also include stabilisation effects such as the AMOC recovery. Beyond just being a theoretical exercise, understanding long-term stabilisation is needed to adequately quantify prominent temperature goals such as the Paris Agreement targets (King et al., 2021b). While constant atmospheric concentrations have been previously addressed in long timescales (e.g. Rugenstein et al., 2019), they lead to a misinterpretation of committed warming and changes compared to net-zero emissions due to the natural carbon sink (Matthews & Weaver, 2010). Long-term net-zero emissions have been studied in models of intermediate complexity (e.g. Zickfeld et al., 2013), but these do not robustly represent regional and extreme changes (King et al., 2025a). Recently, a multi-centennial net-zero emissions framework of Earth system Model simulations has been proposed and carried out (King et al., 2024). These simulations signal long-term changes at multiple regional scales and climatic variables. When analysing further these experiments, I find that the AMOC needs many centuries to recover (Figure 2). Despite these relevant changes, the evolution of temperature extreme events, particularly in Europe, has not been quantified.

3rd research question

In short, I argue that, when compared to transient end-of-century scenarios, European heat extremes have been overlooked for net-zero emissions and long-term timescales relevant for climate stabilisation. These extended timescales are critical given that the AMOC recovery may require centuries, with corresponding impacts on surface temperatures. This research gap can be formulated with the question:

Q3: What is the long-term evolution of European heat extremes under net-zero emissions?

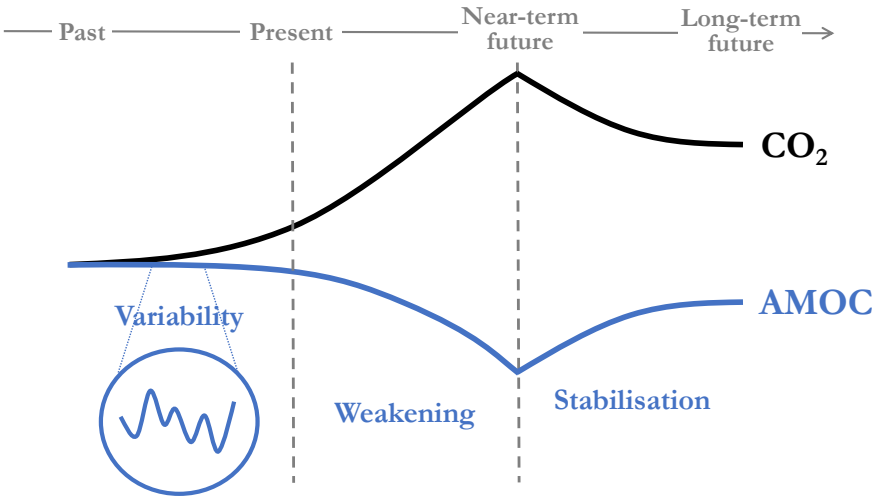

Figure 3: Illustration of the three types of changes in AMOC strength and atmospheric CO_2 concentrations considered in this thesis.

1.6 OVERARCHING QUESTION

The three derived research questions address temperature impacts related to CO_2 forcing and AMOC changes (Figure 3). The first question deals with CO_2 increases until the present day while focusing on AMOC variability. The second question tackles future projected CO_2 increases this century and their interaction with a weakening AMOC. The third question takes on long-term CO_2 emissions cessation and a recovering and stabilising AMOC. They all have a different impact focus, from mechanisms of North Atlantic variability for cold extremes, through reduced ocean carbon uptake affecting global temperatures and causing economic damages, to likelihoods of heat extremes in Europe; but they all address impacts that ultimately manifest through surface temperature changes. Therefore, it is important to consider the added value of combining this research, particularly for mitigating or adapting to climate change temperature impacts. For that reason, the overarching question that will be used at the end to bring together all three topics is:

What is the added value of jointly considering diverse and multitemporal CO_2 and AMOC changes to assess surface temperature impacts?

2

AMOC VARIABILITY AND EUROPEAN COLD EXTREMES

The first publication of this thesis (Article A), whose methods and results are summarised in the following, addresses the research question *"What is the past AMOC interannual variability influence on European extreme cold temperatures?"*. I have motivated this question based on clearly discernible interannual AMOC changes in the past. These changes have also been connected to atmospheric variability over the Atlantic Ocean and Europe. However, since the influence on cold extremes has only been characterised for idealised long-term AMOC weakenings, the connection to realistic past AMOC variability and involved physical mechanisms remains an overlooked scientific gap.

2.1 COLD EXTREMES INFLUENCED BY INTERANNUAL AMOC VARIATIONS

Modelling with a SMILE

As the goal is to quantify the changing likelihood of cold extremes, many event occurrences of such events are required for a robust characterisation. This is not feasible in observations, as the goal is to condition extremes (rare by definition) on AMOC interannual changes, for which measurements span less than two decades (Moat et al., 2025). For that reason, and also to be able to separate variability from the forced signal (Maher et al., 2019; Rodgers et al., 2021), a single model initial-condition large ensemble (SMILE) is the most suitable tool (Maher et al., 2021). The model used is the Max Planck Institute Earth System Model (MPI-ESM) in its low-resolution configuration, which enables many climate realisations with slightly different initial conditions to be simulated. This SMILE, denoted previously as the Max Planck Institute Grand Ensemble (MPI-GE) for CMIP5 (Maher et al., 2019), is now available for CMIP6 with 50 realisations for the historical experiment (MPI-GE CMIP6, Olonscheck et al., 2023) and used in this study. It is initialised in 1850 from different plausible preindustrial conditions, and it simulates potential climates constrained by realistic external forcings until 2014. With this setup, it is possible to analyse the past evolution of the AMOC variability influence on European cold extremes, as CO_2 concentrations considerably increased but the AMOC strength has not yet significantly declined.

Conditioning on AMOC interannual variations

The overall approach is to associate AMOC variations with the subsequent temperature probability distribution functions (PDFs). The idea is to compare the composites of strong and weak AMOC variations (as in Pohlmann et al., 2006), but in our study, the AMOC vari-

ation temporally leads the changes in cold extremes. This is achieved by detrending each analysed period and calculating ensemble-mean composites following the interannual period (3-year means) with a strong or weak AMOC, for variations surpassing one preindustrial standard deviation (Figure 4). By computing the 1% coldest temperatures and their extreme value distributions, the influence of AMOC variations is analysed.

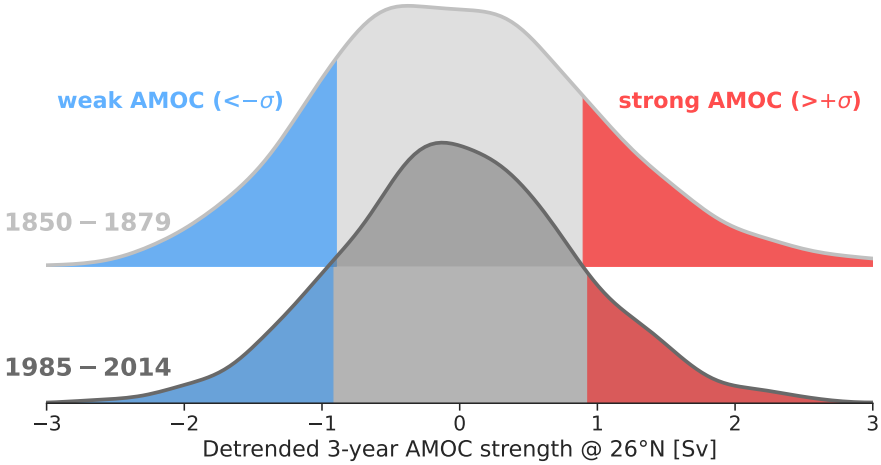

Figure 4: Detrended interannual AMOC strength distributions for the 1850-1879 and 1985-2014 periods in MPI-GE CMIP6. Weak (below one preindustrial standard deviation) and strong (above one preindustrial standard deviation) variations are highlighted in blue and red, respectively.

Distribution shift but contrasting periods

There are two main results from the cold extreme distributions conditioned on AMOC interannual variations. First, in the early period, there is a distribution shift, with colder extremes following weak AMOC years in contrast to strong variations (Figure 5, left). This shift is evident in the European mean distributions, with roughly a 1°C shift. The shift between the distributions can be traced back spatially and to the individual extreme distribution parameters. As a result, the shift is explained by a significant difference in the location parameter, with the largest differences occurring over Northern and Eastern Europe. The second main result is the contrast in the late historical period, where shifts are much smaller (Figure 5, right). In this period, the European mean extreme distributions are very similar as a result of a much smaller and less significant difference in the location parameter. We turn to the analysis of physical mechanisms to explain both the shift in the early period and the contrast between periods.

2.2 EXPLAINING SHIFT AND CONTRASTING PERIODS

Ocean-atmosphere interface mechanisms

Analogously to European cold extremes, mediating physical mechanisms can be inspected by conditioning them on AMOC interannual

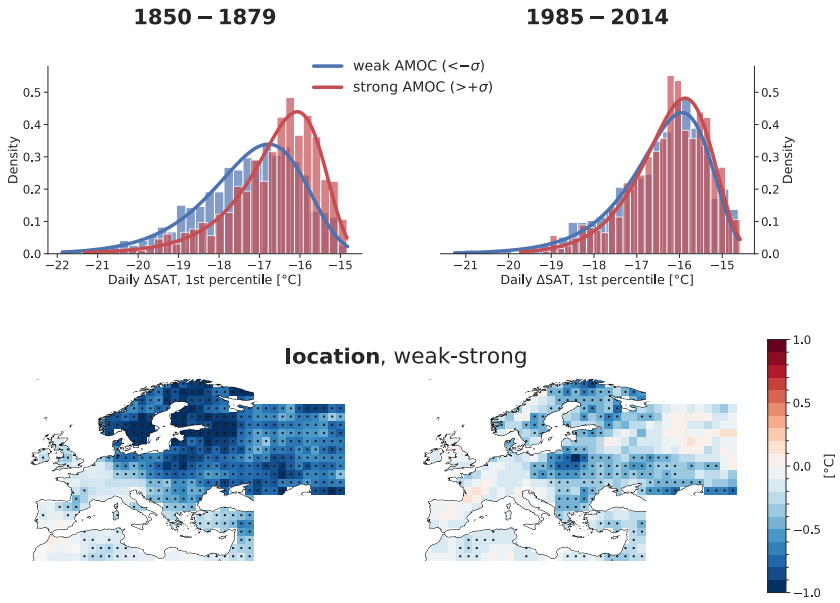

Figure 5: Extreme cold distribution differences between interannual weak and strong AMOC, for the early and late MPI-GE CMIP6 historical periods. Top row: Extreme value distributions of European mean cold extreme temperatures during weak (blue, below -1σ) and strong (red, above 1σ) 3-year AMOC variations. Bottom row: Spatial difference in the location parameter of cold extreme temperatures between weak and strong AMOC composites.

variations. We focus on seasonal averages during cold extreme winters and first address variables at the ocean-atmosphere interface. The analysis of sea surface temperatures (SSTs), sea ice concentrations, and ocean-atmosphere heat fluxes largely reflects the analysed changes in extremes (Figure 6). For the early period shift, and from the perspective following weak AMOC years, SSTs are colder over the subpolar gyre (with a warmer region off the North American coast, consistent with weak AMOC patterns), and over the Labrador, Nordic, and Barents seas. Sea ice concentrations confirm that the cold patterns over the Arctic seas are related to extended sea ice extent at the location of the sea ice edge. As a result, in regions where SSTs are colder following weak AMOC years, latent and sensible heat fluxes into the atmosphere are also reduced. These reduced fluxes favour the formation of North Atlantic atmospheric blocking regimes, which would ultimately lead to colder extremes over Europe. In the late period, while the subpolar gyre pattern is similar, the SST, sea ice, and heat fluxes changes over the sea ice edge regions are practically not present. The hypothesis for this contrast in the later period is the retreated background sea ice state compared to a preindustrial climate, inhibiting the influence of weaker AMOC at the sea ice edge. To understand how these interface effects impact the more direct atmospheric influence on the extreme cold events, the analysis of mechanisms is com-

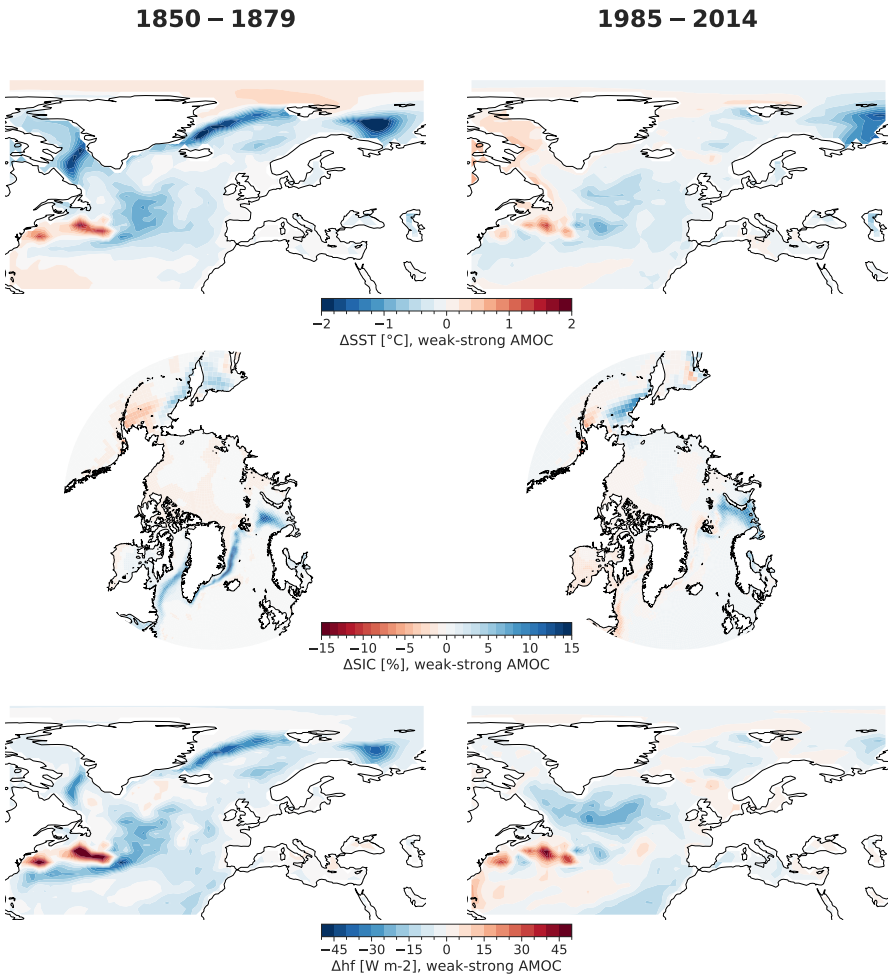

Figure 6: Differences in sea surface temperatures (SSTs, top row), sea ice concentrations (SIC, middle row), and heat fluxes (bottom row, positive upwards) for weak (below -1σ) minus strong (above 1σ) 3-year AMOC variations in MPI-GE CMIP6. Left: 1850-1879; right: 1985-2014.

pleted with the characterisation of Euro-Atlantic atmospheric pressure regimes.

Changes in winter circulation regimes

Changes in AMOC and sea surface properties affect Euro-Atlantic circulation regimes, as shown through the phase space analysis of atmospheric pressure variability modes. Based on an Empirical Orthogonal Function (EOF) analysis, we focus on the three main modes: the North Atlantic Oscillation (NAO), the Atlantic Ridge (AR), and the Scandinavian Blocking (BLO), which together explain 70% of the winter variance (40% of which is the NAO alone). In the early period, the most consistent changes occur in the NAO distributions. The distribution of states slightly drifts towards NAO- phases (pattern inhibiting westerlies, potentially bringing cold air over Northern Europe) after a weak AMOC, and distinctly moves towards NAO+ after a strong AMOC. These early period regime distribution drifts contrast with

the response in the later period, where the NAO states following an anomalous AMOC are not clearly favoured, especially the shift towards NAO+ after a strong interannual AMOC. The last step in dissecting the mechanisms at play is to test the effect of each circulation regime on cold extremes, as well as the changes in these effects when conditioned on AMOC variations.

Extremes conditioned on AMOC and circulation regimes

The analysis of winter circulation regime impacts on cold extremes reveals that the NAO phase remains the primary driver for above- or below-average cold extremes. The expected effect, colder extremes with NAO- and warmer extremes with NAO+, is present in both periods. When accounting for the preceding AMOC variations in the early period, the NAO effect becomes more intense for NAO- and weak AMOC (colder extremes) and for NAO+ and strong AMOC (warmer extremes). This enhanced effect is also present in the late period, but is reduced in magnitude. Taken together, these results show that AMOC interannual variations affect both the likelihood of winter pressure regimes and the effect these regimes have on the intensity of cold extremes. These two effects combine to explain the extreme cold distribution shift in the early period and the contrast with the late period.

Discussion

Altogether, AMOC unforced variability can potentially influence European extreme cold temperature distributions, but recent changes in forcings modulate this relation. We carry out the analysis within the framework of a single Earth system model, which could present biases. While this approach is important to ensure consistency (e.g. of absolute AMOC strengths or variability, which differ widely across models) and accomplish a more in-depth mechanistic analysis, the next step would be to reproduce the analysis with different models. The analysis of future changes in the analysed relationship is another remaining gap, which will need a more careful consideration of AMOC variability in the context of a larger weakening. With regard to preceding studies, our overall results agree with the mean temperature shifts evidenced for annual AMOC variability (Pohlmann et al., 2006), but differ from the mechanisms of a large AMOC weakening on cold extremes (Meccia et al., 2024). Overall, these differences for other types of AMOC changes and the contrasting periods in our results highlight the need to consider an ample diversity of AMOC strengths, and to do it within appropriate climate backgrounds, when assessing potential impacts.

3

ECONOMIC IMPACT OF THE AMOC CARBON FEEDBACK

This thesis's second publication (Article B) focuses on the AMOC weakening until the end of the century to address the question *"What is the projected economic effect of the AMOC carbon feedback?"*. Filling this gap requires not only estimating the feedback's economic imprint, but also the actual quantification of the relationship between AMOC strength and ocean carbon uptake. Addressing such an interdisciplinary topic involves the combination of models that can account for interactions between the physical, biogeochemical, and societal components of the climate system.

3.1 MODELLING THE AMOC CARBON FEEDBACK

AMOC carbon feedback in ESMs

The first step, quantifying the AMOC-carbon uptake relationship, is realised using an Earth system model (MPI-ESM). The magnitude of this relationship is calibrated for a broad range of AMOC strengths first, to later be projected into the future according to multi-model scenarios of AMOC weakening and incorporated into an integrated assessment model.

Calibration with BGC-only hosing experiments

For the calibration, we use freshwater hosing experiments, where an artificial freshwater flux is added to the model in the North Atlantic. This freshwater flux (in practice, a negative salt flux) largely stands for the lack of freshwater input from Greenland, as most Earth system models to date lack interacting ice sheets. Freshwater weakens the AMOC by increasing buoyancy and reducing deep convection. The magnitude of this flux is not meant to be realistic, but to cover a wide range of AMOC strengths by varying its magnitude. The shortcoming with existing hosing simulations is that they are generally performed under preindustrial forcings, to isolate the AMOC weakening effects from those of global warming (e.g. Jackson et al., 2023a). However, the representation of this effect under preindustrial conditions would not be appropriate for assessing the present-day and future carbon cycle, where CO_2 concentrations are fundamentally increased. We propose a novel approach (technically tested once before by Zickfeld et al., 2008, in a model of intermediate complexity) by combining freshwater hosing experiments with biogeochemically-only coupled (BGC-only) experiments (Jones et al., 2016). BGC-only experiments have widespread use in the carbon-cycle-feedbacks community (e.g. Arora et al., 2020; Katavouta & Williams, 2021), and decouple the radiative component of the model from any atmospheric

CO_2 increase. Therefore, in an experiment with freshwater hosing and increasing CO_2 concentrations, the changes in the ocean carbon cycle can be solely attributed to the AMOC weakening, as the CO_2 increase does not cause any warming. To gauge the influence of the chosen freshwater hosing pattern, two different patterns from the North Atlantic Hosing Model Intercomparison Project (NAHosMIP) are tested. To also assess the potential dependence on the emissions scenario, simulations under different pathways are carried out.

Changes in carbon flux scale linearly with AMOC strength

The BGC-only hosing experiments showcase a clear relationship between AMOC and ocean carbon storage (Figure 7a). The larger the freshwater input, the more the AMOC weakens. In general, the induced weakening is larger in experiments where the freshwater is distributed all over the North Atlantic, compared to when it is only around the coast of Greenland. In turn, for larger AMOC weakenings, larger amounts of carbon are not stored in the ocean. Under considerably higher emissions, the reduction of stored carbon is very similar, implying that the relationship solely depends on AMOC strength for a wide range of possible future scenarios. This independence is clearer when, instead of characterising carbon storage, the relation with carbon fluxes is analysed. Carbon flux reductions further show a remarkably linear relationship with AMOC strength (Figure 7b). This depiction indicates that for every Sverdrup that the AMOC is weaker, roughly 0.025 PgC less are taken up by the ocean each year.

3.2 SOCIAL COST OF CARBON EFFECT

The reduced ocean carbon uptake increases atmospheric CO_2 concentrations, leading to additional surface temperature warming. To calculate economic damages and the eventual SCC effect, we use the assessed linear relationship, AMOC strength projections from several Earth system models, and an integrated assessment model.

CMIP6 AMOC projections

The magnitude of the future ocean carbon flux reduction is calculated using projections of AMOC weakening from several CMIP6 models. For the SSP2-4.5 scenario, the available CMIP6 models estimate a relative AMOC weakening between 20 and 50% by 2100. Using each model's AMOC projection and the previously assessed linear relationship of the AMOC carbon feedback, the integrated changes in ocean carbon storage range from 4 to 12 PgC. These values compare to roughly half to one year of CO_2 emissions at present-day rates. While not a large effect, such an increase in CO_2 concentrations will further warm the surface, potentially with a negative economic impact.

Economic modelling: META

The IAM used, the Model for Economic Tipping Analysis (META), is particularly designed to include the feedback effects of major climate system components such as the AMOC (Dietz et al., 2021). The previously existing version, however, does simply include the direct

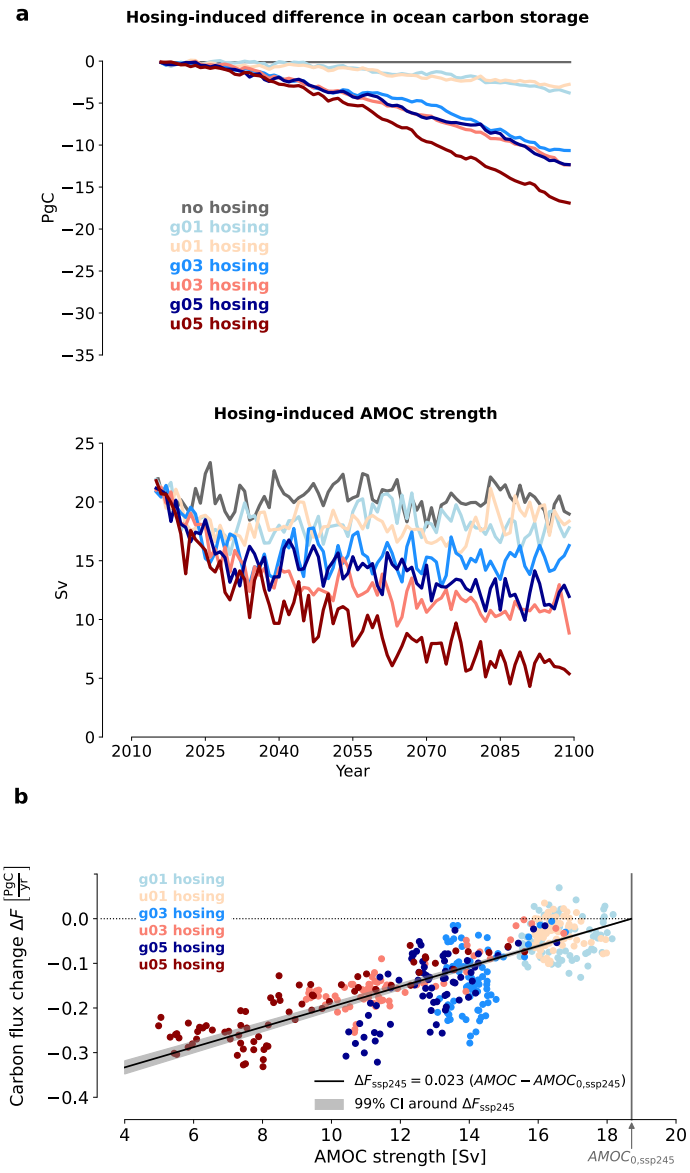

Figure 7: AMOC carbon feedback calibration with MPI-ESM. a) Cumulative carbon (top) and AMOC strength (middle) time series for the different hosing BGC-only experiments along an SSP2-4.5 scenario. b) Changes in carbon flux into the ocean as a function of AMOC strength, with respect to years with a preindustrial AMOC strength.

cooling effect of the AMOC, and it does it without an explicit representation of AMOC strength evolution. In our study, this representation is now included, based on the projected AMOC strengths from different models and scenarios. Given the AMOC strength in a given year, the corresponding additional CO_2 is added to the carbon cycle of the climate module in the model, which calculates the resulting global mean surface temperature change, given also the emissions

from the particular scenario. For reference, the additional warming from including the feedback in the different AMOC projections under a SSP2-4.5 scenario ranges between 0.4 and 0.8 % in 2100. Once the yearly global temperature change is estimated, the model's economic module downscales this global temperature change for each country, and calculates country-specific damages (based on Burke et al., 2015). This component then outputs the corresponding change in utility and welfare. By comparing the results with and without the AMOC carbon feedback implementation, the resulting change in SCC can finally be assessed.

A potential net cost to society

Compared to the previously assessed direct cooling effects, the SCC changes from the additional warming caused by the AMOC carbon feedback are of similar magnitude but reversed sign (Figure 8). The SSP2-4.5 relative SCC changes for the different models range between +0.5 and +1.6%, implying a significant relative increase in the social cost of carbon. The central estimates of the direct cooling effect were roughly a -1% change in Dietz et al., 2021, although both estimates are not directly comparable due to the model changes and developments introduced in the carbon feedback representation. Repeating the carbon feedback SCC estimation for different scenarios widens the range from 0.2 to almost 4%. Remarkably, the effect becomes larger for lower emissions scenarios. This apparent contradiction is caused by similar AMOC weakening between scenarios until 2060, resulting in a comparable AMOC-related increase in CO_2, which is then larger in relative terms under low emissions. Altogether, these estimations show that already including one additional impact channel to the direct cooling effect, the AMOC carbon feedback, could flip the SCC impact of a weakening AMOC from a net benefit to a net cost to society.

Discussion

In summary, we quantify the size of the AMOC carbon feedback and show that an AMOC weakening would negatively impact the economy. The size of the effect is opposite and about as large as the previous estimate of a positive economic impact from the direct cooling effect on the Northern Hemisphere. There are possible pitfalls in the calculation of the relationship between AMOC and ocean carbon uptake, such as only using one model or possible deviations from the linear model. Nevertheless, we corroborate the approximate size of the overall effect by constructing a multi-model AMOC carbon-climate feedback (using the estimates from Katavouta & Williams, 2021) and also by similarity to recent studies (Boot et al., 2024). When estimating the economic effect, large uncertainties apply to both the representation of physical processes and the value judgments and parameter choices that come with economic assumptions. We mitigate this latter impact by working with relative social carbon changes

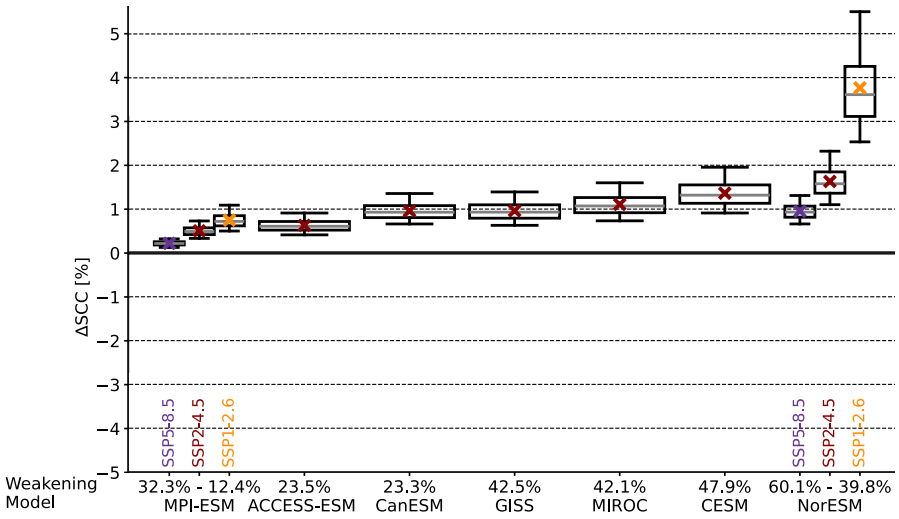

Figure 8: Relative SCC change due to the AMOC carbon feedback with multi-model AMOC projections (SSP2-4.5 when not indicated). Uncertainties are calculated by Monte Carlo sampling, drawing from uncertainties in the climate module, the preindustrial AMOC strength, internal variability around AMOC projections, and the linear fit between AMOC strength and ocean carbon uptake.

(rather than absolute), reducing the sensitivity to normative assumptions. While the consideration of multiple scenarios and models for possible weakening paths is a significant contribution from our study, scenarios of rapid AMOC weakening or collapse are possible but not accounted for, and could result in larger impacts. Nonetheless, we show the large impact that adding a single impact channel can have, laying the groundwork for the incorporation of more AMOC projections and impacts in the pursuit of a thorough economic assessment.

4

LONG-TERM EUROPEAN HEAT UNDER NET ZERO

The third and last publication of this thesis (Article C) concerns post-net-zero climate stabilisation in multi-centennial timescales, particularly on the question: *"What is the long-term evolution of European heat extremes under net-zero emissions?"*. While European heat extremes have been carefully studied in a plethora of future climate projections, the existing net-zero frameworks have not yet thoroughly inspected the expected changes in these events. Given that recent net-zero research highlights the significance of long-term timescales and mitigation delay impacts on various climate system components, there is a compelling rationale to investigate European heat extremes within a similar paradigm.

4.1 EXTREMES IN LONG-TERM NET-ZERO SIMULATIONS

1000-year-long ACCESS-ESM experiments

Earlier, I briefly introduced a recently developed modelling framework to answer long-term stabilisation under net-zero (King et al., 2024). The innovative aspects of these experiments are that they focus on net-zero emissions (not concentrations), extend beyond just one or two centuries, branch from more realistic scenarios than idealised experiments, and are available for different net-zero branching times to analyse the effect of cessation delay. These experiments are performed with the Australian Community Climate and Earth System Simulator - Earth System Model (ACCESS-ESM), in its 1.5 version developed for CMIP6 (Ziehn et al., 2020). These experiments set CO_2 emissions instantaneously to zero (from a high-emissions scenario) at five-year intervals from 2030 to 2060. The rest of the anthropogenic forcings are instantaneously returned to preindustrial levels. Hence, while still idealised, this design and framework present a clear step forward in understanding long-term post-net-zero climate changes.

Mean surface temperature and AMOC evolution after net zero

In all experiments, global mean surface temperature first responds to the drastic change in forcing by cooling slightly in the first decades, but then slowly warms for the remaining centuries. As I show in Figure 2, the AMOC strength, after a decline of roughly 30% before net zero, recovers slowly in all simulations to around 90% of its preindustrial strength. Even though the recovery in each experiment is statistically significant in less than a century, the AMOC trajectories are not significantly different between the net-zero experiments (King et al., 2025b). The AMOC strength similarity between experiments could imply that, while the temperature impact of the AMOC recovery will determine temperatures over Europe, it will likely not drive

the temperature differences between experiments. In fact, European temperatures follow a similar evolution to the global mean, but the behaviour of heat extremes is, as justified in the derivation of the research question, still unknown.

Extreme heat metric and evaluation

This gap is mostly addressed using an intensity-based standard index, the annual TXx (e.g. Sillmann et al., 2013). It represents the hottest maximum daily temperature in each year. When analysing a specific region, TXx is averaged separately over the whole of Europe or over each of the four European regions in the Sixth Assessment Report of the Intergovernmental Panel on Climate Change (IPCC AR6): Northern Europe, Western and Central Europe, Northern Europe, and the Mediterranean (Iturbide et al., 2020). While the TXx analysis would quantitatively differ for other indices, conclusions are qualitatively robust for other indices (as we tested for the frequency-related TX90p index). To better interpret the significance of this index in comparison to current heat records, as well as the evaluation of the model's ability to represent the observed past, the same metric is computed in the Fifth generation of the European Centre for Medium-Range Weather Forecasts Retrospective Analysis (ERA5). The spatial representation of ERA5 records indicates that the spatially-averaged TXx records in European regions result from years where each specific region undergoes a very severe heatwave. For the spatial average over the whole of Europe, the records often represent years with several episodes in different regions. The model evaluation through rank frequency analysis (a method to test initial-condition large ensembles, e.g. Suarez-Gutierrez et al., 2018) shows that observed variability is within the model range (in its initial-condition large ensemble of the past climate, Figure 9). Eventually, we also use attribution metrics such as risk ratios (RRs) or fractions of attributable risk (FARs) to quantify the role of differences in experiments in changing likelihoods in extremes above thresholds.

4.2 A STATIONARY FUTURE AND PATH DEPENDENCE

Europe mean TXx remains elevated for centuries

The spatially-averaged time evolution of TXx shows a steady strength over many centuries of net-zero emissions (shown here for the European mean, Figure 10a). This remarkable stability also holds for the mean over the different European regions. There is no long-term trend but strong annual variability, which is largest over Northern and Eastern Europe and smallest over the Mediterranean region. The distributions of these extremes are significantly different from the present-day distributions (Figure 10b). Moreover, the distributions are also significantly different among each pair of net-zero experiments. These differences imply that five-year delays in emissions cessation along a high-emissions scenario (where five years are between 75 and 130 PgC of additional emissions) lead to consistently more

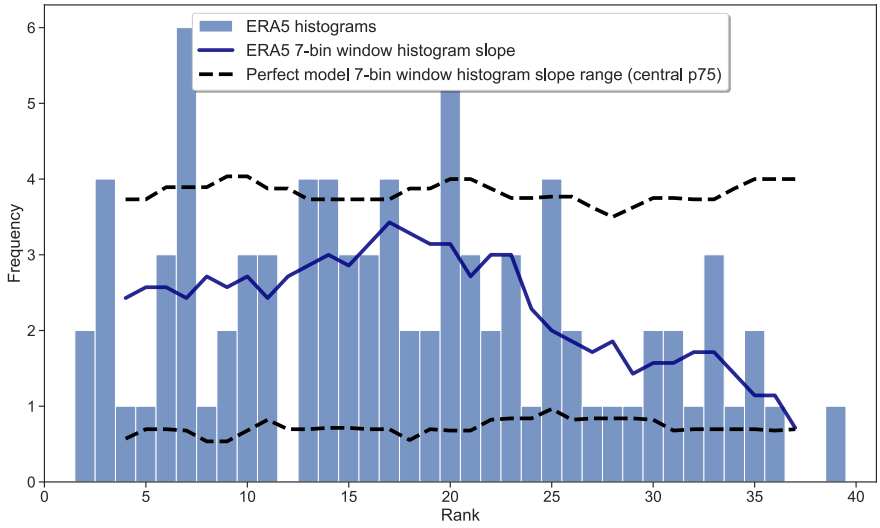

Figure 9: European TXx evaluation through rank histogram analysis of the ACCESS-ESM-1.5 historical+SSP5-8.5 ensemble with ERA5.

intense heat extremes for many centuries. These distribution shifts also hold for the separate European regions, with the smallest absolute but largest relative shift for the Mediterranean region. The likelihoods above thresholds, as represented by risk ratios with respect to the present-day distribution, also show significant increases (Figure 10c). These ratios, valuable in interpreting potential impacts, portray observed records to be two to five times more likely for the next centuries, with higher probabilities for later emissions cessation years. Once again, the Mediterranean region stands out, with the likelihood of events as current records becoming, in the net-zero simulations with emissions cessation in 2060, up to 30 times more likely. Even higher thresholds present larger increases in likelihood, meaning that unprecedented extreme heat intensities will not only become possible but much more likely unless CO_2 emissions are promptly reduced.

Path dependence at global warming levels

While multiple studies have previously characterised European extreme heat intensities at a transient global warming level (GWL), we can use this long-term framework to test whether those results would be applicable centuries after net-zero emissions. We use a similar GWL definition as King et al., 2024, where a difference is made between a transient, an early stable, and a late stable climate at 1.5, 2, and 3°C. The results of this approach clearly highlight that the transient extreme heat distributions are always at larger values than the stabilised ones (Figure 11). This difference between transient and stable becomes larger at higher GWLs. When comparing the two stable distributions, analysing a low GWL (1.5 and 2°C) at an early stable period might already be a good estimate of the late-stable distribution.

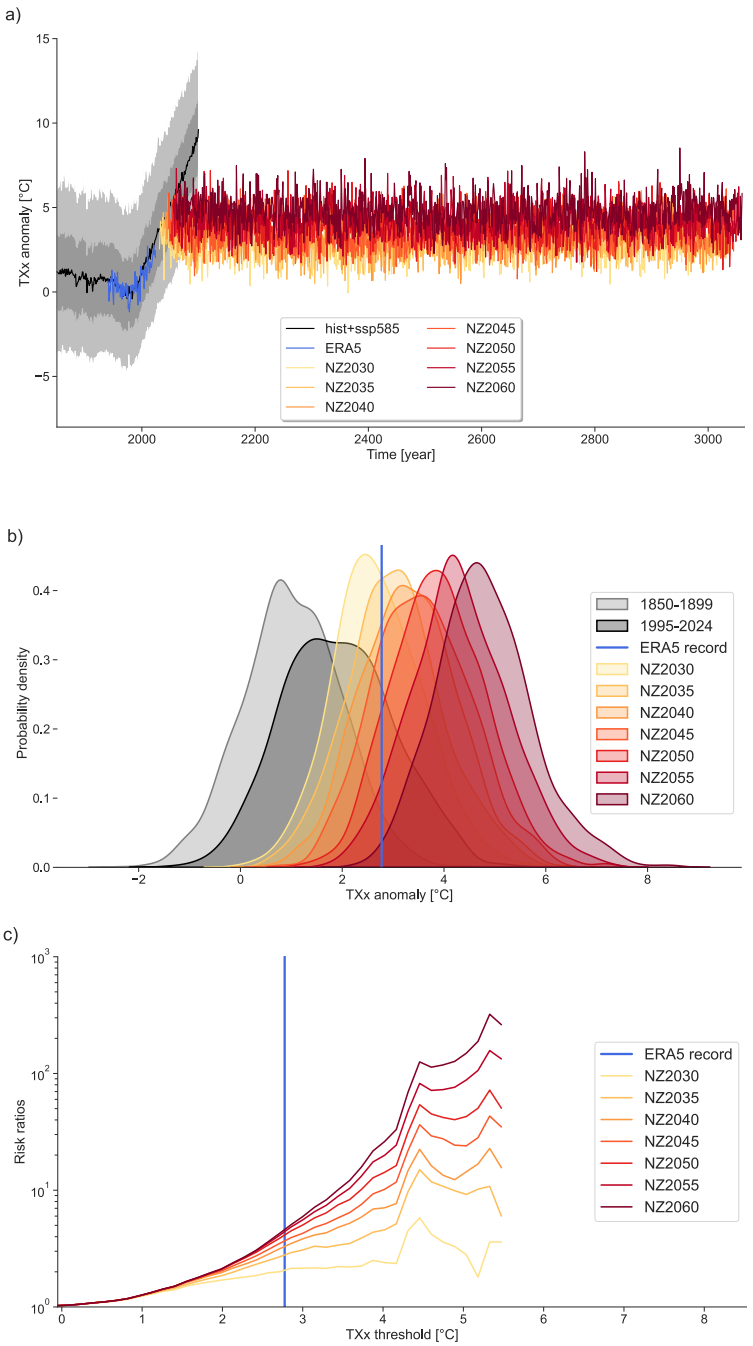

Figure 10: Characterisation of European TXx likelihoods in 1000-year ACCESS-ESM-1.5 net-zero experiments. a) Time series. b) Probability distribution functions. c) Risk ratios.

However, this similarity breaks down at higher GWLs, emphasising that an early evaluation could lead to an overestimation of future intensities. In general, this global warming level analysis shows that these distributions are path-dependent, showcasing even more the value of long-term net-zero studies and experiments.

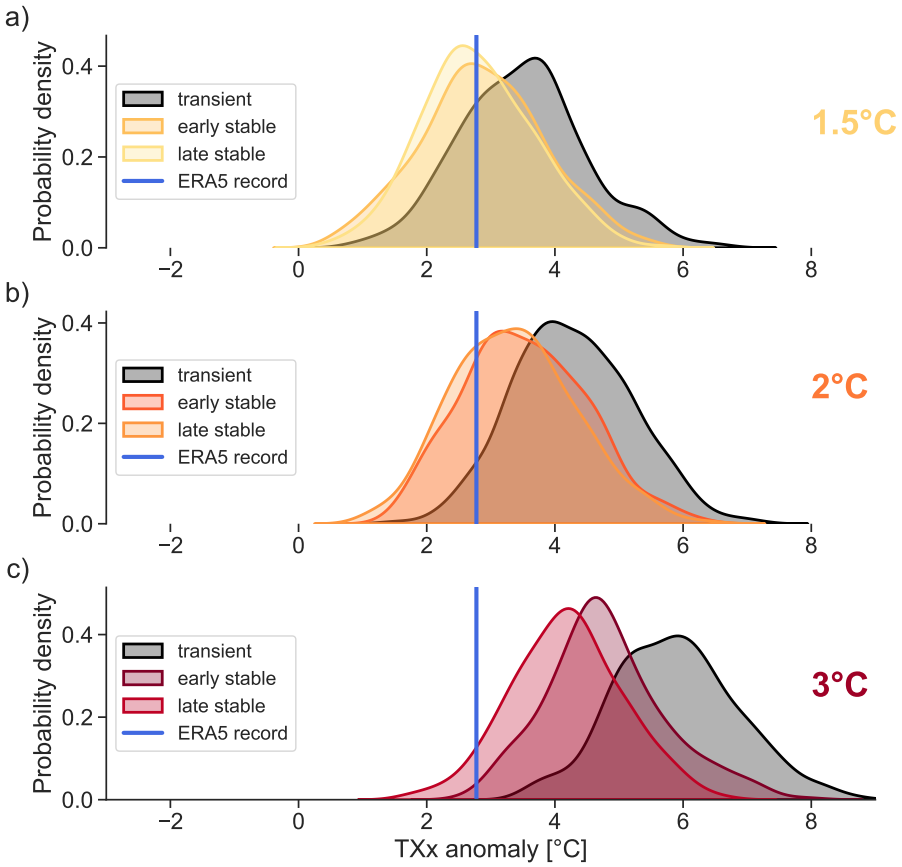

Figure 11: Probability distribution functions of European mean annual TXx anomalies at global warming levels of a) 1.5°C, b) 2°C, and c) 3°C in ACCESS-ESM-1.5 net-zero simulations.

Discussion

We find stationary intensities of European heat extremes for centuries, even under net-zero emissions, as well as significant effects from short delays in emissions cessation, and differences between transient and stabilised climates, even at the same level of global warming. Even though analysing the role of physical mechanisms is not an explicit part of the study, research suggests that the recovering AMOC trend (Figure 2) plays a crucial role in setting Northern Hemispheric temperatures throughout the simulations. MacDougall et al., 2022 show that the multi-model short-term temperature response to net zero is highly variable over the Arctic and North Atlantic, partly determined by the different AMOC responses. If the AMOC recovers at different speeds or to different levels, the impact on surface temperatures (and thus heat extremes) in Europe could differ (e.g. Sigmond et al., 2020). The temperature impact of a recovering AMOC under net-zero emissions is further controlled by mechanisms such as heat fluxes and cloud dynamics (Schwinger et al., 2022a) or even determined by salinity differences preceding emissions cessation (Lee et al., 2025). All these variables possibly introduce more sources of multi-model uncertainty. Since the setup of long-term net-zero sim-

ulations used here only exists with one Earth system model, more models are needed to understand the impact that different AMOC strengths or other model differences could have on post-net-zero responses over Europe. Regardless, we provide with this study a first in-depth characterisation of heat extremes under net-zero emissions on long-term timescales, hoping to establish the foundation for future extreme event studies.

5 CONCLUSIONS AND OUTLOOK

5.1 ANSWERING THE RESEARCH QUESTIONS

I have argued for three research questions on the surface temperature impacts of different combinations of AMOC and atmospheric CO_2 changes. I here summarise the main conclusions of the studies addressing these individual research gaps.

Q1: What is the past AMOC interannual variability influence on European extreme cold temperatures?

The first research question is framed in the context of past to present-day CO_2 increases and AMOC variability. The primary conclusions we reach in Article A are:

- **Interannual AMOC variations have the potential to change the distribution of winter cold extremes in Europe**. This change, in a preindustrial climate, occurs mainly as a distribution shift of about 1°C over Scandinavia, Northern and Eastern Europe.
- **The shifts can be understood from changes in Atlantic winter physical mechanisms at the ocean-atmosphere interface and circulation regimes**. For instance, strong interannual AMOC variations lead to warmer sea surface temperatures over the subpolar gyre and Arctic regions along the sea ice edge. Reduced sea ice concentrations follow, increasing heat fluxes to the atmosphere, eventually resulting in more atmospheric anti-blocking regimes that oppose the occurrence of cold extremes.
- **There is a contrast with the present-day climate, where the distribution shift is largely reduced**. The period contrast in mechanisms originates mainly over the sea ice edge region, where AMOC variations no longer lead to shifts. We hypothesise that a retreated sea ice state with climate change prevents AMOC variations from influencing the sea ice edge, reducing the influence on the atmosphere and Europe.

Q2: What is the projected economic effect of the AMOC carbon feedback?

This second research question focuses on a weakening AMOC and projected CO_2 increases until the end of the century. The main conclusions of Article B are the following:

- **There is a robust linear relationship between AMOC weakening and reduced ocean carbon uptake**. For every Sverdrup of AMOC weakening, each year approximately 0.025 PgC less go into the ocean. This relationship is governed by the AMOC strength, implying that it can be used to project the size of the effect along different scenarios of CO_2 emissions and AMOC strengths.
- **By the end of the century, and in an intermediate warming scenario, between half and a full year of present-day CO_2 emissions would stay in the atmosphere due to a weakened AMOC**. These cumulative reductions in ocean carbon storage result from multi-model AMOC projections, where the AMOC weakens between 20 and 50 % by 2100.
- **The additional atmospheric CO_2 would enhance surface warming and lead to additional economic damages of around 1%**. The social cost of carbon effect is of a similar magnitude but opposite sign to the direct cooling effect, and larger in low-emissions scenarios. Thus, the consideration of a single impact channel could be enough to reverse the economic impact of AMOC weakening into a net cost to society.

Q3: What is the long-term evolution of European heat extremes under net-zero emissions?

The third question is posed in the context of a recovering AMOC in long-term net-zero emissions futures. I answer this question in Article C, concluding that:

- **European heat extreme intensity and frequency might stay elevated for centuries after net-zero emissions**. While the AMOC slowly recovers and global mean temperature gradually increases, extremes over all European regions show no trend but have large year-to-year variability.
- **Short delays in emissions cessation result in significant shifts towards more intense extreme heat distributions**. These shifts also apply to all individual European regions and are most pronounced over the Mediterranean region.

- **Compared to today's heat records, delaying emissions cessation will result in substantial intensity increases**. For the European mean, heat intensities will increase two- to five-fold. The Mediterranean will experience the largest differences, reaching up to 30-fold increases if emissions cessation is postponed until 2060.
- **Comparing extreme heat distributions at global warming levels shows path dependence, with different distributions between transient and stabilised climates**. At warmer levels (i.e. 3°C), these differences are larger, with discrepancies even between early and late stable distributions.

5.2 OUTLOOK

Individual outlook of each study

The three articles of this thesis provide a tentative but conclusive answer to the associated research questions. In addition, each study's significance will reside in its capacity to encourage further related research. For instance, Article A highlights the role of variability in impacting extremes, inciting other studies to repeat the same analysis with other models and types of extreme events. Article B is an innovative example of how to combine experiments from different disciplines (AMOC and carbon cycle feedbacks) and how to coordinate these results with economic modelling, hopefully stimulating novel approaches that incorporate more impact channels of AMOC into socioeconomic assessments. Article C asserts the value of swiftly reducing CO_2 emissions, motivating more analyses considering AMOC and extreme events in plausible high-mitigation short- and long-term scenarios.

Future modelling, observational, and theoretical efforts

Evidently, all parts of this thesis heavily rely on modelling. Modelling the AMOC is here an essential strategy, and ample effort has to be devoted to improving such modelling tools. Progress should be directed at increasing the process representation, as well as improving the computational capabilities towards better resolved models and with the capacity to perform multiple experiments (Jackson et al., 2023b). Still, this strategy must come alongside a push for a better theoretical and observational understanding of the AMOC. As direct AMOC observational products extend further in time, robust analyses of its changes and impact will become possible (e.g. Frajka-Williams et al., 2023). Many of these discoveries can only be attainable when supported by solid theoretical frameworks and conceptual models (Johnson et al., 2019), which have been and will continue to be essential for foundational work on the AMOC.

5.3 OVERARCHING QUESTION

While the three research questions conform to a clear temporal framework, addressing past, future, and long-term CO_2 and AMOC changes, they also tackle rather distinct surface temperature impacts. For that reason, I previously raised an overarching question encompassing all three studies:

What is the added value of jointly considering diverse and multi-temporal CO_2 and AMOC changes to assess surface temperature impacts?

At first glance, the different impacts addressed here seem difficult to combine. They affect diverse timescales (years, decades and centuries), temporal resolutions (averages to extremes), seasons (both summer heat and winter cold extremes) or even regions of influence (European to global temperatures). Thus, I argue that the value of integrating these timescales is not in the specific way the three impacts combine to form a singular response, but rather in the cross-temporal and context-dependent framework of AMOC impacts they support.

These three papers highlight the importance of accounting for CO_2 changes when assessing AMOC impacts. Notably, prominent impact studies often consider AMOC weakening in isolation within a preindustrial climate background (e.g. Jackson et al., 2015; Orihuela-Pinto et al., 2022; van Westen et al., 2024b). This approach is present even though the AMOC's (and its impacts') dependence on the CO_2 state and pathway has been clearly identified (e.g. Bellomo et al., 2021; Bellomo & Mehling, 2024; Hankel, 2025). In that spirit, the first study of this thesis already demonstrates how this consideration is key even for past internal variability effects, with changing temperature impacts as the climate background state evolves. The second and third studies also show that different future scenarios and mitigation pathways yield substantially different results, even when AMOC strengths are comparable. Therefore, while the broad conclusions on the value of the climate background for different AMOC impacts are not new, there has not been to date a unified frame of reference bringing these impacts together across timescales.

Furthermore, combining these different AMOC impact studies with changing CO_2 concentrations across timescales adds value for climate mitigation and adaptation strategies. Scattered knowledge and deep uncertainties on AMOC changes are often used as a justification for inaction among policymakers. For instance, when the United Kingdom Government recently admitted in a written answer to Parliament that it "has not assessed the effect of any slowing or collapse of the Atlantic Meridional Overturning Circulation (AMOC) on economic planning" (UK Parliament, 2024). This disregard sim-

ilarly motivated an open letter to the Nordic Council of Ministers by more than forty climate scientists, warning about the risks of AMOC changes ("Open Letter by Climate Scientists to the Nordic Council of Ministers," 2024). The many remaining questions around the AMOC's past and future evolution justify a deep-uncertainty decision-making approach. In such an approach, the focus is not on finding the most likely future scenario, but instead on considering and assessing a broader set of responses (e.g. Gu et al., 2024; Lee et al., 2025), while creating a more robust set of solutions and monitoring strategies (Biesbroek et al., 2025). My main contribution with this thesis is to highlight that adopting such a deep uncertainty framework is imperative, and that AMOC and CO_2 changes from multiple timescales must be considered jointly.

Part II

ARTICLES

A

CHANGING PAST INFLUENCE OF INTERANNUAL AMOC VARIABILITY ON EUROPEAN COLD EXTREMES

The work in this chapter is to be submitted for publication on *Geophysical Research Letters* as:

Alastrué de Asenjo, E., Borchert, L. F., Sillmann, J., & Baehr, J. (in preparation). Changing past influence of interannual AMOC variability on European cold extremes.

Contributions: Together with J. Baehr and J. Sillmann, I conceptualised the study. I curated the data, implemented the software, performed the analysis and investigation, visualised the results, and wrote the original draft. All authors participated in discussing the methodology and results, and in revising the final manuscript.

Changing past influence of interannual AMOC variability on European cold extremes

Eduardo Alastrué de Asenjo[1,2], Leonard Borchert[1], Jana Sillmann[1,3], Johanna Baehr [1]

[1] Center for Earth System Research and Sustainability (CEN), University of Hamburg, Hamburg, Germany.
[2] International Max Planck Research School on Earth System Modelling, Max Planck Institute for Meteorology, Hamburg, Germany.
[3] Center for International Climate and Environmental Research (CICERO), Oslo, Norway.

ABSTRACT
Beyond a potential future weakening or collapse, the Atlantic Meridional Overturning Circulation (AMOC) exhibits interannual variability, but whether this variability influences European winter cold extremes remains unknown. We quantify this influence and mediating mechanisms using a large ensemble of historical simulations. In the early historical period, weaker interannual AMOC strengths are associated with colder European extreme temperatures. This distribution shift is linked to colder sea surface temperatures, increased Arctic sea ice concentrations, and reduced ocean-atmosphere heat transport, favouring atmospheric blocking regimes. In the late historical period, extreme temperature distributions barely shift when conditioned on interannual AMOC variations. We hypothesise this period contrast arises from a retreated background Arctic sea-ice state, ultimately leading to no evident shift in pressure regimes. Altogether, we show that short and unforced AMOC variability can influence European extreme temperatures, while highlighting the role of forced climate change in mediating this impact.

PLAIN LANGUAGE SUMMARY
The Atlantic Meridional Overturning Circulation (AMOC) is a major ocean current system regulating heat transport in the climate system. While most studies focus on its potential future collapse and associated impacts, scientists still debate whether it is currently in decline. However, the AMOC also varies on short timescales, but how these year-to-year changes affect the surface climate is not well known, particularly for extreme events. We quantify the influence of interannual AMOC variations on European cold extremes using a large number

of model simulations of Earth's past. We find that, while AMOC variations shift the distributions of European extreme cold events in a preindustrial climate, this influence has disappeared in recent decades. We trace the preindustrial shift and its absence in the recent past by analysing mediating physical mechanisms, such as Arctic sea ice, sea surface temperatures, ocean-atmosphere heat transports, and winter pressure regimes. Overall, we show how natural AMOC variations can lead to changes in European cold extremes and highlight that this internal influence depends on the changing background climate.

A.1 INTRODUCTION

The Atlantic Meridional Overturning Circulation (AMOC), a crucial system of ocean currents redistributing heat northward (e.g. Mecking & Drijfhout, 2023), is often linked to its potential impact on surface temperatures (e.g. Liu et al., 2017; Chen & Tung, 2018; van Westen et al., 2024b). Previous studies investigate these impacts in the context of a potential future large AMOC weakening, typically using idealised modelling experiments (such as freshwater hosing, Stouffer et al., 2006; Jackson et al., 2023a). For such long-term AMOC weakening that reduces poleward oceanic heat transport, a mean cooling was found over Europe, being strongest for winter (Jackson et al., 2015; Bellomo et al., 2023; Ma et al., 2024). Only recently have studies also investigated the potential impact of a large AMOC weakening on winter extreme cold temperatures, for instance, over North America (Yin & Zhao, 2021) or Europe (Meccia et al., 2024; van Westen & Baatsen, 2025). Yet, impacts from other timescales of AMOC variability have not been so thoroughly investigated, even though the AMOC exhibits variability across a wide range of timescales (e.g. McCarthy et al., 2012; Buckley & Marshall, 2016). Among these, interannual variability is notably relevant for European winter weather, coinciding with some major atmospheric modes of variability such as the North Atlantic Oscillation (NAO). Despite this relevance, the effect of short-term AMOC variability on European temperatures has only been previously investigated for annual mean temperatures (with idealised simulations in coupled atmosphere–ocean models, Pohlmann et al., 2006), remaining an open research question for extreme events such as winter cold extremes.

Beyond quantifying this relationship, the physical mechanisms linking European cold extremes with interannual AMOC variability remain unclear. Sea surface temperatures (e.g. Tandon & Kushner, 2015; Borchert et al., 2018) and sea level pressures and regimes (e.g. Frankignoul et al., 2013; Bryden et al., 2014) are plausible hypothesised surface changes with AMOC variations, although the explicit link to extremes has not been made for AMOC interannual variabil-

ity. For a long-term large AMOC weakening, European cold extremes get colder due to an overall colder North Atlantic, but also less frequent as an advanced sea ice edge and an intensified meridional temperature gradient strengthen the jet stream and reduce atmospheric blocking (Meccia et al., 2024; van Westen & Baatsen, 2025). However, as short-term AMOC variability might produce smaller and spatially dissimilar mean temperature shifts, it is uncertain whether mechanisms play the same role. Therefore, we examine the corresponding differences in mediating oceanic and atmospheric variables, with a particular focus on winter pressure regimes, to identify the physical mechanisms linking interannual AMOC variability and European cold extremes.

A.2 DATA AND METHODS

MPI-GE CMIP6

We probabilistically quantify the past and present-day influence of interannual AMOC variability on European winter cold extreme events. A robust statistical representation of variability and extremes requires many occurrences, which observations cannot provide due to the rarity of extremes and the short 20-year period of AMOC direct observations (by the RAPID project, Moat et al., 2025). Instead, we employ a large ensemble of Earth system model simulations (with identical model and physics but different initial conditions), specifically the Max Planck Institute Grand Ensemble in its latest version, the MPI-GE CMIP6 (Eyring et al., 2016; Olonscheck et al., 2023). MPI-GE CMIP6 uses the low-resolution version of MPI-ESM1.2 (Mauritsen et al., 2019), with 1.8° resolution and 47 hybrid sigma-pressure levels in the atmosphere, and 1.5° and 40 vertical levels in the ocean. To study past and present variability, we analyse the 50-member historical ensemble (1850-2014) and compare early (1850-1879, quasi-preindustrial) and late (1985-2014, present-day) 30-year periods. For the overlap with the RAPID observational period, the model AMOC strength is within the observational range (Jungclaus et al., 2013), and MPI-ESM1.2-LR performs notably well in correlations and mean bias against other CMIP6 models (Alastrué de Asenjo et al., in preparation). We detrend all variables separately for each ensemble member, removing the ensemble mean trend for each respective period (e.g. Frankcombe et al., 2018).

Interannual AMOC variations

We characterise AMOC states using a widely adopted metric: the AMOC strength (meridional streamfunction maximum for all depths) at 26.5°N latitude (e.g. Frajka-Williams et al., 2019). The interannual

AMOC is defined using a 3-year centred moving average. This 3-year window captures interannual variability while avoiding annual aliasing caused by irregular seasonal cycles and preserving variability that longer averaging windows would smooth out.

The method to analyse the AMOC variability effects on European cold extreme temperatures and mediating variables is inspired by Pohlmann et al., 2006, i.e. conditioning variables on concurrent anomalously weak or strong AMOC variations. To establish temporal precedence, we analyse other variables in the final year of each 3-year window. This approach ensures that AMOC variations temporally lead the examined climate responses, while we acknowledge that complex feedbacks between components and timescales (e.g. between AMOC and Arctic sea ice, Liu & Fedorov, 2022) prevent definitive causal attribution with our methodology. We calculate composite maps and probability distribution functions (PDFs) following weak and strong AMOC years, defined as negative and positive variations exceeding one reference standard deviation (σ, 0.90 Sv) from a 1000-year preindustrial control simulation. Different thresholds characterising weak/strong AMOC variations do not qualitatively alter the relationship with European temperatures (Figure A.S1), and the one-sigma threshold balances a large enough signal with sufficient sample size. The detrended PDFs for 3-year AMOC variations are nearly symmetric for both the early and the late period, enabling unbiased comparisons between periods (Figure A.S2).

European cold extremes

We define cold extremes using daily-mean 2-meter air temperatures over European land areas (all four IPCC AR6 European reference regions, Iturbide et al., 2020). For each grid cell and each ensemble member, we compute the 1st percentile of all daily temperatures. While the definition of cold extremes influences the obtained results, our findings are not particularly sensitive to small variations in the chosen percentile. We employ a simpler extreme definition that captures both intensity and frequency changes, although standardised cold extreme indices (i.e. TNn or TN10p, Sillmann et al., 2013) are more common. We categorise each extreme cold temperature based on its preceding anomalous 3-year AMOC variation and analyse the events' extreme value distributions separately, disaggregating the changes in each distribution parameter (location, scale, and shape).

Physical mechanisms

We examine mediating mechanisms by comparing winter distributions of relevant variables during weak and strong interannual AMOC years. These mechanisms include winter oceanic surface vari-

ables linked to AMOC changes, such as sea surface temperatures, ocean-atmosphere heat fluxes, and Arctic sea ice concentrations (e.g. Frankignoul et al., 2013; Tandon & Kushner, 2015; Liu & Fedorov, 2022). We also thoroughly inspect winter sea level pressures (extending as well over land), as these directly determine the atmospheric systems that favour the occurrence of cold extremes (e.g. Straus et al., 2016; Riebold et al., 2023). For sea level pressures, we identify winter Euro-Atlantic circulation regimes using Empirical Orthogonal Function (EOF) analysis, computed over the region 20-90°N latitude and 80°E-40°W longitude using the algebraic method of singular value decomposition. Considering the three dominant modes of variability, we construct phase space diagrams to examine the distribution of pairwise mode combinations.

A.3 RESULTS

Cold extremes

The distributions of European-averaged extreme cold temperatures (detrended anomalies) during interannual weak or strong AMOC years exhibit a notable contrast between both examined periods (Figure A1). In the early period (1850-1879), the distribution of extreme cold temperatures is colder following weak interannual AMOC compared to strong AMOC years (Figure A1, top left). A shift in the same direction, with colder temperatures following weak AMOC, occurs for annual mean temperatures (roughly 0.5°C, Figure A.S3), but the magnitude is larger for extreme distributions, reaching approximately 1°C. In the late period, the distributions of cold extremes (and also mean annual temperatures) show only a minor shift between weak and strong interannual AMOC years (Figure A1, top right).

To find the disaggregated contributions to these spatially averaged results, we repeat the same comparison of extreme cold distributions during weak and strong AMOC at the grid point level. For each location, we separately compute the difference (weak minus strong AMOC years) for each extreme value distribution parameter (Figure A1, bottom three rows): location (distribution position), scale (distribution spread), and shape (distribution tail behaviour). In the early period, the location parameter shifts in the same direction as the European mean for virtually all grid points, with colder extremes for weak AMOC variations. These cold shifts are largest (around 1°C) over Scandinavia and parts of northeastern Europe, and also occur for mean temperatures (Figure A.S3). The scale parameter also shows some spatially coherent and significant shifts of the opposite sign (warmer extremes for weak AMOC), but of smaller magnitude and without a clear spatial pattern. The shape parameter differences are small and exhibit no clear pattern resembling noise. In the late period,

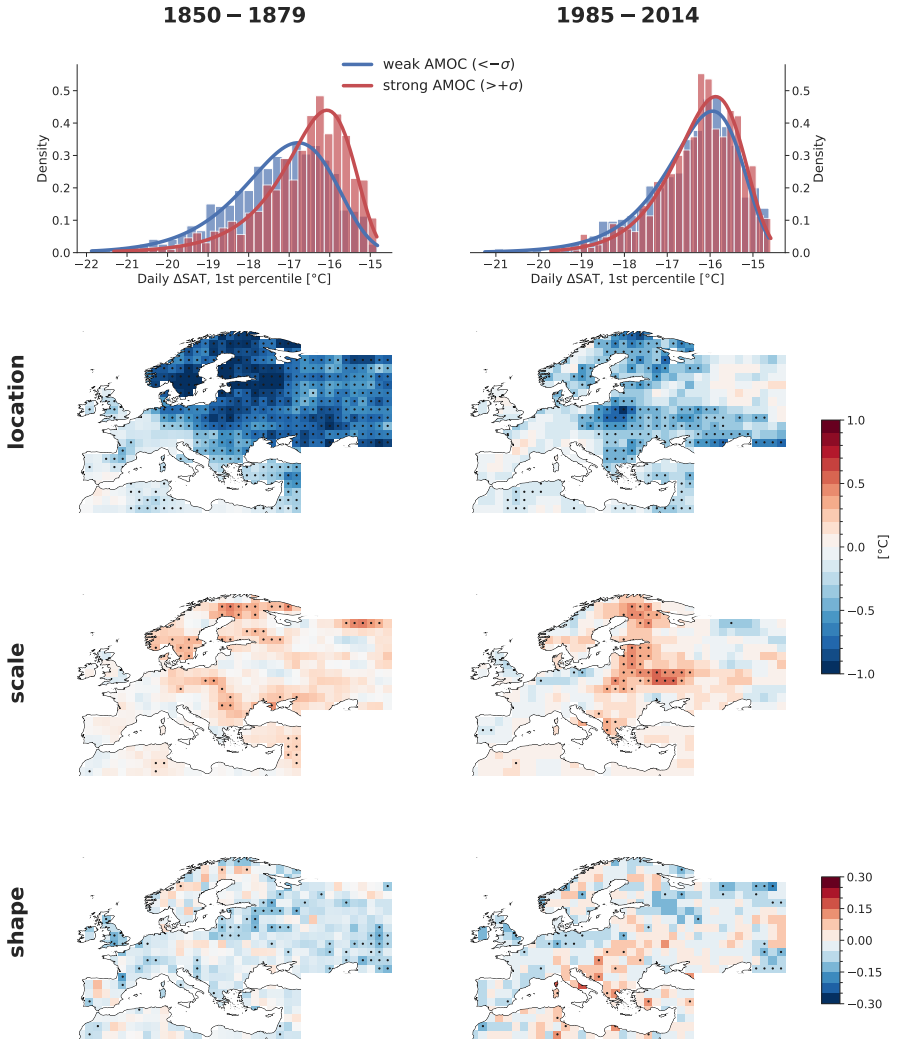

Figure A1: Daily extreme cold (1st percentile) surface air temperatures for the detrended early (1850-1879, left), and late (1985-2014, right) historical periods in MPI-GE CMIP6, conditioned on interannual AMOC variations. Top row: Histograms and extreme value distributions of European mean cold extreme temperatures during weak (blue, below -1σ) and strong (red, above 1σ) 3-year AMOC variations. Bottom three rows: Difference in distribution parameters (location, scale, and shape) of cold extreme temperatures between weak and strong AMOC years, per grid cell. Dots indicate significance at the 99% level.

the location parameter shows smaller differences between weak and strong years for most locations, with only a slight cold shift following weak AMOC in some regions of central Europe. The scale parameter increases in magnitude for weak AMOC, as in the early period, but is now more clustered and significant over central Europe. The shape parameter again exhibits a noisy pattern, suggesting that the type of distribution tail is not substantially affected by the preceding interannual AMOC variation. In summary, cold extreme distributions show

location parameter shifts in the early period but minimal shifts in the late period, prompting further investigation into the source of these contrasting differences.

Ocean surface mechanisms

North Atlantic winter ocean surface properties (temperatures, heat fluxes, and sea ice) differ between weak and strong interannual AMOC years, with contrasting differences between early and late periods (Figure A2).

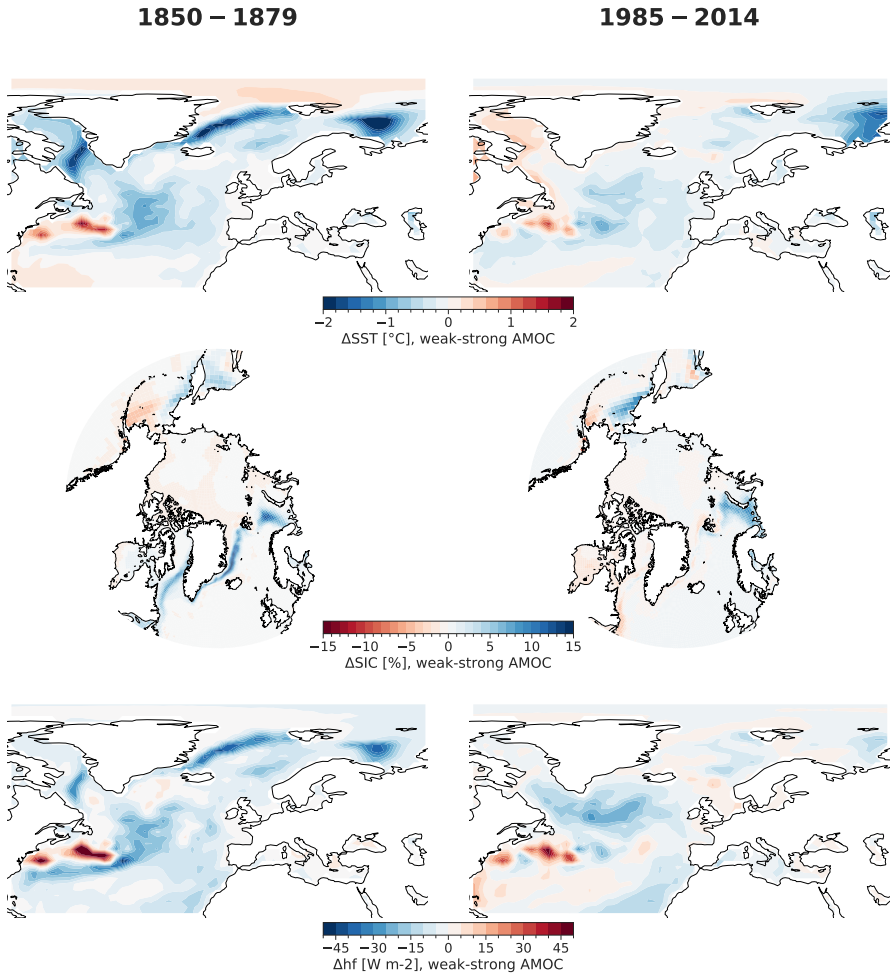

Figure A2: Differences in sea surface temperatures (SSTs, top row), sea ice concentrations (SIC, middle row), and heat fluxes (bottom row, positive upwards) for weak (below -1σ) minus strong (above 1σ) 3-year AMOC variations in MPI-GE CMIP6. Left: 1850-1879; right: 1985-2014.

Sea surface temperatures (SSTs, Figure A2, top row) are generally slightly colder following a weak AMOC in both periods. In the early period, weak AMOC leads to notably colder SSTs in the Labrador, Nordic, and Barents Seas, seemingly along the winter sea ice edge.

At lower latitudes, weak AMOC also leads to a pattern of cooling in the subpolar gyre and warming along the Gulf Stream extension. This pattern roughly matches the dipole observed for longer-term AMOC weakening (e.g. Caesar et al., 2018) and sustained in interannual timescales for anomalous meridional ocean heat transport anomalies in the North Atlantic (Borchert et al., 2018). In the late period, the SST differences at the sea ice edge largely disappear (except in the Barents Sea, where they dissipate and shift eastward) and the subpolar gyre pattern persists, albeit diffused and reduced in magnitude.

Consistent with SST patterns, winter sea ice plays a key role in determining the high-latitude contrast between the two periods, with similar patterns found for sea ice concentrations (Figure A2, middle row). In the early period, weak interannual AMOC years increase sea ice concentrations where SSTs cool along the sea ice edge compared to strong AMOC years. In the late period, this increase is virtually absent in the Labrador and Nordic Seas, and more spatially dispersed in the Barents Sea. We hypothesise that this contrast between periods originates from the different background sea ice states. In the late period, Arctic winter sea-ice area declined by 1.5-2 million km^2 compared to the early period, possibly decoupling the dynamic and thermodynamic processes through which interannual AMOC variations interact with the sea ice edge. Although an in-depth analysis of sea ice changes and related processes would be needed to understand how this decoupling occurs, previous studies already indicate a changing relationship between AMOC variability and its effect on sea ice (e.g. Liu & Fedorov, 2022).

The differences in winter SSTs and sea ice concentrations combine to produce consistent changes in ocean-atmosphere heat exchange (Figure A2, bottom row). In the early period, regions with increased sea ice extent (and colder SSTs) following a weak interannual AMOC show a decreased heat flux into the atmosphere. This decreased heat flux stems from reductions in both sensible and latent heat fluxes (Figure A.S4). Reduced latent heat flux also occurs in the subpolar gyre region that cools during weak AMOC, and increased latent heat flux accompanies warming along the Gulf Stream path. In the late period, these heat flux differences are absent over sea ice edge regions and reduced in the subpolar gyre.

Ultimately, these anomalous heat fluxes influence weather patterns by affecting sea level pressure systems. For instance, reduced heat flux to the atmosphere decreases vertical motion in the lower troposphere, opposing low-pressure system development and altering the prevalent pressure regime. However, since different regime types respond differently to pressure anomaly location, we must analyse surface pressures to understand the specific effects on predominant winter regimes.

Euro-Atlantic winter circulation regimes

Empirical Orthogonal Function (EOF) analysis reveals that the three leading winter patterns are consistent across both periods (Figure A.S5). The leading mode corresponds to the North Atlantic Oscillation (NAO) pattern, explaining approximately 40% of the variance. The second and third modes are the Atlantic Ridge (AR) and the Scandinavian Blocking (BLO), explaining 18% and 12% of the variance, respectively. Specific phases of these patterns promote atmospheric blocking and potentially transport cold air over large parts of Europe (e.g. Sillmann et al., 2011; Brunner et al., 2018): negative NAO (decreased pressure gradient between the Azores High and Icelandic Low), positive AR (high-pressure system over the central North Atlantic), and positive BLO (persistent high pressures over Scandinavia). Therefore, understanding how these regimes depend on interannual AMOC states provides direct insights into cold extreme changes.

We analyse how winter regime distributions in two-dimensional phase space change with interannual AMOC variations. The NAO|AR phase space (two leading modes) exhibits substantial shifts when conditioned on AMOC variations (Figure A3). During the early period, the distribution of all years is radially symmetric. Weak AMOC slightly shifts the distribution towards NAO-, while strong AMOC shifts it towards NAO+/AR-. In the late period, weak AMOC produces only a slight shift towards AR+, and for strong AMOC, it remains centred with increased spread in the AR+ direction. Therefore, while the early period shows very distinct distributions, particularly favouring NAO- (NAO+) for weak (strong) AMOC, the late period shows similar distributions for both AMOC variations. The NAO|BLO phase space shifts, in the early period, towards more likely NAO-/BLO- for weak AMOC and NAO+/BLO- for strong AMOC (Figure A.S6). In the late period, weak AMOC still favours NAO- (but not BLO-), while strong AMOC favours BLO- (but not NAO+). Overall, winter regime distributions support the prevalence of atmospheric anticyclonic (cyclonic) regimes for weak (strong) AMOC in the early but not the late period, which experiences a reduced shift towards NAO+ during strong AMOC.

Having established changes in mechanisms and winter regimes, we now test whether winter regimes affect cold extremes as hypothesised. We calculate composites of European cold extremes for each quadrant of the two-dimensional phase space, defined by positive or negative phases of the winter regimes. For all years, regardless of AMOC state, effects on cold extremes are primarily controlled by the NAO phase (Figures A4, A.S7, top row). In both periods, winters dominated by NAO- exhibit colder extremes across most of Europe (measured by the extreme distribution shift) compared to all winters, while NAO+ winters show less severe cold extremes.

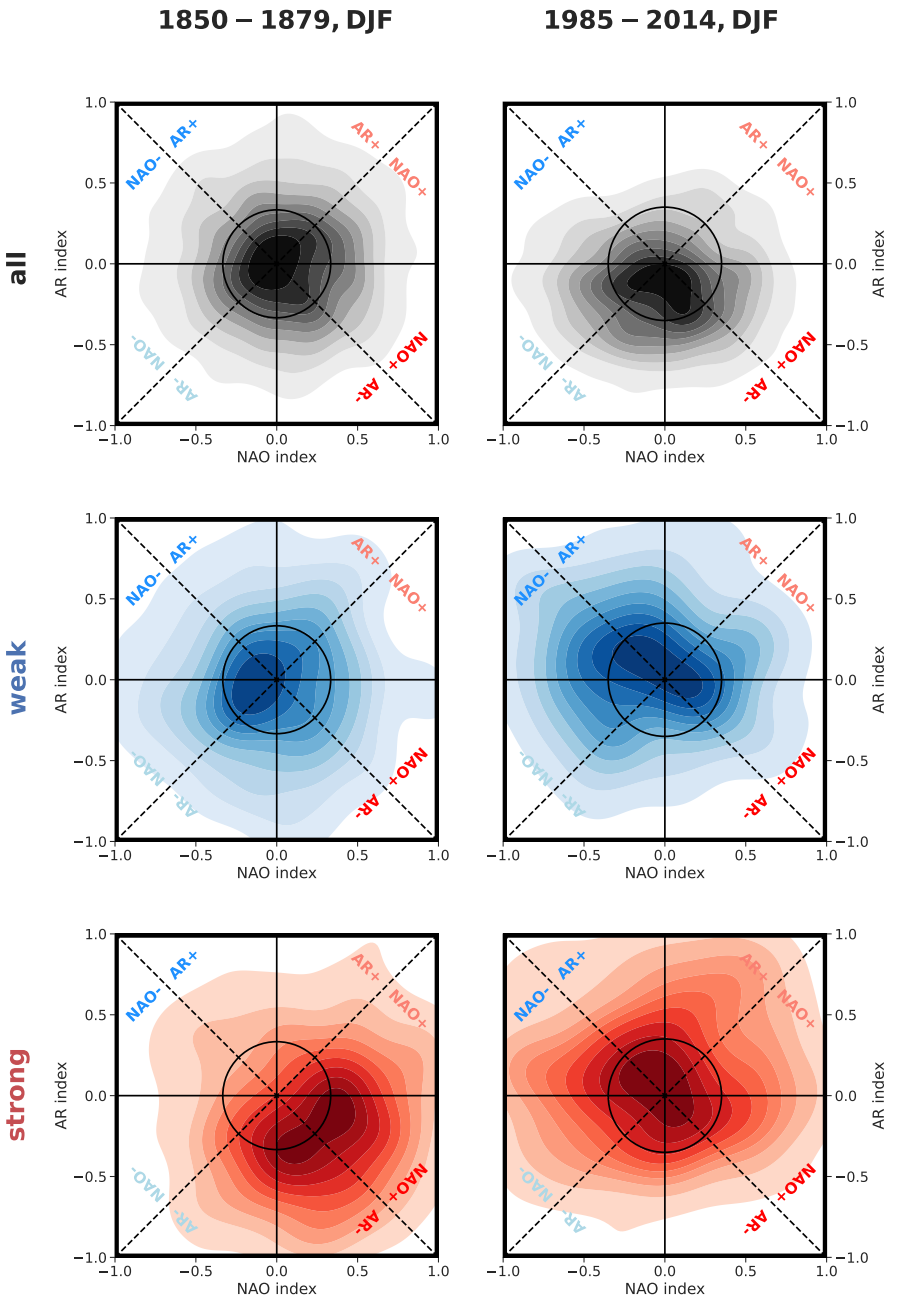

Figure A3: Phase space diagrams of NAO|AR, from winter (DJF) sea level pressures for early (1850-1879, left) and late (1985-2014, right) periods in MPI-GE CMIP6. Rows show distributions for all years (black, first row), years following 3-year weak AMOC (below -1σ, blue, second row), and strong AMOC (above 1σ, red, third row). Circles indicate one standard deviation of the NAO index for all years in each period.

When AR or BLO patterns have the same sign as the NAO, they enhance the spatial extent and intensity of the NAO-induced shift. Crucially, these regime-extremes relationships provide the basis sup-

porting how AMOC-induced shifts in regimes lead to the inspected shifts in extreme cold temperature distributions.

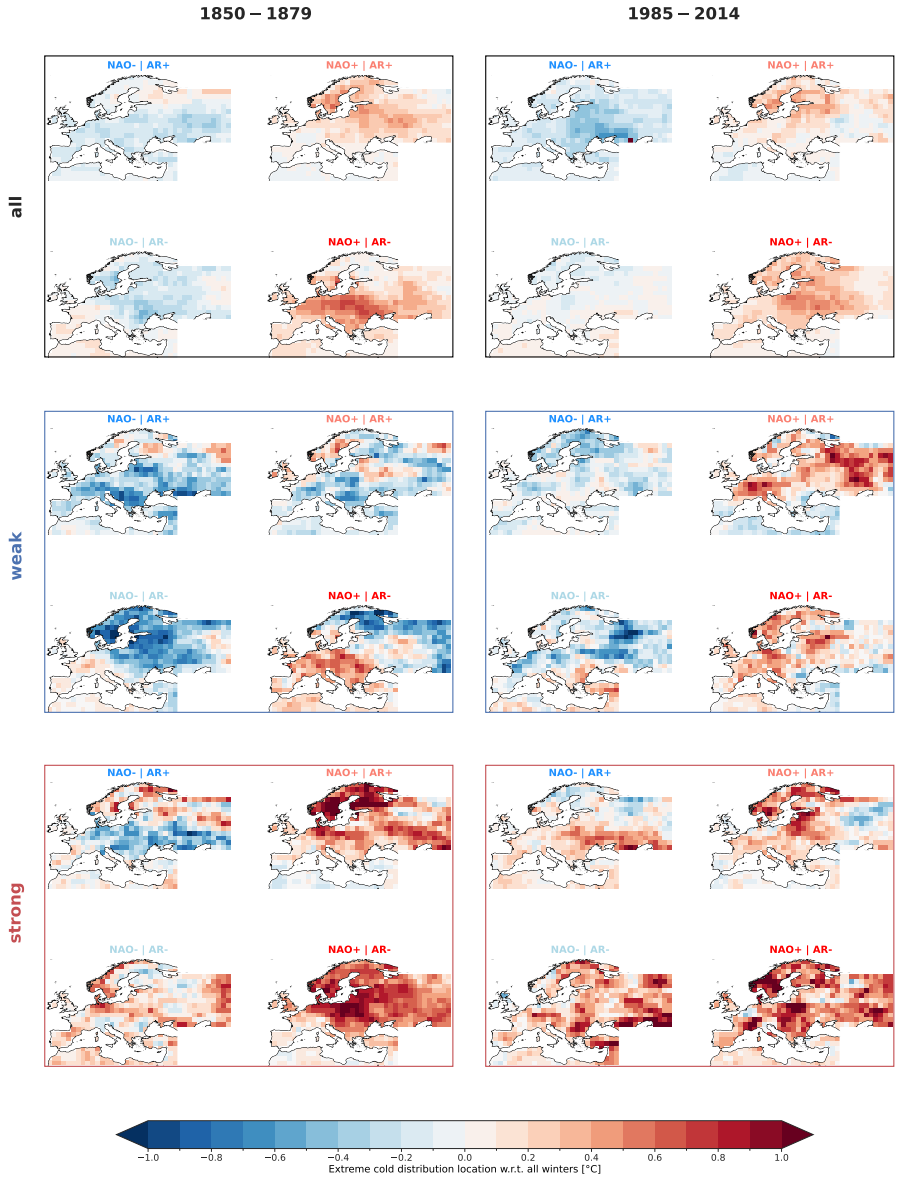

Figure A4: Daily extreme cold (1st percentile) surface air temperatures composites conditioned on that winter (DJF) NAO|AR phase, for the detrended early (1850-1879, left), and late (1985-2014, right) periods in MPI-GE CMIP6. Rows of panels differentiate between all years (black, first row), years in a 3-year weak (below -1σ, blue, second row) or strong (above 1σ, red, third row) AMOC.

While these results support the hypothesised regime-extreme connection, we now test whether AMOC variations further modulate this relationship. The temperature effects of each regime combination are indeed further enhanced during anomalous AMOC (Figures A4, A.S7, bottom rows). The shift is larger in the early period, where weak (strong) AMOC mainly determines if cold extremes will be colder

(warmer). Among pressure regimes, the NAO phase remains dominant for enhancing (and occasionally even reversing) the shifts in extreme cold temperatures. In summary, AMOC variations influence European cold extremes in two ways: by directly altering the likelihood of winter circulation regimes and by modulating the direct temperature impacts of those regimes, with both effects substantially decreasing in the recent past.

A.4 DISCUSSION AND CONCLUSIONS

We found that interannual AMOC variations significantly influence extreme cold temperature distribution across Europe, with this influence diminishing in a warming climate. However, it is difficult to contrast these findings with existing literature, as no previous studies analysed the effects of interannual AMOC variability. Nonetheless, the general pattern of temperature responses to short-term AMOC variations aligns with the results for annual variations reported by Pohlmann et al., 2006. Recent studies examining European cold extremes related to the AMOC have instead focused on the effects of long-term AMOC weakening, broadly agreeing that a weaker AMOC results in colder overall temperatures but reduced atmospheric blocking - findings that contrast with our results. Meccia et al., 2024 and van Westen and Baatsen, 2025 link this decreased blocking to an increased meridional temperature gradient and strengthened jet stream and storm track. Meccia et al., 2024 further link these changes to less persistent cold extremes. For interannual variations, we find no substantial jet stream position or strength changes (Figure A.S8) nor changes in the length of cold spells (Figure A.S9). We hypothesise that this contrasting atmospheric response results from distinct AMOC-induced SST changes between interannual variations and long-term weakening. Following a weak interannual AMOC, there is no widespread meridional temperature gradient increase; instead, changes are localised near the sea ice edge. Thus, while the overall jet stream is less impacted, the likelihood of different low-pressure regimes can change, ultimately leading to the resulting contrast in extreme temperature distributions.

Our study has several limitations that also suggest directions for future research. First, while the general effect of interannual AMOC on cold extremes extends to large parts of Europe, it is not uniform across all regions. A detailed subregional analysis would improve understanding of the link with winter regimes, as the location of atmospheric pressure anomalies differently impacts specific parts of Europe. For such regional analysis, a large ensemble of high-resolution simulations, when computationally feasible, would be ideal for characterising small-scale features that might be insufficiently represented in our low-resolution model. Second, our results are based on a single-

model large ensemble and are therefore susceptible to model biases. This approach, while motivated by the need to analyse many occurrences to characterise extreme events, could be repeated with other existing large ensembles (e.g. Deser et al., 2020) to test for robustness. However, other CMIP6 models may have substantially different AMOC strengths and variability, making inter-model comparisons difficult. Third, the historical simulations analysed here are suitable for capturing the AMOC-extremes relationship under changing external forcings, but are not optimal for separating the AMOC contribution from other interactions and feedbacks. Therefore, we acknowledge that the relationships found here, although at least temporally directional, are not causal and could be confounded by other factors. Experimental designs such as freshwater hosing experiments (Jackson et al., 2023a) or deep-ocean thermohaline nudging simulations (Oelsmann et al., 2020) are typically available only in small ensembles or in preindustrial forcings, but could potentially be more suitable to isolate the AMOC effect on extremes.

A fundamental question arising from our analysis is whether the interannual AMOC influence on cold extremes will continue to change in the future. Our methodology to study interannual variability (e.g. detrending) is likely unsuitable when the AMOC weakens considerably, so we limit our analysis to past and present-day climate where the AMOC has not yet substantially changed. However, increased warming is expected to substantially decrease not only AMOC strength (Weijer et al., 2020) and Arctic sea ice extent (Notz & SIMIP Community, 2020), but also the frequency and intensity of cold extremes (Blackport et al., 2024). Even as the occurrence of these events diminishes, understanding how they are affected by forced climate change and internal variability will be challenging, but it remains fundamental for adapting to their potential impacts. Likewise, a weakening AMOC could also drive changes in other variables or extremes (such as heat extremes, Meccia et al., 2025; Duarte et al., 2025), and our work may serve as a blueprint for determining how internal variability may influence these changes in the future.

Ultimately, we show that even short-term AMOC variations are associated with European extreme cold distribution shifts, but that climate change might have altered this relationship, highlighting how forced climate change can shape the impact of internal variability on extreme events.

OPEN RESEARCH SECTION

All variables from the historical experiment of the MPI-GE CMIP6 can be downloaded from the DKRZ's ESGF server at https://esgf-data.dkrz.de/search/cmip6-dkrz/. The scripts needed to analyse the

data and produce the figures will be made available upon revision on GitHub.

AUTHOR CONTRIBUTIONS

Conceptualisation: E. Alastrué de Asenjo, J. Baehr, J. Sillmann. **Data curation:** E. Alastrué de Asenjo. **Formal analysis:** E. Alastrué de Asenjo. **Investigation:** E. Alastrué de Asenjo. **Methodology:** E. Alastrué de Asenjo, J. Baehr, J. Sillmann, L. Borchert. **Supervision:** J. Baehr, J. Sillmann. **Software:** E. Alastrué de Asenjo. **Visualisation:** E. Alastrué de Asenjo. **Writing - original draft:** E. Alastrué de Asenjo. **Writing - Review & Editing**: E. Alastrué de Asenjo, J. Baehr, J. Sillmann, L. Borchert.

ACKNOWLEDGEMENTS

EAdA, LFB, JS, and JB were funded by the Deutsche Forschungsgemeinschaft (DFG, German Research Foundation) under Germany's Excellence Strategy - EXC 2037 'CLICCS - Climate, Climatic Change, and Society'- Project Number: 390683824, contribution to the Center for Earth System Research and Sustainability (CEN) of Universität Hamburg.

A.5 SUPPORTING INFORMATION

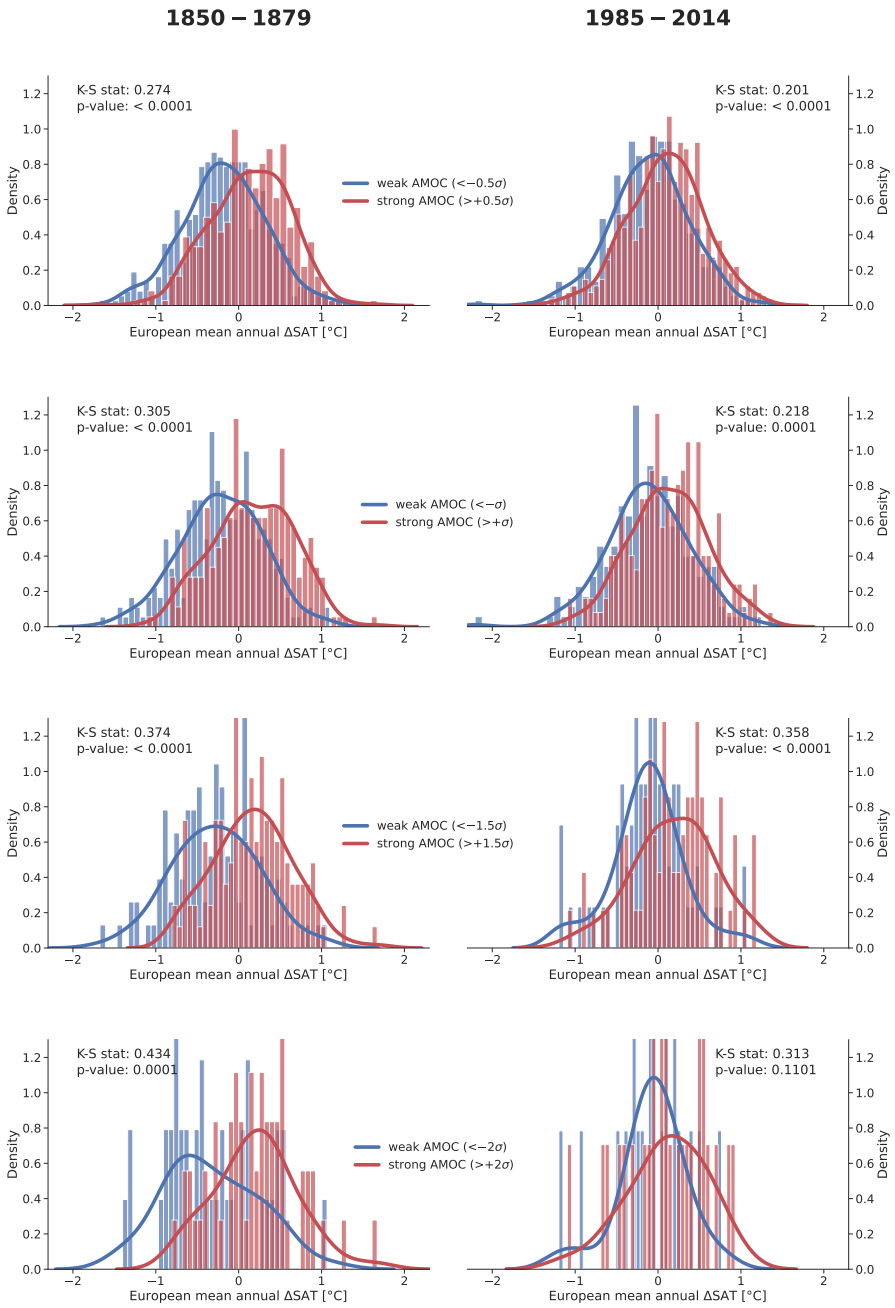

Figure A.S1: Equivalent to top panel in Figure A1, but now each row represents the European mean annual SAT distributions considering a different AMOC threshold for weak/strong variations: ±0.5, ±1, ±1.5, and ±2 σ (preindustrial standard deviations).

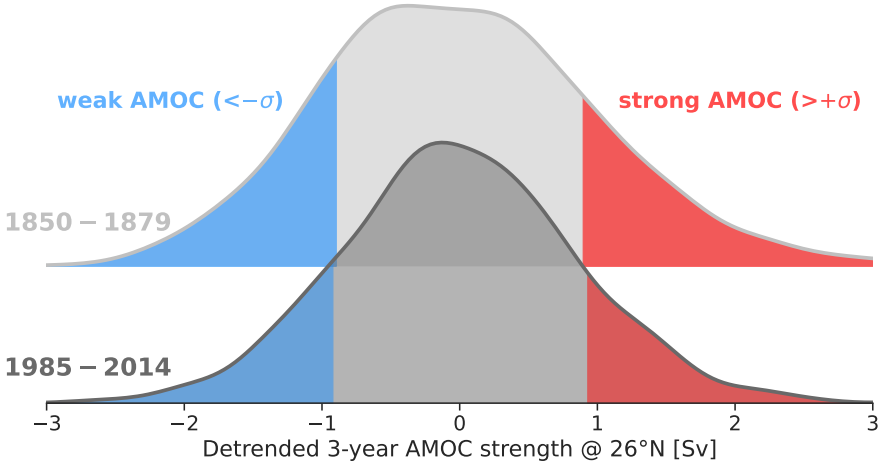

Figure A.S2: Interannual (3-year) AMOC strength (at 26.5°N) distributions for the 1850-1879 and 1985-2014 periods in MPI-GE CMIP6. Weak (below -1σ, blue) and strong (above 1σ, red) strengths are highlighted.

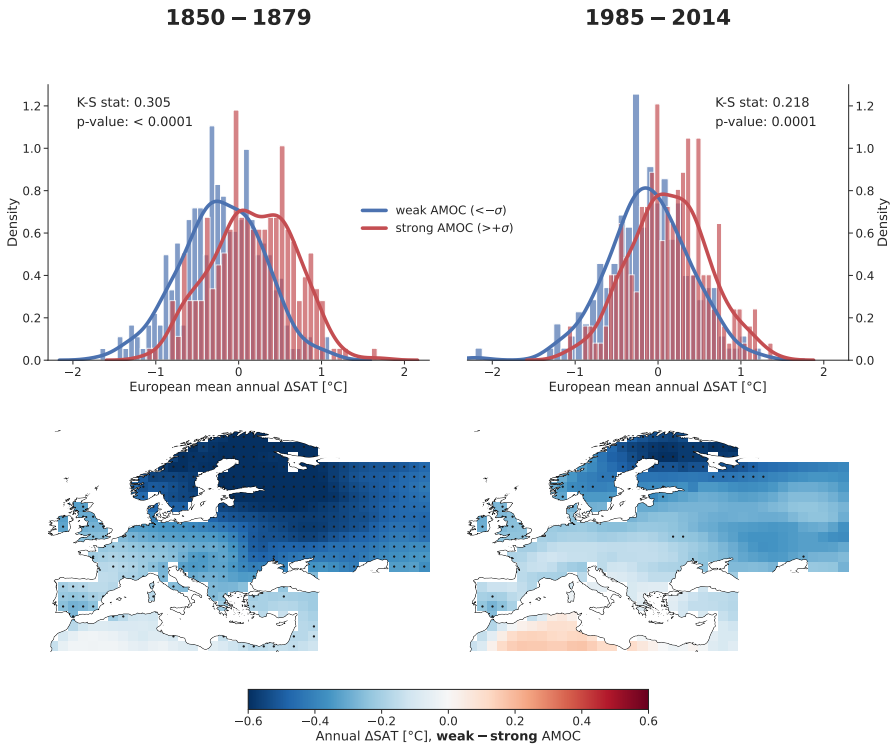

Figure A.S3: Annual surface air temperatures (SATs) for the detrended early (1850-1879, left), and late (1985-2014, right) periods in MPI-GE CMIP6, conditioned on interannual AMOC strength variations. Top: PDFs and histograms of detrended annual European mean SATs, preceded by 3-year 26.5°N AMOC strength stronger (red) or weaker (blue) than one preindustrial standard deviation (σ). The Kolmogorov-Smirnov test statistic and p-value are computed between each strong and weak distribution. Bottom: SATs of weak minus strong AMOC for each grid cell. Dots indicate significance at the 99% level.

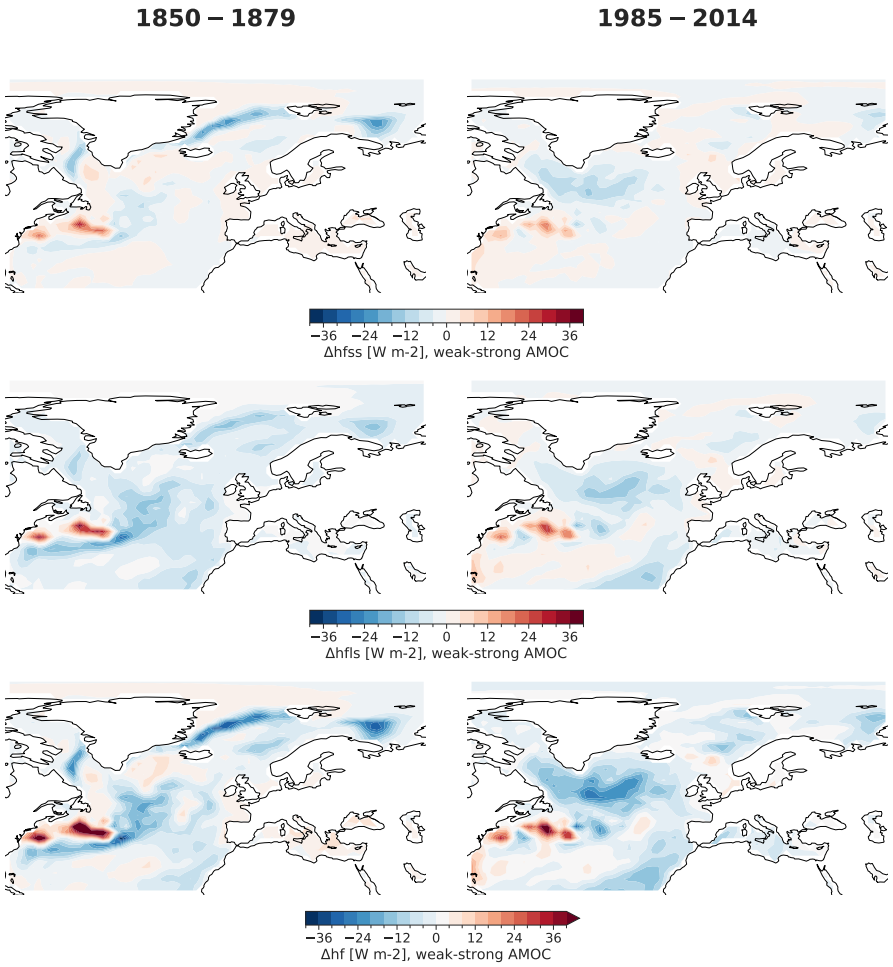

Figure A.S4: Equivalent to Figure A2, but now the first row displays sensible heat fluxes, the second row latent heat fluxes, and the third row the turbulent heat flux (sum of the previous two). Fluxes are positive upwards, from the ocean to the atmosphere.

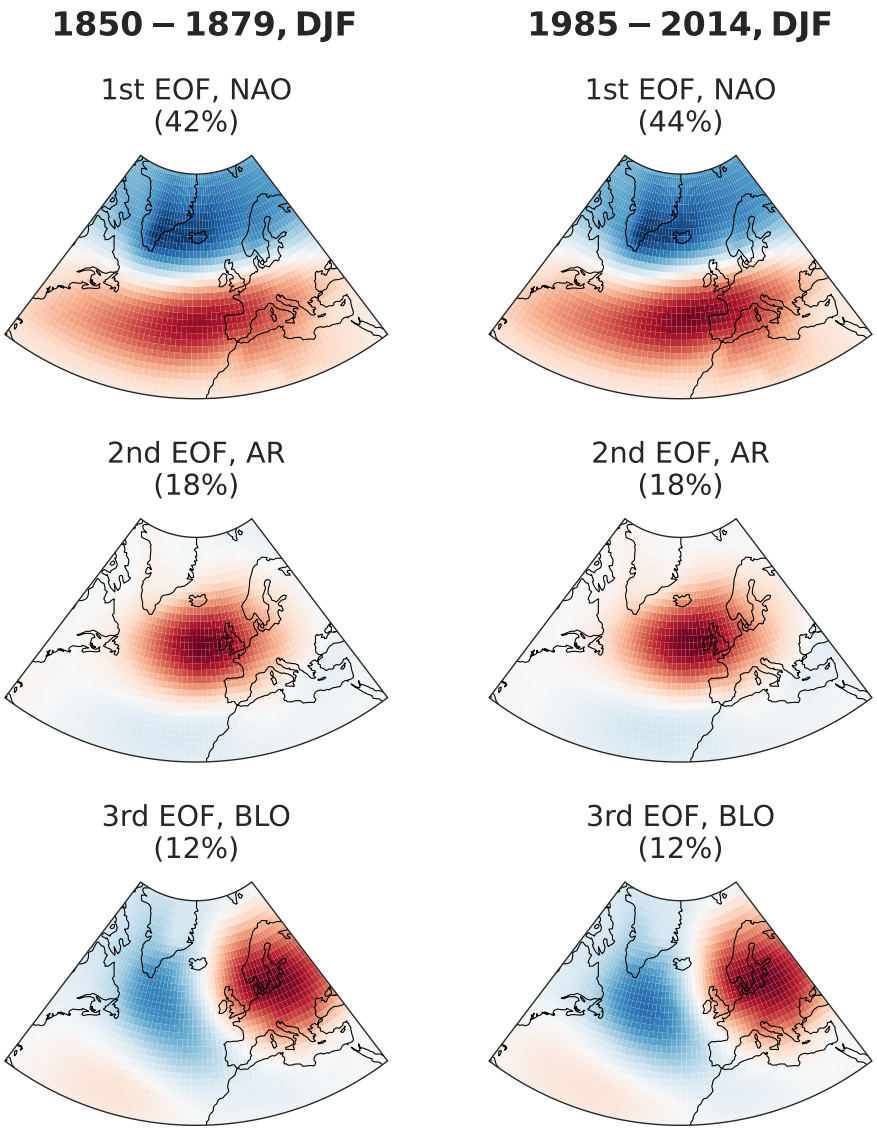

Figure A.S5: First three EOFs of winter (DJF) North Atlantic (20-80°N, -80-40°W) sea level pressures for the detrended early (1850-1879, left), and late (1985-2014, right) historical periods in the MPI-GE CMIP6. The first EOF/row is identified with the North Atlantic Oscillation (NAO), the second with the Atlantic Ridge (AR), and the third with the Scandinavian Blocking (BLO). Percentages represent the variance explained in each case.

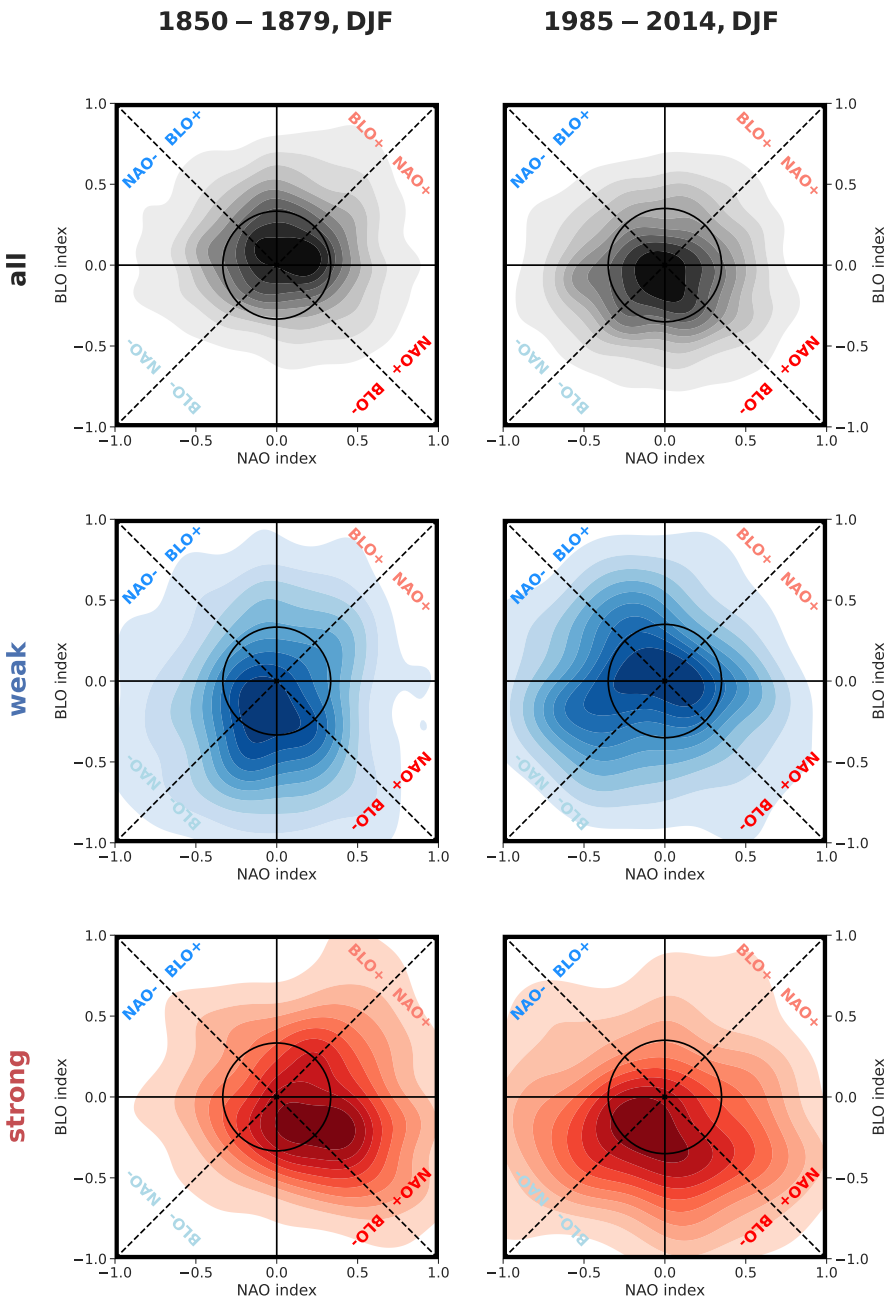

Figure A.S6: Equivalent to Figure A3, but for NAO|BLO phases.

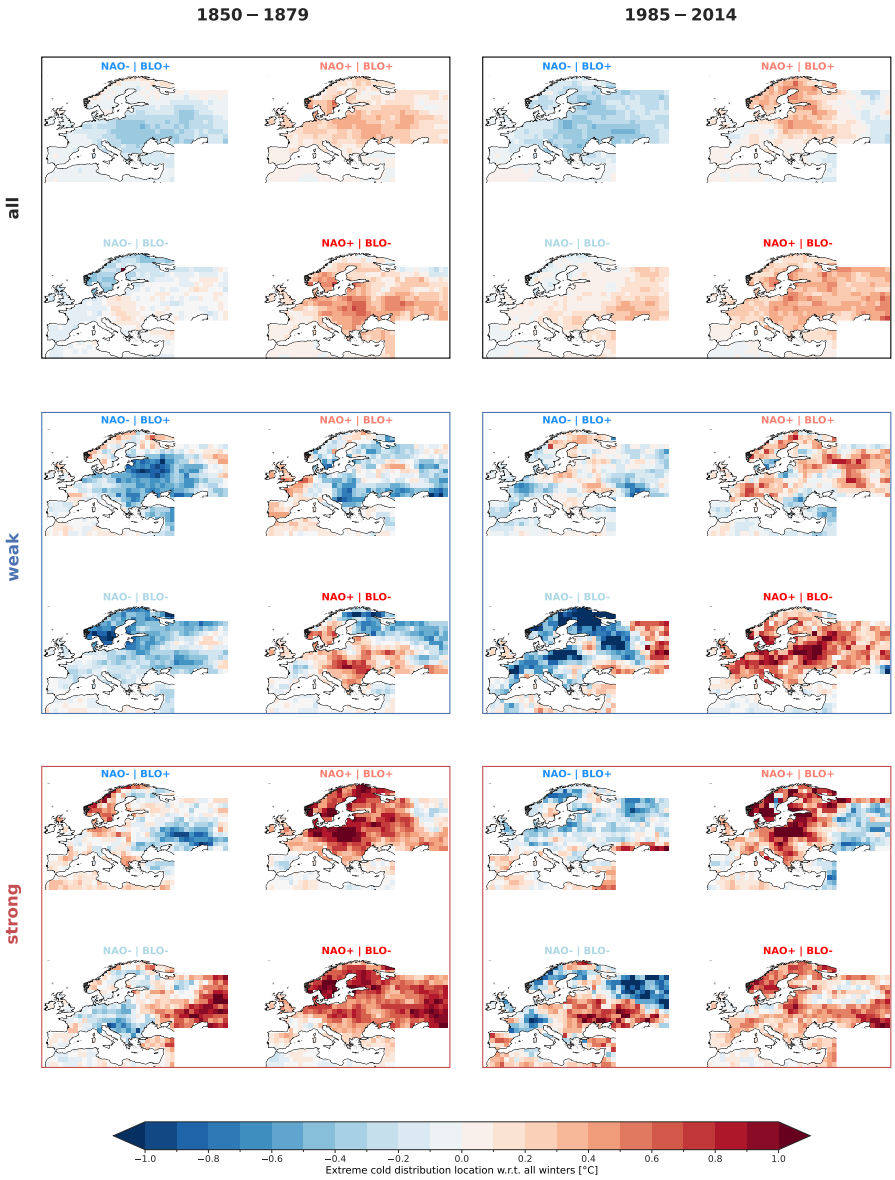

Figure A.S7: Equivalent to Figure A4, but for NAO|BLO phases.

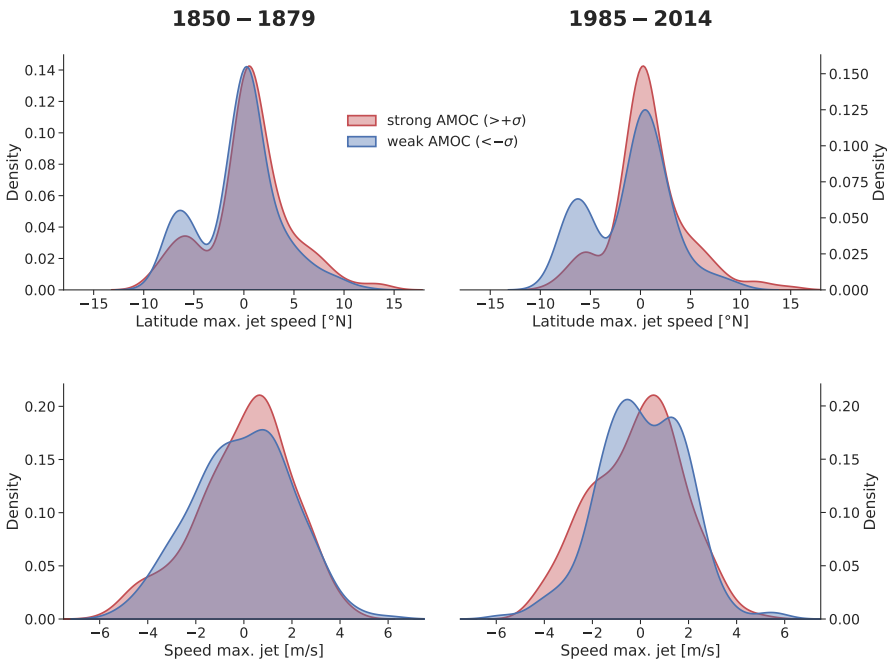

Figure A.S8: Distributions of anomalies of winter (DJF) North Atlantic jet stream latitudes (top row) and maximum speeds (bottom row), in the detrended early (1850-1879, left column), and late (1985-2014, right column) historical periods in the MPI-GE CMIP6. The jet stream is calculated from the maximum speed of zonal wind averaged between the 925 and 700 hPa pressure levels, and restricted to longitudes 0-60°W and latitudes 15-75°N.

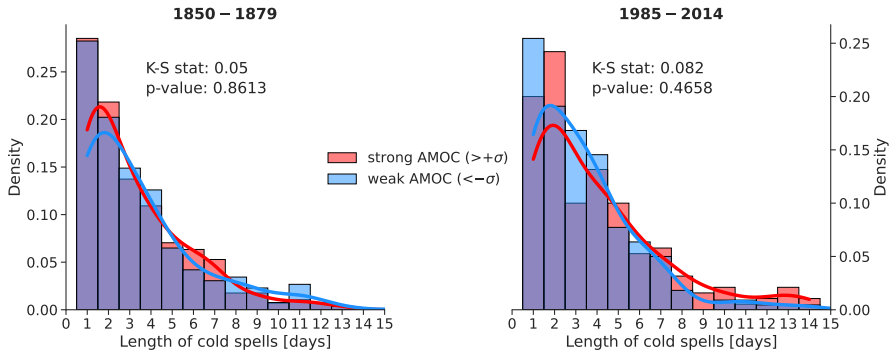

Figure A.S9: Histograms and PDFs for occurrences of different lengths of consecutive daily extreme cold (1st percentile) surface air temperatures (SATs), for the detrended early (1850-1879, left), and late (1985-2014, right) historical periods in the MPI-GE CMIP6. Red lines display temperature distributions preceded by 3-year 26.5°N AMOC strengths stronger than one preindustrial standard deviation (σ), while blue are those weaker than -1σ. The Kolmogorov-Smirnov test statistic and p-value are computed between each strong and weak distribution.

B

WEAKENING AMOC REDUCES OCEAN CARBON UPTAKE AND INCREASES THE SOCIAL COST OF CARBON

The work in this chapter was published as:

Schaumann, F., & **Alastrué de Asenjo, E.** (2025). Weakening AMOC reduces ocean carbon uptake and increases the social cost of carbon. *Proceedings of the National Academy of Sciences*, *122*(9), e2419543122. https://doi.org/10.1073/pnas.2419543122

Contributions: F. Schaumann proposed the idea for this study. I implemented and performed the MPI-ESM freshwater hosing simulations and curated the Earth system model data. F. Schaumann implemented and performed the integrated assessment model simulations. Both F. Schaumann and I performed the analysis and investigation, visualised and discussed the results and wrote and revised the manuscript.

Note: The version here included contains minor formatting changes with respect to the published version.

Weakening AMOC reduces ocean carbon uptake and increases the social cost of carbon

Felix Schaumann[1,2], Eduardo Alastrué de Asenjo[2,3]

[1] Department of Economics, Center for Earth System Research and Sustainability, University of Hamburg, Hamburg 20146, Germany.
[2] International Max Planck Research School on Earth System Modelling, Max Planck Institute for Meteorology, Hamburg 20146, Germany.
[3] Institute of Oceanography, Center for Earth System Research and Sustainability, University of Hamburg, Hamburg 20146, Germany.

ABSTRACT
A weakening of the Atlantic Meridional Overturning Circulation (AMOC) has been found to be globally beneficial by economic assessments. This result emerges because AMOC weakening would cool the Northern Hemisphere, thereby reducing expected climate damages and decreasing estimates of the global social cost of carbon dioxide (SCC). There are, however, many other impacts of AMOC weakening that are not yet taken into account. Here, we add a second impact channel by quantifying the effects of AMOC weakening on ocean carbon uptake, using biogeochemically-only coupled freshwater hosing simulations in the MPI-ESM Earth system model. Our simulations reveal an approximately linear relationship between AMOC strength and carbon uptake reductions, constituting a carbon cycle feedback that leads to higher atmospheric CO_2 concentrations and stronger global warming. This AMOC carbon feedback, when incorporated into an integrated climate-economy model, leads to additional economic damages of several trillion US dollars and raises the SCC by about 1%. The SCC increase is similar in magnitude, but of opposite sign, to the SCC effect of Northern Hemisphere cooling. While there are many other potentially relevant economic impact channels, the AMOC carbon feedback alone could thus flip the consequences of AMOC weakening into a net cost to society.

SIGNIFICANCE
The Atlantic Meridional Overturning Circulation (AMOC) is crucial for controlling the state of the Earth system, and it is projected to weaken within this century, with potentially dramatic global conse-

quences. However, current economic impact studies focus solely on AMOC-related surface cooling, the impact of which is seen as globally beneficial. By quantifying the AMOC-related reduction of ocean carbon uptake, which leads to more atmospheric CO_2 and more global warming, we find economically negative effects that are not yet accounted for in impact assessments of AMOC weakening. Our study develops projections of the AMOC carbon feedback, estimates the associated economic consequences, and provides a blueprint for how different model types can be combined to comprehensively assess impacts of future AMOC changes.

B.1 INTRODUCTION

Assessments of the social cost of carbon dioxide (SCC) – the most important economic impact metric of climate change, which quantifies the economic cost of an additionally emitted ton of CO_2 (Nordhaus, 2014; Nordhaus, 2017; Carleton & Greenstone, 2022; Rennert et al., 2022) – have started integrating climate feedbacks and tipping dynamics (Anthoff et al., 2016; Cai et al., 2015, 2016; Nordhaus, 2019; Dietz et al., 2021). However, a recent expert survey and meta-analysis on the SCC indicates that insufficient representation of Earth system dynamics is still a major driver of underestimated SCC values (Moore et al., 2024) – an issue also pointed out by the U.S. Environmental Protection Agency (EPA, 2023). We tackle this issue using the example of economic impacts arising from the projected weakening of the Atlantic Meridional Overturning Circulation (AMOC, Weijer et al., 2019, 2020). The AMOC is crucial for regulating the Earth's climate, and its projected weakening (Liu et al., 2017; Weijer et al., 2020; Boers, 2021) could severely impact temperature and weather patterns across the globe (Jackson et al., 2015; Liu et al., 2020). Yet, the economic assessment of these impacts has been the source of heated debates (Keen et al., 2022; Dietz et al., 2022).

The controversy stems from the fact that existing economic estimates of the impacts of AMOC weakening only take into account direct changes in surface temperature patterns (Anthoff et al., 2016; Dietz et al., 2021). As the AMOC transports large amounts of heat northward, its weakening would lead to large-scale cooling in the Northern Hemisphere alongside warming in the Southern Hemisphere. Pronounced cooling in the Northern Hemisphere locally reduces warming-induced climate damages and thereby decreases estimates of the global SCC (Dietz et al., 2021). But AMOC weakening would have impacts far beyond cooling the Northern Hemisphere (Jackson et al., 2015; Kopp et al., 2016; Armstrong McKay & Loriani, 2023), for example on precipitation (Ben-Yami et al., 2024a), sea levels (Levermann et al., 2005), or the carbon cycle (Sarmiento & Le

Quéré, 1996; Obata, 2007; Swingedouw et al., 2007b; Zickfeld et al., 2008; Boot et al., 2024) – all of which come with large uncertainties and have yet to be incorporated into economic assessments. Here, we focus on adding one key mechanism: the impact of AMOC weakening on ocean carbon uptake. The contribution of this paper is twofold; first, we quantify the impact of AMOC weakening on ocean carbon uptake with Earth system model (ESM) simulations; and second, we assess the effect of carbon uptake reductions on the SCC with an integrated assessment model (IAM).

Carbon uptake is affected by AMOC weakening because the North Atlantic currently takes up a large fraction of anthropogenic CO_2 (Gruber et al., 2019; Brown et al., 2021), facilitated by the AMOC transporting dense and carbon-rich water masses from the surface to the deep ocean (Pérez et al., 2013; Khatiwala et al., 2013; DeVries et al., 2017). As the AMOC is projected to weaken due to global warming, this uptake of atmospheric carbon is expected to weaken accordingly (Swingedouw et al., 2007b; Obata, 2007; Zickfeld et al., 2008; Nielsen et al., 2019; Katavouta & Williams, 2021; Liu & Fedorov, 2022; Boot et al., 2024). Consequently, more carbon will remain in the atmosphere and increase global warming. We call this the *AMOC carbon feedback*. The approximate magnitude of the AMOC carbon feedback can be inferred from existing studies that model AMOC weakening alongside an interactive carbon cycle (Swingedouw et al., 2007b; Zickfeld et al., 2008; Boot et al., 2024), but the exact relationship between AMOC strength and the resulting reduction in carbon uptake is still uncertain (Monteiro et al., 2021; Marotzke, 2023). In order to assess the dynamics and the strength of this relationship, we conduct combined carbon cycle and hosing simulations in the Max Planck Institute Earth System Model (MPI-ESM, version 1.2-LR, Mauritsen et al., 2019). Specifically, we combine biogeochemically-only coupled experiments, common in the carbon cycle feedback literature (Friedlingstein et al., 2006; Jones et al., 2016; Arora et al., 2020), with freshwater hosing experiments, common in the AMOC modeling literature (Stouffer et al., 2006; Jackson et al., 2022). Based on these simulations, we establish an approximately linear relationship between AMOC strength and the reduction of ocean carbon uptake.

This reduction in carbon uptake will – through the AMOC carbon feedback – lead to higher atmospheric carbon concentrations and thereby higher global mean temperatures. The rise in global mean temperatures increases expected economic damages from climate change and leads to an increase in the SCC, the economic metric used to quantify the aggregate welfare impact of emitting an additional ton of CO_2. For estimating how strongly the AMOC carbon feedback affects the SCC, we employ an IAM developed for investigating the economic effects of climate feedbacks and tipping dynamics, called Model for Economic Tipping Analysis (META, Dietz

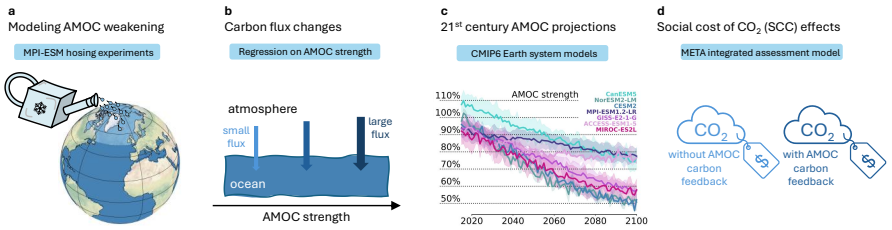

Figure B1: **Overview of the modeling approach.** (**a**) The MPI-ESM model is used to simulate climate states with an artificially weakened AMOC. (**b**) The resulting changes in annual ocean carbon storage are then analyzed as a function of the simulated AMOC, yielding a quantitative relationship between AMOC strength and changes in carbon fluxes. (**c**) We use AMOC projections from CMIP6 models to estimate the strength of the AMOC carbon feedback until 2100 along the SSP2-4.5 scenario. (**d**) The economic impact of these projected changes is then analyzed in the META IAM, by calculating the relative change in SCC that follows from explicitly incorporating the AMOC carbon feedback into the model structure.

et al., 2021). We include a new modular AMOC carbon component into META, which we calibrate to our quantification of the AMOC carbon feedback, as well as to CMIP6 projections of AMOC strength over the 21st century (Weijer et al., 2020). With this modular setup, we can then assess the economic impact of including the AMOC carbon feedback into META and compare it to the SCC effects of previously studied AMOC-induced surface cooling (Anthoff et al., 2016; Dietz et al., 2021).

Overall, our approach consists of four elements (Fig. B1). We start by simulating AMOC weakening together with the carbon cycle in MPI-ESM (a). We then use these simulations to quantify the dependence of carbon fluxes on AMOC strength (b). With this, we proceed to project the strength of the AMOC carbon feedback throughout the 21st century based on CMIP6 models (c); and for each of these projections, we finally quantify the economic impacts using the META integrated assessment model (d).

B.2 MODELING A WEAKENING AMOC

Studying the carbon cycle effects of AMOC weakening requires ESM simulations with varying AMOC strengths and realistic atmospheric CO_2 concentrations. Most ESM simulations of AMOC weakening are conducted with preindustrial CO_2 concentrations, which makes them unsuitable for studying effects on the modern-day carbon cycle (Jackson et al., 2022). While there are ESM simulations of AMOC weakening that include the anthropogenic rise in atmospheric carbon along with the resulting global warming (Swingedouw et al., 2007b; Boot et

al., 2024), this warming will itself strongly affect ocean circulations. In these simulations, it is therefore difficult to disentangle the carbon cycle effects of AMOC weakening from the carbon cycle effects of global warming. We circumvent this issue by combining *freshwater hosing experiments* (Stouffer et al., 2006) for modeling AMOC weakening with a *biogeochemically-only coupled* (BGC-only) setup (Friedlingstein et al., 2006) for neutralizing the carbon cycle effects of global warming. In freshwater hosing experiments, the AMOC is artificially weakened by reducing the salinity of the North Atlantic (Methods, Jackson et al., 2022). This freshening of high-latitude waters is supposed to account for the melting of land ice, which is neglected in ESMs without interacting ice sheets. It reduces the density of water masses in the North Atlantic regions of deep water formation so that less water sinks into the deep ocean and the AMOC as a whole is weakened. BGC-only simulations, on the other hand, are a key element of carbon cycle feedback studies (Friedlingstein et al., 2006; Arora et al., 2020). Usually, a fully coupled ESM simulation is compared to a BGC-only simulation, in which the radiative module is decoupled so that rising carbon concentrations have no effect on temperatures. This comparison allows to disentangle temperature effects from other changes affecting the carbon cycle.

We leverage the BGC-only setup for estimating the effects of AMOC weakening on the carbon cycle without picking up temperature-related carbon cycle changes. In contrast to carbon cycle feedback experiments, we do not compare the BGC-only simulations with fully coupled simulations. Instead, we compare a set of BGC-only simulations which vary in AMOC strength. The variation in AMOC strength is generated by applying different magnitudes and spatial patterns of freshwater hosing to BGC-only simulations in MPI-ESM (Methods, Mauritsen et al., 2019; Jackson et al., 2022). Because the rise in carbon concentrations is decoupled from global temperature responses, ocean circulation and the oceanic carbon cycle are only affected by changes in AMOC strength, not by other mechanisms linked to warming. Thereby, we can cleanly identify the effect that a certain amount of AMOC weakening has on carbon uptake in the model.

We conduct our simulations for two different CO_2 concentration configurations. As is common in carbon cycle feedback studies, we use an experimental setup where atmospheric CO_2 concentrations increase by 1% per year, until quadrupling after 140 years. However, this so-called *1pct experiment* exhibits much larger CO_2 concentrations than expected in reality. We therefore repeat our simulations with an SSP2-4.5 scenario of CO_2 concentrations (Fricko et al., 2017), which can be seen as representing a future of intermediate warming (Hausfather & Peters, 2020) and which is commonly used in SCC research (Dietz et al., 2021). The results from these simulations show that, as

expected, the model runs with the weakest AMOC are associated with the lowest ocean carbon storage (Fig. B2). Remarkably, though, in both the 1pct experiment and the SSP2-4.5 scenario, AMOC weakening reduces ocean carbon storage by comparable amounts. This indicates that, at least between 400 and 1120 ppm, the effect of AMOC weakening on ocean carbon uptake barely depends on the CO_2 concentration in the atmosphere.

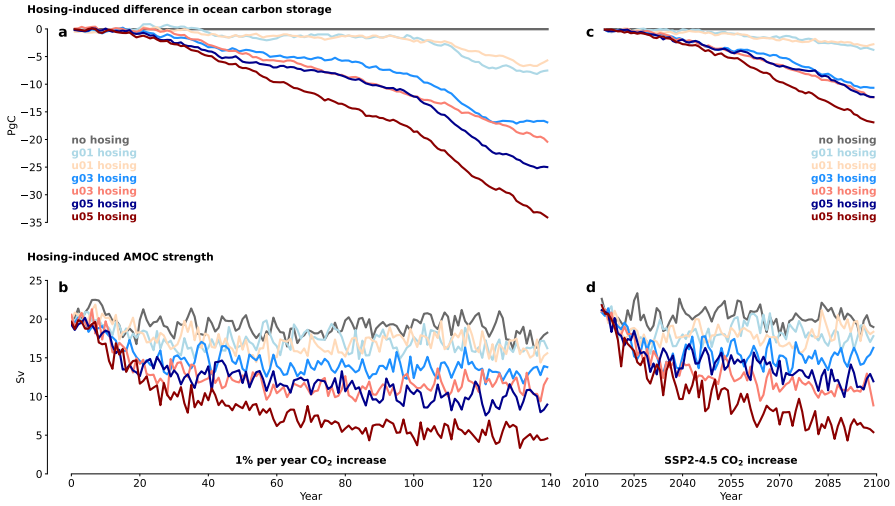

Figure B2: **AMOC strength and difference in ocean carbon storage** for the 1pct experiment (**a**, **b**) and the SSP2-4.5 scenario (**c**, **d**), as simulated by MPI-ESM. Difference in ocean carbon storage describes the change of ocean carbon storage in a hosing simulation compared to the no-hosing simulation (Methods). The colored labels denote six different hosing configurations: *g* and *u* stand for Greenland and Uniform hosing pattern, whereas *01*, *03*, and *05* denote a freshwater flux of 0.1, 0.3, and 0.5 Sv, respectively (SI Appendix, Table B2). Each hosing configuration is applied throughout the modeling period.

By the end of the modeling period, AMOC weakening leads to changes in ocean carbon storage of more than 30 PgC for the 1pct experiment and more than 15 PgC for the SSP2-4.5 scenario (Fig. B2). To contrast these findings with multi-model evidence, we construct an AMOC-related carbon-climate feedback based on Katavouta and Williams, 2021, which comprises only those carbon pools and ocean basins for which the feedback strength correlates significantly with the AMOC strength across models (Methods). For strong AMOC weakening of 15 Sv, comparable to the u05 hosing run, this results in carbon storage reductions of 32 PgC at the end of the 1pct experiment. Thus, carbon-climate feedback estimates that harness variation of AMOC strength among CMIP6 models yield very similar results to our 1pct hosing experiments in MPI-ESM. The effects of AMOC weakening on ocean carbon storage in SSP scenarios are also estimated by Boot et al., 2024, who find carbon storage reductions of between 7.5

and 15 PgC by 2100. Importantly, though, they compare hosing simulations against fully coupled simulations, which already exhibit a weakened AMOC. The resulting carbon storage reductions are thus only a partial estimate of the overall effect of AMOC weakening. Nevertheless, these other two estimates – both of which come from ESM simulations where AMOC weakening occurs alongside global warming – corroborate the effect size of AMOC-related carbon storage reduction that results from our own simulations in MPI-ESM.

B.3 AMOC-INDUCED CARBON FLUX CHANGES

Beyond the overall size of the effect on end-of-century ocean carbon storage, the dynamics of AMOC weakening and carbon storage matter – that is, how exactly the change in carbon storage in a given year depends on the AMOC strength. In order to quantify this relationship, we compute year-on-year changes in ocean carbon storage, which we refer to as *carbon fluxes*, for each simulation. By subtracting carbon fluxes in the simulation without hosing from carbon fluxes in the hosing simulations, we can define the change in carbon fluxes that is directly caused by hosing – which we call the AMOC-induced *carbon flux change*. We find that there is an approximately linear relationship between the AMOC strength in a given year and the resulting change of carbon fluxes into the ocean (Fig. B3). For illustration, if the AMOC strength is 10 Sv, the yearly carbon flux into the ocean is reduced by about 0.2 PgC, compared to an AMOC of preindustrial strength (19 Sv).

To capture the emerging relationship between AMOC strength and carbon flux changes, we perform a linear regression for the 1pct experiment and the SSP2-4.5 scenario (Fig. B3 and SI Appendix, Table B3). The regression coefficient is slightly higher for the 1pct experiment than for the SSP2-4.5 scenario ($0.025 \frac{\text{Pg}}{\text{yr Sv}}$ vs. $0.023 \frac{\text{Pg}}{\text{yr Sv}}$), but the results are remarkably similar. This provides further evidence that, under climate change, carbon fluxes into the ocean do not seem to be limited by atmospheric CO_2 concentrations, but rather by the transport of carbon-rich upper-ocean water masses into the deep ocean. Because the SSP2-4.5 scenario of CO_2 concentrations is more realistic than the 1pct experiment, as well as for the sake of being conservative and consistent with the SCC literature, we use the SSP2-4.5 coefficient of $0.023 \frac{\text{Pg}}{\text{yr Sv}}$ for further calculations. With this relationship at hand, we can now proceed to 21$^{\text{st}}$-century projections of AMOC weakening, whereby every annual value of AMOC strength can be associated with a change of carbon fluxes into the ocean.

Table B1: Projections for SSP2-4.5 (SSP5-8.5, SSP1-2.6) for 10,000 Monte Carlo runs.

Model	AMOC strength (preindust.)	AMOC strength (2100)	Relative weakening	Carbon storage reduction (2100)	Additional warming (2100)	Additional damages	SCC change
MPI-ESM1.2-LR	19.0 ± 1.1 Sv	12.8 ± 1.0 Sv	32.3 ± 6.8 %	6.7 ± 1.3 PgC	0.16 ± 0.06 %	2.3 ± 1.0 trillion $	+0.22 ± 0.06 %
MPI-ESM1.2-LR	19.0 ± 1.1 Sv	14.7 ± 0.8 Sv	22.5 ± 6.4 %	5.9 ± 2.8 PgC	0.38 ± 0.23 %	3.9 ± 2.5 trillion $	+0.50 ± 0.12 %
MPI-ESM1.2-LR	19.0 ± 1.1 Sv	16.6 ± 0.8 Sv	12.4 ± 6.8 %	5.0 ± 1.9 PgC	0.61 ± 0.36 %	2.1 ± 1.4 trillion $	+0.75 ± 0.19 %
ACCESS-ESM1-5	18.1 ± 1.0 Sv	13.9 ± 0.6 Sv	23.5 ± 5.1 %	7.3 ± 2.8 PgC	0.47 ± 0.26 %	4.6 ± 2.8 trillion $	+0.63 ± 0.15 %
CanESM5	11.4 ± 0.8 Sv	8.7 ± 0.7 Sv	23.3 ± 8.4 %	3.9 ± 4.0 PgC	0.26 ± 0.30 %	3.1 ± 3.4 trillion $	+0.96 ± 0.22 %
GISS-E2-1-G	24.1 ± 1.7 Sv	13.8 ± 0.7 Sv	42.5 ± 5.0 %	9.9 ± 4.1 PgC	0.63 ± 0.37 %	6.7 ± 4.4 trillion $	+0.96 ± 0.24 %
MIROC-ES2L	12.8 ± 1.0 Sv	7.4 ± 0.8 Sv	42.1 ± 7.7 %	11.4 ± 4.6 PgC	0.74 ± 0.43 %	7.5 ± 4.9 trillion $	+1.11 ± 0.27 %
CESM2	18.0 ± 0.8 Sv	9.4 ± 0.4 Sv	47.9 ± 3.3 %	11.8 ± 4.6 PgC	0.77 ± 0.45 %	8.1 ± 5.4 trillion $	+1.36 ± 0.33 %
NorESM2-LM	20.2 ± 0.8 Sv	8.1 Sv	60.1 %	13.9 ± 4.9 PgC	0.34 ± 0.19 %	4.7 ± 2.8 trillion $	+0.95 ± 0.20 %
NorESM2-LM	20.2 ± 0.8 Sv	10.3 ± 1.0 Sv	49.3 ± 5.1 %	12.4 ± 4.9 PgC	0.81 ± 0.49 %	8.4 ± 5.7 trillion $	+1.63 ± 0.38 %
NorESM2-LM	20.2 ± 0.8 Sv	12.2 Sv	39.8 %	13.5 ± 9.5 PgC	1.71 ± 1.55 %	5.9 ± 6.4 trillion $	+3.76 ± 0.94 %

Uncertainty ranges correspond to one standard deviation. The monetary values of additional damages are aggregated and discounted over the whole projection period (2015-2100) and expressed in 2024 US dollars (Methods). Uncertainty estimates of AMOC strength are derived from ensembles of projections. Given that we only have access to one ensemble member for NorESM along the SSP1-2.6 and SSP5-8.5 scenarios, we do not provide standard deviations for these projections.

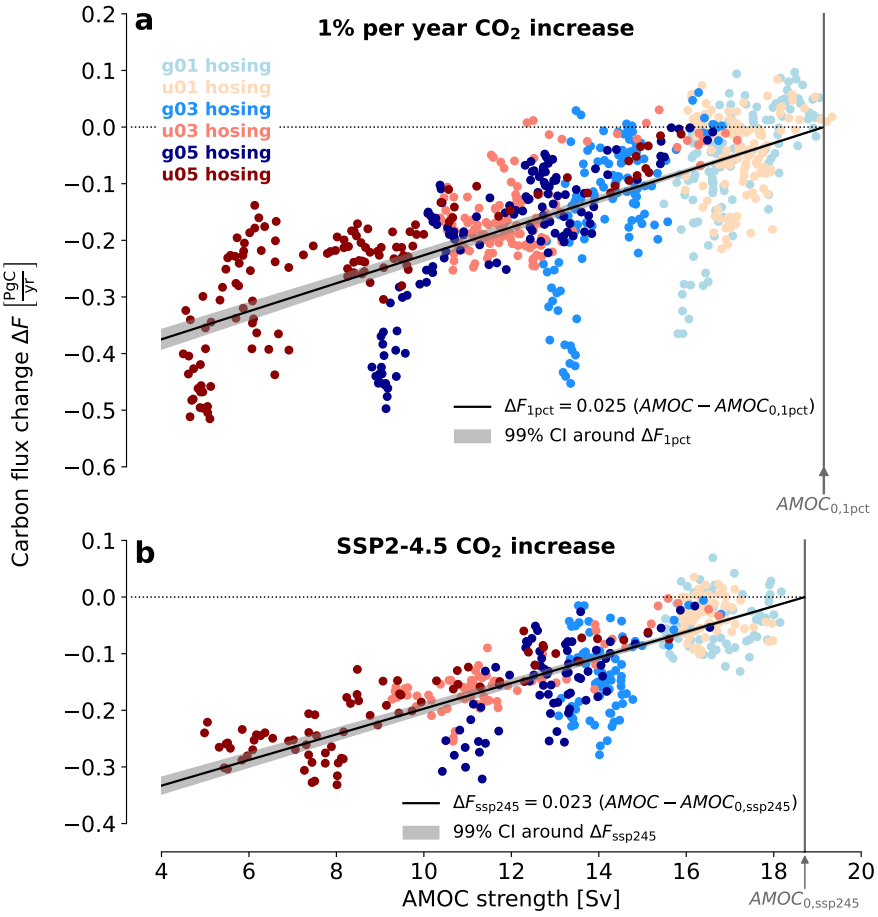

Figure B3: **Carbon flux changes as a function of AMOC strength** for the 1pct experiment (**a**) and for the SSP2-4.5 scenario (**b**). Both the AMOC strength and the carbon flux time series are smoothed with a 10 year running mean (Methods, SI Appendix Fig. B.S1 for different running mean windows). Vertical gray lines denote the mean AMOC strength of the simulation without hosing. Black lines are linear regressions with zero intercepts (Methods), and gray shading is the 99% confidence interval of the regression coefficient.

B.4 PROJECTING THE AMOC CARBON FEEDBACK

CMIP6 models project a substantial amount of AMOC weakening along the SSP2-4.5 scenario, but both initial AMOC strengths and amounts of weakening vary strongly across models (Table B1, Fig. B4). We compare CMIP6 projections based on their relative AMOC weakening compared to preindustrial AMOC strength and use them to calibrate a newly created AMOC carbon component of the META model. In contrast to the existing AMOC component in META, we do not define a probability for stochastic AMOC weakening, but instead include an explicit representation of AMOC strength, which can be calibrated to match projections by CMIP6 models (Methods).

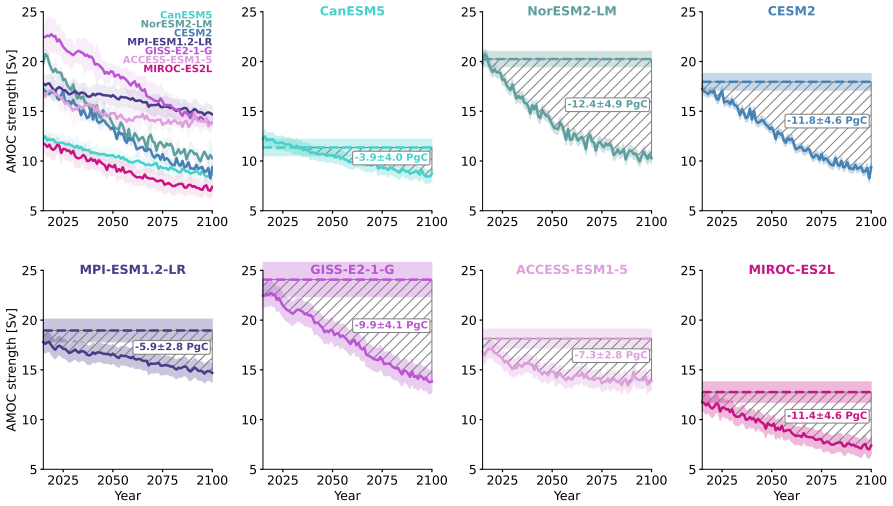

Figure B4: **Projected reductions in ocean carbon storage.** The top-left panel shows all seven SSP2-4.5 ESM projections for AMOC strength that are used in this paper. Each of them has at least three ensemble members; the thick lines represent the ensemble mean and the shading the ensemble standard deviation. The other panels show one ESM projection each, together with the preindustrial strength of the respective ESM. For the preindustrial AMOC strength, the dotted line represents the mean strength and the shading one standard deviation. The difference between projected AMOC strength and preindustrial AMOC strength governs the strength of carbon flux change, so the hatched area symbolizes the cumulative amount of carbon that is not stored in the ocean by 2100. The labels on the hatched areas show this carbon storage reduction in 2100, calculated with 10,000 Monte Carlo runs, with the uncertainty range corresponding to one standard deviation. Note that the reductions in ocean carbon storage are not exactly proportional to the size of hatched areas in this plot, because we model carbon flux changes as depending on relative AMOC weakening compared to preindustrial AMOC strength, not on absolute AMOC weakening as portrayed here.

Hereby, we make sure to only use CMIP6 models with several ensemble members so that we can account for internal variability in our projections (Schwarzwald & Lenssen, 2022). In our own projections with the META model, we use the internal variability of CMIP6 ensemble projections as well as a constrained parameter set of the FaIR climate emulator (Leach et al., 2021) to obtain 10,000 Monte Carlo parameter samples (Methods).

By the end of the century, the AMOC weakens between 20 and 50% in our projections along the SSP2-4.5 scenario (Table B1). As a result of this AMOC weakening, the ocean carbon storage in 2100 is reduced by between 3.9 and 12.4 PgC (Fig. B4). For comparison, yearly CO_2 emissions from fossil fuels are currently at around 10 PgC (Friedlingstein et al., 2023). The projected reduction in ocean

carbon storage corresponds to additional carbon in the atmosphere (Goodwin & Lenton, 2009), which affects global temperatures. This additional warming due to the AMOC carbon feedback is small, as it leads to relative global temperature increases between 0.26% and 0.81% by 2100 (Table B1). Nevertheless, even this slight increase in global temperatures has a non-negligible impact on economic damages from climate change. We aggregate the discounted future climate damages that occur between 2015 and 2200 due to the AMOC carbon feedback with the damage function calibrated to Burke et al., 2015 (Methods). This yields projected additional damages of between 3.1 and 8.4 trillion US dollars (Table B1). Beyond a projected increase in expected climate damages, however, the AMOC carbon feedback also affects the main metric with which the societal damage from an additional ton of CO_2 emissions is estimated: the SCC.

B.5 EFFECTS ON THE SCC

The SCC increase of including the AMOC carbon feedback based on SSP2-4.5 projections lies between 0.5% and 1.63% (Table B1), when using the welfare and persistence parameters shown in the box of Fig. B5. SCC effects are estimated by calculating the SCC in META for both the base setup and a setup with AMOC carbon feedback and then calculating the relative change in percent (Methods). The results are robust to assumptions about the spatial pattern of warming; because AMOC weakening will impact surface temperature patterns, we have also estimated these SCC effects against the backdrop of different AMOC-induced temperature patterns. We used the same four spatial patterns as previous studies on the subject (Anthoff et al., 2016; Dietz et al., 2021), which go back to transient hosing simulations under greenhouse gas forcing (Vellinga & Wood, 2008; Swingedouw et al., 2013), but none of these AMOC-induced temperature patterns affect relative SCC changes caused by the AMOC carbon feedback (SI Appendix, Table B4). Contrasting the impacts of the AMOC carbon feedback with the previously studied AMOC cooling effects (Fig. B5, left; Dietz et al., 2021) shows that the SCC effects of the AMOC carbon feedback are similar in magnitude, but of opposite sign, to the SCC effects of AMOC-induced cooling.

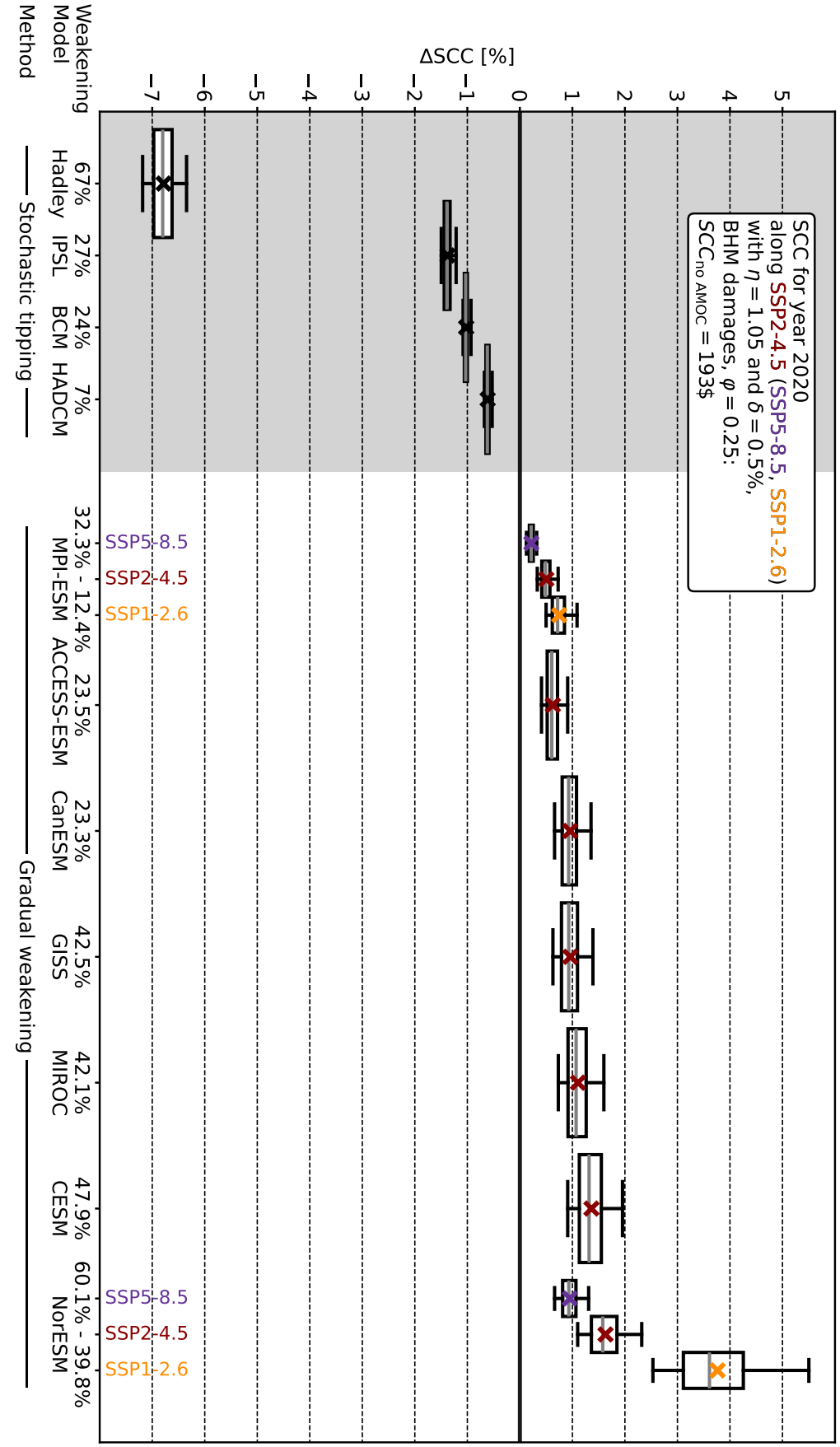
META temperature effect
CMIP6-calibrated carbon effect
SCC for year 2020
along SSP2-4.5 (SSP5-8.5, SSP1-2.6)
with η = 1.05 and δ = 0.5%,
BHM damages, φ = 0.25:
SCC no AMOC = 193$
ΔSCC [%]
5
4
3
2
1
0
−1
−2
−3
−4
−5
−6
−7
Weakening
Model
Method
67%
Hadley
Stochastic tipping
27%
IPSL
24%
BCM
7%
HADCM
32.3% - 12.4%
MPI-ESM
SSP5-8.5
SSP2-4.5
SSP1-2.6
23.5%
ACCESS-ESM
23.3%
CanESM
42.5%
GISS
42.1%
MIROC
47.9%
CESM
60.1% - 39.8%
NorESM
SSP5-8.5
SSP2-4.5
SSP1-2.6
Gradual weakening

Figure B5: **Percentage change in SCC due to AMOC effects.** In the gray panel (left), the relative SCC effects of AMOC-induced surface cooling are reproduced based on Dietz et al., 2021. In the white panel (right), the relative SCC effects of the AMOC carbon feedback are estimated based on different 21st-century AMOC projections by CMIP6 models. *Stochastic tipping* refers to the way in which the AMOC component is implemented in the META model, whereby the probability of tipping increases with global temperatures and, once the AMOC is tipped, surface temperature patterns change over the course of 35 years (Dietz et al., 2021). On the other hand, *gradual weakening* refers to our approach of calibrating AMOC scenarios to CMIP6 models, whereby the modeled AMOC strength exactly follows ESM projections along a given emission scenario. *AMOC weakening* describes the relative AMOC decrease in the tipped state (stochastic tipping) or the relative AMOC decrease between preindustrial conditions and 2100 (gradual weakening). Boxes show interquartile ranges, with medians in gray. Crosses mark the mean effect, and whiskers show the 5th and 95th percentile. Each box covers a distribution of results that emerge from 10,000 Monte Carlo results, with uncertainty in the FaIR climate module, as well as about preindustrial AMOC strength, AMOC projections, and the coefficient linking AMOC strength to reduced carbon uptake. We show the full distribution of 10,000 Monte Carlo samples – versions with 0.1% or 1% of results trimmed at each tail are shown in the SI Appendix (Fig. B.S5). The text box on the top left lists important parameters for the SCC calculation, with η denoting the elasticity of intertemporal substitution, δ the rate of pure time preference, and φ the persistence parameter (Methods, Dietz et al., 2021). BHM damages refer to the damage function based on Burke et al., 2015.

For the AMOC carbon feedback, there is a stable relationship between the amount of AMOC weakening that a certain model projects and the resulting rise in SCC estimates (Table B1). This relationship, however, breaks down when comparing changes along different socioeconomic scenarios. For the two models with weakest and strongest SCC effect, respectively, we also calculated the SCC effect of the AMOC carbon feedback along SSP5-8.5 and SSP1-2.6 (Fig. B5). For both models, the SCC increase is diminished under a high-emission scenario and magnified under a low-emission scenario. This disproportionate SCC effect of AMOC changes under low-emission scenarios is caused by the fact that projections of AMOC strength along different SSP scenarios are barely distinguishable until late in the 21st century (Weijer et al., 2020). At the same time, global warming levels differ strongly across these scenarios. Therefore, relative to the amount of global warming, AMOC weakening is much more pronounced in low-emission scenarios (Table B1). Hence, the AMOC carbon feedback becomes more economically relevant the

more the world moves towards limiting global warming to internationally agreed levels.

B.6 DISCUSSION

We provide new estimates of the AMOC carbon feedback and find an approximately linear relationship between AMOC strength and carbon flux changes. This allows us to make projections for a range of CMIP6 models, whose ScenarioMIP output currently does not capture the AMOC carbon feedback because of being forced by CO_2 concentrations instead of CO_2 emissions (Sanderson et al., 2024). As a second contribution, we incorporate this relationship into an IAM, with which we explore the economic impacts of the AMOC carbon feedback. This yields SCC changes of a magnitude that could flip economic impact assessments of AMOC weakening from a global benefit into a global cost. Both parts of our study are subject to uncertainties and limitations. The estimates of AMOC-induced carbon flux changes rest on our simulations with the MPI-ESM model. Some features of the ocean and carbon cycle dynamics would likely be different in equivalent simulations with other ESMs, for example the late intensification of carbon uptake reductions in the 1pct experiment (Fig. B3 and SI Appendix, Fig. B.S2). This implies that the confidence interval of our regression coefficient might not be capturing the full amount of uncertainty. Nevertheless, the fact that multi-model evidence from CMIP6 carbon cycle feedback experiments as well as other hosing-based studies (Boot et al., 2024) yield similar results increases confidence in the dynamics and magnitude of our findings. The economic impact estimation is also subject to uncertainties as well as normative and structural modeling choices (Moore et al., 2024). As demonstrated by many studies, the SCC is very sensitive to choices of discounting and damage function parameters (Dietz & Stern, 2015; Howard & Sterner, 2017; Hänsel et al., 2020; Rennert et al., 2022; Nesje et al., 2023). Our absolute SCC values, as well as the additional damages we estimate, are equally sensitive to these parameter choices (SI Appendix, Table B5). For this reason, we focus on the relative change in SCC as our main outcome variable. While the absolute SCC value can change drastically, the relative SCC impact of including the AMOC carbon feedback is more robust to alternative discounting and damage function parameters (SI Appendix, Table B5).

Of all the possible impacts of AMOC weakening, the literature has so far only included a single one: the change in surface temperature patterns, which is dominated by Northern Hemisphere cooling. Here, we add a second important mechanism that acts through the impact of AMOC weakening on the carbon cycle. By considering a single additional mechanism through which AMOC weakening might affect the economy, we find SCC changes that might flip the sign of the

overall effect. But there are many more potential impacts of AMOC weakening, such as changes in precipitation, sea level, or North Atlantic storm tracks. Therefore, our results should not be interpreted as an impact estimate of AMOC weakening as such, but rather as the second step of a long journey towards assessing the full economic consequences of AMOC weakening. Recent studies have been warning about the possibility of a complete AMOC collapse (Boers, 2021; Ditlevsen & Ditlevsen, 2023; van Westen et al., 2024a), a scenario which we do not cover in this study. Our results are conservative, as they are based on SSP2-4.5 AMOC projections from CMIP6 models — none of which feature AMOC collapse. Using the same scenario across all parts of this study is important for the internal consistency of our results, but it should be noted that, in the event of stronger AMOC weakening than projected by current models, SCC impacts would increase considerably.

B.7 METHODS

ESM simulations

Freshwater hosing

We perform freshwater hosing experiments in the MPI-ESM1.2-LR model (Mauritsen et al., 2019). There are two common ways of introducing the freshwater flux (implemented as a negative salinity flux) in these experiments (Jackson et al., 2022): either as a uniform field across the whole Atlantic north of 50°N, or as a field around Greenland that decays exponentially with distance to the coast. While Greenland hosing is arguably the more realistic setup, uniform hosing fields are more common in the literature; we therefore run both types of hosing patterns. For both patterns, we use different hosing strengths, corresponding to freshwater fluxes of 0.1, 0.3, and 0.5 Sv, respectively. Given that 0.1 Sv is already on the higher end of estimates of expected input from future Greenland ice sheet melting, these hosing experiments should not be interpreted as a realistic freshwater forcing, but rather as a means for generating internally consistent model worlds that span a wide range of AMOC strengths.

CO_2 forcing

In contrast to the hosing simulations studied in Jackson et al., 2022, which are conducted against the background of preindustrial climate conditions, we apply anthropogenic CO_2 forcing. We do that in two different experimental setups. In the first setup, we run one set of simulations where atmospheric CO_2 concentrations increase by 1% per year, in accordance with the literature on carbon cycle feedbacks (Jones et al., 2016). In the second setup, we prescribe more realistic at-

mospheric CO_2 concentrations, following a historical simulation first and branching into the SSP2-4.5 emission scenario from 2015 until 2100 (Fricko et al., 2017). The hosing for the SSP2-4.5 setup is only applied after 2015. All the conducted ESM simulations are listed in the SI Appendix, Table B2.

Biogeochemical-only coupling

Our simulations feature freshwater forcing and CO_2 forcing, both of which affect the oceanic carbon cycle; the freshwater forcing by reducing water mass density and weakening the AMOC, and the CO_2 forcing by causing global warming which again causes changes in, among others, solubility, carbonate chemistry, density, mixed layer depth, and biological activity. For this study, we are exclusively interested in carbon cycle changes caused by AMOC-related reductions in physical water mass transport into the deep ocean. All warming-induced carbon cycle changes are potential confounders for this analysis, which we address by running biogeochemically-only coupled (BGC-only) simulations. BGC-only simulations artificially decouple atmospheric CO_2 concentrations from the model's radiation component so that there is no warming impact from CO_2. This ensures that the ocean carbon cycle is not affected by CO_2-induced warming, but only by the AMOC changes we induce through freshwater hosing. At the same time, the carbon cycle as such is undisturbed, and with the 1pct experiment and the SSP2-4.5 scenario, we can study how different amounts of atmospheric CO_2 concentrations influence carbon fluxes into the ocean and how these depend on AMOC strength.

AMOC-related carbon-climate feedback

A second method for estimating the influence of AMOC strength on ocean carbon uptake takes the overall oceanic carbon-climate feedback (Arora et al., 2020) and disentangles it by ocean basin and by carbon pool in order to determine which parts of the carbon-climate feedback depend on AMOC weakening (Katavouta & Williams, 2021).

Three carbon-climate feedback is differentiated by three carbon pools: *saturated carbon*, which reflects changes in solubility governed by warming and carbonate chemistry; *disequilibrium carbon*, which reflects changing amounts of water masses sinking before reaching chemical equilibrium with the atmosphere; and *regenerated carbon*, which reflects changes in biological processes and residence times of water masses in the ocean interior. Katavouta and Williams, 2021 find that the carbon-climate feedbacks of the Atlantic disequilibrium carbon pool ($\gamma_{\text{Atl, dis}}$) and the carbon-climate feedbacks of the Atlantic regenerated carbon pool ($\gamma_{\text{Atl, reg}}$) across different CMIP6 models both correlate with the amount of AMOC weakening that the respective model exhibits.

We harness this correlation to construct an *AMOC-related carbon-climate feedback* γ_{AMOC}

$$\gamma_{AMOC} = \gamma_{Atl,\,dis} + \gamma_{Atl,\,reg} \tag{1}$$

Regressing this on AMOC strength at the end of the carbon cycle feedback experiments yields the following equation (SI Appendix, Fig. B.S3):

$$\gamma_{AMOC} = -0.58 \frac{PgC}{SvK} (\Delta AMOC - 3.84\ Sv)$$

To calculate end-of-simulation ocean carbon storage reductions, we need to choose a value for AMOC weakening $\Delta AMOC$ and multiply γ_{AMOC} with global mean surface temperature at the end of the simulation, as carbon-climate feedback values are normalized with respect to temperature change. From Arora et al., 2020, we get $T_{1pct}(140) = 4.87K$, which simplifies the AMOC-related ocean carbon storage reduction ΔC_{AMOC} to

$$\Delta C_{AMOC}(\Delta AMOC) = -\gamma_{AMOC}(\Delta AMOC) \cdot T_{1pct}(140) \tag{2}$$

$$= 2.825 \frac{PgC}{Sv} (\Delta AMOC - 3.84\ Sv) \tag{3}$$

Analyzing AMOC strength and ocean carbon storage

We define AMOC strength as the maximum meridional flow of water at 26.5°N in the Atlantic Ocean for all depths z and integrated from west to east:

$$AMOC(t) = \max_z \left\{ \int_{W_{Atl}}^{E_{Atl}} \int_0^z v(lat = 26.5°N, lon, z)\, dz\, dlon \right\}, \tag{4}$$

where $v(lat, lon, z)$ is the meridional northward velocity of water at a specific point in the ocean.

We define global ocean carbon storage as the volumetric integral of dissolved inorganic carbon (DIC) concentrations:

$$C_{ocean}(t) = c \int_V DIC(t)\, dV, \tag{5}$$

with $c = 12.01 \frac{g}{mol}$.

For both of these quantities, we extract annual values for all MPI-ESM simulations, which form the basis of further calculations. The annual dataset of AMOC strength and carbon storage is available as part of our open-access code repository.

AMOC-induced carbon flux changes

We define yearly global carbon fluxes $F(t)$ as the year-on-year change in $C_{ocean}(t)$. In order to investigate the impact of different AMOC strengths on carbon fluxes into the ocean, we consider the difference between yearly carbon fluxes in hosing simulations and yearly carbon fluxes in the respective simulation without hosing; we call this quantity the AMOC-induced carbon flux change $\Delta F_{AMOC}(t)$

$$\Delta F_{AMOC}(t) = F_{hosing}(t) - F_{no\ hosing}(t) \tag{6}$$

To relate the carbon flux change $\Delta F_{AMOC}(t)$ to the amount of AMOC weakening, we plot it as a function of $AMOC(t)$, as in Fig. B3. For both ΔF_{AMOC} and $AMOC$, we apply a 10-year running mean in order to capture the overall dynamics rather than short-term fluctuations in carbon storage and AMOC strength. The same results for different running mean windows are shown in the SI Appendix, Fig. B.S1. We then perform two linear regressions, which we call ΔF_0 and ΔF_1:

$$\Delta F_0 = 0 + c_0 \cdot (AMOC - AMOC_0) \tag{7a}$$

$$\Delta F_1 = c_1 + c_2 \cdot (AMOC - AMOC_0), \tag{7b}$$

where $AMOC_0$ is the average AMOC strength of the simulations without hosing.

The difference between the two regressions is that ΔF_0 has no oth-order term so that the AMOC-induced carbon flux change vanishes by definition if the AMOC strength is unchanged. For internal consistency, this is a desirable property. Given that the linear regression coefficients $c_0 = 0.023 \frac{PgC}{yr\ Sv} \left(= 0.025 \frac{PgC}{yr\ Sv}\right)$ and $c_2 = 0.022 \frac{PgC}{yr\ Sv} \left(= 0.026 \frac{PgC}{yr\ Sv}\right)$ for the SSP2-4.5 scenario (the 1pct experiment) are very similar (SI Appendix, Table B3), we use ΔF_0 for further calculations.

Impacts of the AMOC carbon feedback

Integration into META IAM

We use the most recent version of the META IAM (Dietz et al., 2021) for assessing the 21st-century impacts of the AMOC carbon feedback on carbon storage, temperature, climate damages, and the SCC. The META model has a base configuration that comprises socioeconomic and emission scenarios, the FaIR 2.0.0 simple climate model (Leach et al., 2021), pattern-scaling, a country-level damage function, and a discounted utility component. On top of that, META has several modules for tipping dynamics and climate feedbacks, among them

the AMOC-induced cooling effect. We build a new AMOC carbon module that differs from the existing AMOC cooling module in that it does not follow stochastically triggered tipping dynamics, but instead comes with an explicit representation of yearly AMOC strength, which again depends on global temperatures. We introduce the variable $\Delta AMOC$, which describes AMOC weakening and depends on the change in atmospheric temperatures since the beginning of the scenario modeling period in 2015:

$$\Delta AMOC(t) = \beta_{AMOC}(t)\,(T_{atm}(t) - T_{atm}(2015)) \tag{8}$$

The parameter β_{AMOC} describes the sensitivity of the AMOC to global warming. For stylized scenario analyses, this parameter can be taken to be constant, but it can also be calibrated such as to follow annual projections of AMOC strength. Note that $\Delta AMOC$ is positive when the AMOC weakens.

Absolute AMOC strength $AMOC$ is obtained by

$$AMOC(t) = AMOC(2015) - \Delta AMOC(t) + \epsilon_{AMOC}(t), \tag{9}$$

where ϵ_{AMOC} is a random fluctuation in AMOC strength that can be calibrated to AMOC projection uncertainty.

The AMOC-induced reduction in carbon uptake is formally equivalent to additional emissions, which we model through the AMOC-induced carbon flux change ΔF_{AMOC}

$$\Delta F_{AMOC}(t) = (c_0 + \epsilon_{c_0}) \cdot (AMOC_{pi} + \epsilon_{AMOC_{pi}} - AMOC(t)) \cdot \frac{AMOC_{pi,MPI}}{AMOC_{pi}}. \tag{10}$$

Here, c_0 relates AMOC strength to carbon flux changes (Eq. 7a, SI Appendix Table B3), and ϵ_{c_0} represents the uncertainty about c_0. $AMOC_{pi}$ is the preindustrial AMOC strength of a given model that the AMOC carbon module is calibrated to, and $\epsilon_{AMOC_{pi}}$ the associated uncertainty. The second term in Eq. 10 describes AMOC weakening in year t, and the third term converts the weakening into equivalent weakening in MPI-ESM. We model the carbon flux change as dependent on the AMOC weakening with respect to preindustrial values, not 2015 values, because in our MPI-ESM simulations, we compare hosing-induced changes to no-hosing simulations that don't exhibit any warming; the appropriate reference is thus the preindustrial AMOC strength. Since our estimates of c_0 are obtained with MPI-ESM and absolute AMOC weakening differs widely between ESMs, we convert model-specific weakening into equivalent weakening in MPI-ESM through the ratio of respective preindustrial AMOC strengths. The additional CO_2 flux ΔF_{AMOC} is then passed on to the emissions module of META, from where it influences global temperatures and climate damages.

Calibration to CMIP6 AMOC projections

The AMOC carbon module of META can be calibrated to stylized scenarios of AMOC weakening, but also to ESM projections. We collected those historical and SSP2-4.5 simulations by ESMs participating in CMIP6 that are available from the Earth System Grid Federation (ESGF) node of the German Climate Computing Center (DKRZ) and include the variable *msftmz* for calculating AMOC strength. Of these, we use only the ones that have at least three ensemble members. For MPI-ESM1.2-LR and NorESM2-LM, we additionally collected SSP5-8.5 and SSP1-2.6 AMOC projections; here, we have only one ensemble member of NorESM2-LM and hence no ensemble standard deviation. We also collected preindustrial control simulations of all the models for which we have AMOC projections. From these preindustrial control simulations, we get the mean and standard deviation of preindustrial AMOC strength.

For calibrating the AMOC carbon component, we first extract the time series for global mean surface temperature from META along the SSP2-4.5 scenario. Then we choose $\beta_{AMOC}(t)$ such that for every year, the deterministic SSP2-4.5 temperature scenario leads to AMOC weakening that exactly corresponds to a given ESM projection of AMOC strength. This implies that for warming scenarios above (below) the deterministic SSP2-4.5 in META, the AMOC will weaken more (less) than projected by a given ESM.

Uncertainty treatment

For all projections and SCC calculations, we run 10,000 Monte Carlo samples. For this, we sample parameters for the simple climate model FaIR from the constrained parameter ensemble in Leach et al., 2021, following the implementation in Errickson and Rennels, 2021.

To calibrate the uncertainty about the preindustrial AMOC strength of a given ESM, we use the standard deviation of the distribution of AMOC strength in the model's historical experiment. For every Monte Carlo sample, we draw from a normal distribution with this standard deviation and use this draw as the value for $\epsilon_{AMOC_{pi}}$. To calibrate the uncertainty about AMOC projections, we average the ensemble standard deviation over time and then, for every year, draw from a normal distribution with this standard deviation. This gives a time series of $\epsilon_{AMOC}(t)$, which is able to emulate the year-on-year fluctuations that we observe in both projections and observations of AMOC strength. To calibrate the uncertainty about the carbon flux change resulting from a certain AMOC strength value, we take the standard error of the regression coefficient c_0 in Eq. 7a and for every Monte Carlo sample, we draw an ϵ_{c_0} value from a normal distribution.

Economic damage estimation

To calculate additional climate damages caused by the AMOC carbon feedback, we extract the path of total climate damages from each Monte Carlo simulation of the META model and then take the difference between total damages in a model configuration with the AMOC carbon feedback and a model configuration without the AMOC carbon feedback. This time series of additional damages is aggregated and discounted to 2015 net present values, which is when the SSP2-4.5 scenario, and hence the AMOC weakening, starts. We use a social discount rate based on the deterministic Ramsey rule, with elasticity of marginal utility of consumption $\eta = 1.05$ and rate of pure time preference $\delta = 0.5\%$ as in META, and the global growth rate as projected by the SSP2-4.5 scenario. Because the META model variables for consumption and damages are given in 2010 US dollar values, we adjust them to 2024 US dollar values by multiplying with 1.44 based on inflation rates.

For all economic calculations, we retain the parameter values of the most recent version of META (Github, Dietz et al., 2021); the values are also given in the text box of Fig. B5. The damage persistence parameter φ describes the amount of climate damage that is still felt in the year after the damage is caused. A φ value of 1 means there is no persistence; a φ value of 0 means there is full persistence. The value $\varphi = 0.25$, as used in the META model, is calibrated based on Nath et al., 2024. The results of a sensitivity analysis on η, δ, φ, and the damage function coefficient are shown in the SI Appendix, Table S4.

Assessing SCC changes

The SCC effect of the AMOC carbon feedback is estimated in the base META model, without any further feedbacks or tipping dynamics activated. Since META does not optimize, this SCC estimate is contingent on the underlying socioeconomic scenario, in our case SSP2-4.5 (and for two AMOC projections also SSP5-8.5 and SSP1-2.6). We always report values for the SCC in 2020.

We determine the relative SCC impact of including the AMOC carbon feedback through

$$\Delta SCC = \frac{SCC_{\text{AMOC}} - SCC_{\text{no AMOC}}}{SCC_{\text{no AMOC}}}. \tag{11}$$

We always compare the base META model ("no AMOC") and the META model with the activated AMOC carbon feedback ("AMOC") for the same Monte Carlo sample so that the difference between these two values stems only from the inclusion of the AMOC carbon feedback, not from uncertain parameters that differ between runs. This results in 10,000 estimates of the relative SCC effect ΔSCC of the AMOC carbon feedback, which are depicted in Fig. B5.

Code availability

All code used to analyze the data and produce the results and figures of this paper can be accessed at https://doi.org/10.5281/zenodo.14290084. The ESM output data required to reproduce the results are all located in the data subfolder of this repository. The modified version of the META model that is used to integrate the AMOC carbon feedback can be found here https://doi.org/10.5281/zenodo.14290001.

ACKNOWLEDGMENTS

We are grateful for comments and support from Moritz Drupp, Johanna Baehr, Chao Li, Tatiana Ilyina, Leonard Borchert, Helmuth Haak, Karl-Hermann Wieners, Alexandra Herter, Jochem Marotzke, David Nielsen, and Paul Waidelich. We also thank audiences at AGU23, EGU24, and EAERE24 for insightful comments and questions, as well as the META developers for making their model open-source, and the German Climate Computing Center (DKRZ) for providing computational resources. We acknowledge funding by the Deutsche Forschungsgemeinschaft (DFG, German Research Foundation) under Germany's Excellence Strategy – EXC 2037 'CLICCS - Climate, Climatic Change, and Society' – Project Number: 390683824.

AUTHOR CONTRIBUTIONS

F.S. designed the research; F.S. and E.A. performed the research, analyzed the data, and wrote the paper. The authors declare no competing interests.

B.8 SUPPLEMENTARY INFORMATION

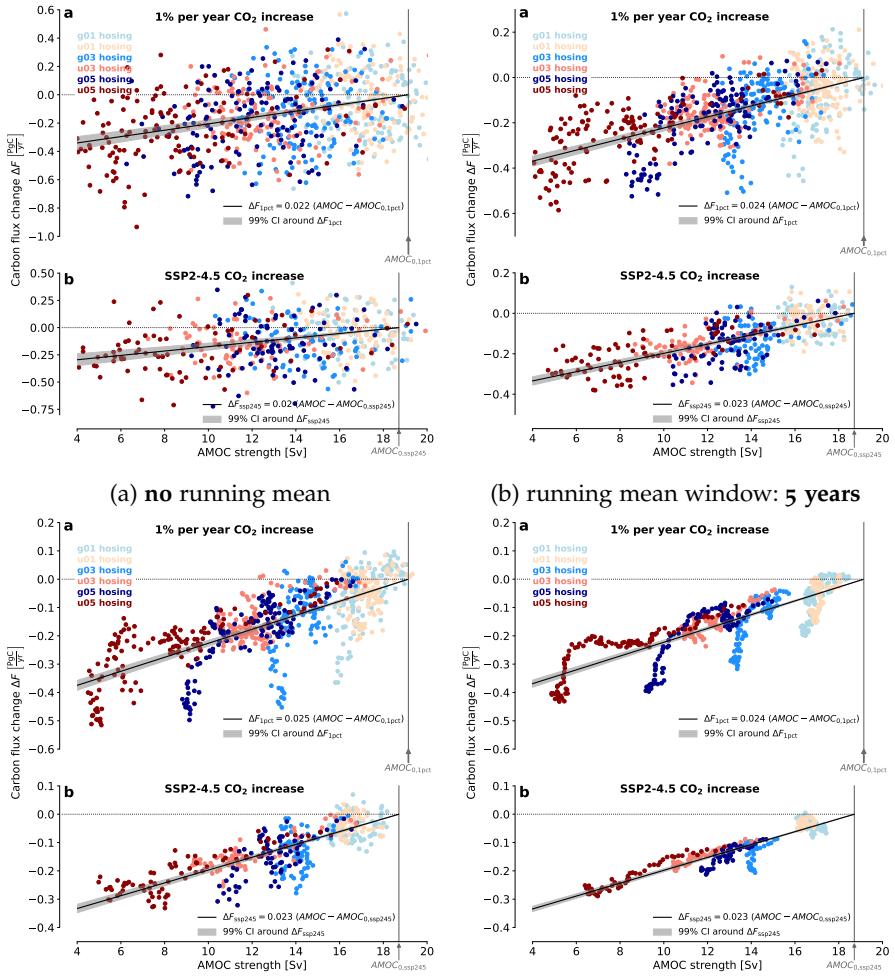

(a) **no** running mean

(b) running mean window: **5 years**

(c) running mean window: **10 years**

(d) running mean window: **30 years**

Figure B.S1: Each panel shows a version of Fig. B3 in the paper, but for different running mean windows. The main specification is a running mean window of 10 years, such that panel **(c)** corresponds exactly to Fig. B4. The same running mean is applied to both the AMOC strength and the carbon storage time series. Note that panels **(a)** and **(b)** have wider y-axes due to higher fluctuations in the unsmoothed data. The regression coefficients, as plotted in each panel for both 1pct experiment and SSP2-4.5 scenario, are recalculated in for each running mean window size and are approximately constant across the different running mean configurations.

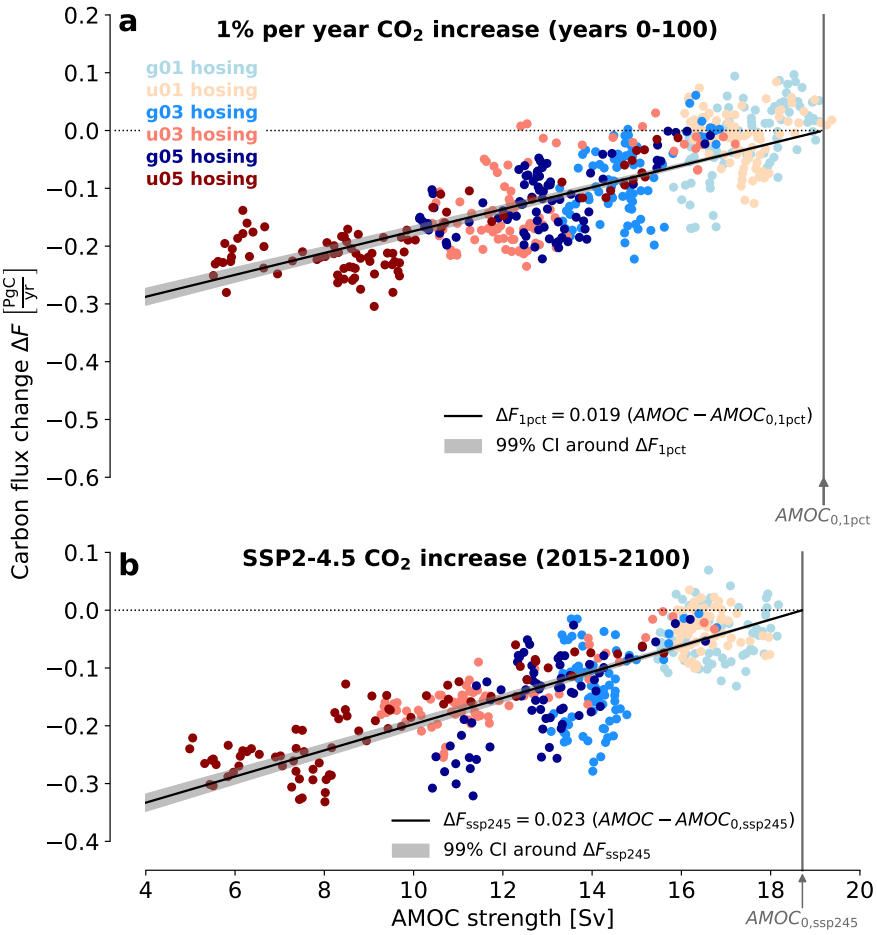

Figure B.S2: A version of Fig. B3 in the paper, but omitting all data points of the 1pct experiment between year 100 and year 140. The reason for this robustness check is that between years 100 and 140, most 1pct hosing simulations show a substantial increase in carbon flux reductions (see also Fig. B2 in the paper). When omitting these 40 years of simulations, the linear regression coefficient weakens by around one quarter (0.019 rather than 0.025).

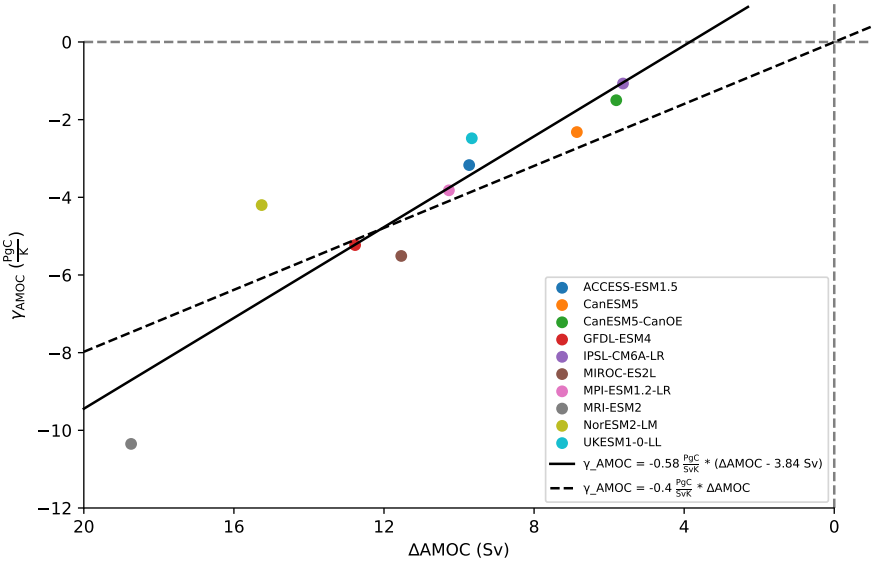

Figure B.S3: AMOC-related carbon-climate feedback γ_{AMOC} as a function of AMOC weakening $\Delta AMOC$. All values are taken from Katavouta and Williams, 2021, and as in Katavouta and Williams, 2021, the CNRM model is omitted due to unrealistic values for regenerated carbon. Two regression lines are estimated, the thick line as a linear linear regression with a constant order term, and the dashed line while forcing the intercept to be zero. For further calculations, we use the thick line which provides a better fit of the model data.

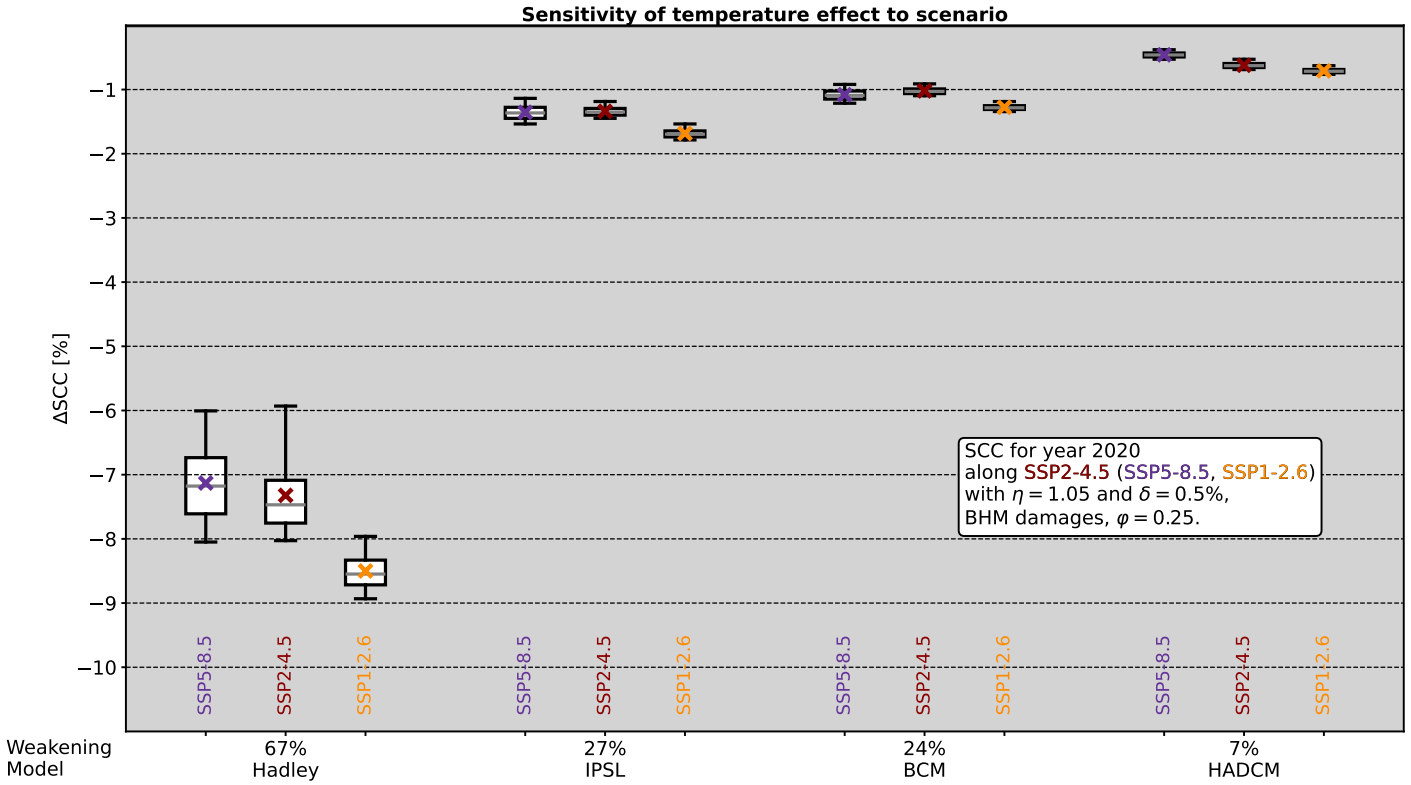

Figure B.S4: A version of Fig. B5 in the paper, but focusing only on the SCC effects of AMOC-induced temperature pattern changes in META (Dietz et al., 2021). For each climate model calibration, three different SSP scenarios are run for 1,000 Monte Carlo samples. The qualitative dependence of SCC changes on scenarios is the same as for the AMOC carbon feedbacks (effects are less/more pronounced in the SSP5-8.5/SSP1-2.5 scenario), but the dependence is weaker in the case of the temperature effect.

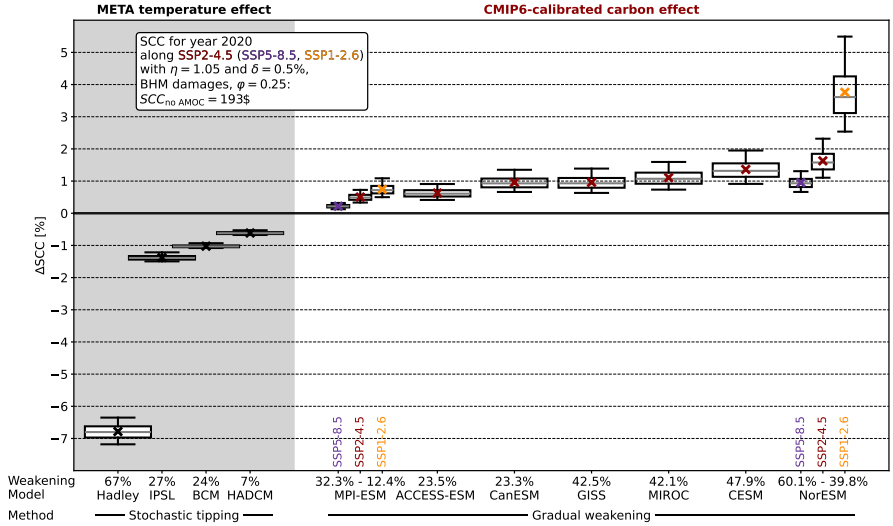

(a) A version of Fig. B5 in the paper with 0.1% of the most extreme Monte Carlo values trimmed on each tail of the distribution.

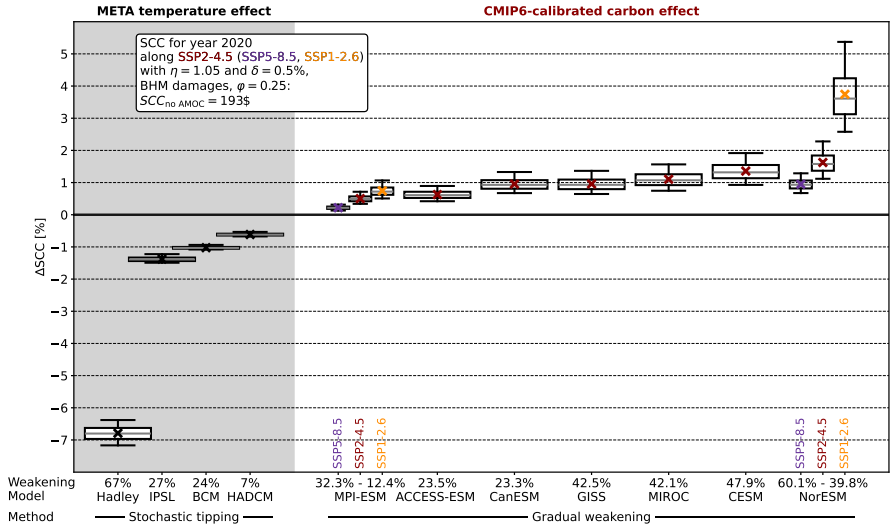

(b) A version of Fig. B5 in the paper with 1% of the most extreme Monte Carlo values trimmed on each tail of the distribution.

Figure B.S5: The effect of trimming the tails of Monte-Carlo-generated SCC distributions. Fig. B5 in the paper shows the distribution of all 10,000 Monte Carlo samples. In order to test the robustness of these results to trimming extreme values at the tails of the distribution, we here show two additional versions of Fig. B5 with trimmed distributions. Panel **(a)** shows trimming of the 0.1% most extreme values at each tail; panel **(b)** shows trimming of the 1% most extreme values at each tail.

Table B2: BGC-only simulations conducted in MPI-ESM1.2-LR.

Atm. CO_2 concentration	Hosing period	Hosing pattern	Hosing strength	Label
1% per year CO_2 increase	—	—	—	no hosing
1% per year CO_2 increase	year 0 - 140	uniform in North Atlantic	0.1 Sv	u01 hosing
1% per year CO_2 increase	year 0 - 140	uniform in North Atlantic	0.3 Sv	u03 hosing
1% per year CO_2 increase	year 0 - 140	uniform in North Atlantic	0.5 Sv	u05 hosing
1% per year CO_2 increase	year 0 - 140	decaying around Greenland	0.1 Sv	g01 hosing
1% per year CO_2 increase	year 0 - 140	decaying around Greenland	0.3 Sv	g03 hosing
1% per year CO_2 increase	year 0 - 140	decaying around Greenland	0.5 Sv	g05 hosing
SSP2-4.5 scenario	—	—	—	no hosing
SSP2-4.5 scenario	2015 - 2100	uniform in North Atlantic	0.1 Sv	u01 hosing
SSP2-4.5 scenario	2015 - 2100	uniform in North Atlantic	0.3 Sv	u03 hosing
SSP2-4.5 scenario	2015 - 2100	uniform in North Atlantic	0.5 Sv	u05 hosing
SSP2-4.5 scenario	2015 - 2100	decaying around Greenland	0.1 Sv	g01 hosing
SSP2-4.5 scenario	2015 - 2100	decaying around Greenland	0.3 Sv	g03 hosing
SSP2-4.5 scenario	2015 - 2100	decaying around Greenland	0.5 Sv	g05 hosing

Table B3: Regressions of carbon flux changes on AMOC strength.

Name	Intercept $\left[\frac{\text{Pg}}{\text{yr}}\right]$	Slope c_0/c_2 $\left[\frac{\text{Pg}}{\text{yr Sv}}\right]$	Std. error of slope $\left[\frac{\text{Pg}}{\text{yr Sv}}\right]$
$\Delta F_{0,\,\text{ssp245}}$	0 by definition	0.023	0.0004
$\Delta F_{1,\,\text{ssp245}}$	-0.0013	0.022	0.0008
$\Delta F_{0,\,\text{1pct}}$	0 by definition	0.025	0.0004
$\Delta F_{1,\,\text{1pct}}$	0.010	0.026	0.0008

See Methods for underlying regression equations.

Table B4: Sensitivity analysis with respect to modified surface temperature patterns.

AMOC projection	ΔSCC pattern scaling	ΔSCC Hadley pattern	ΔSCC IPSL pattern	ΔSCC BCM pattern	ΔSCC HADCM pattern
MPI-ESM1.2-LR	0.50 %	0.51 %	0.50 %	0.50 %	0.51 %
ACCESS-ESM1-5	0.63 %	0.63 %	0.63 %	0.63 %	0.64 %
CanESM5	0.95 %	0.95 %	0.95 %	0.95 %	0.95 %
GISS-E2-1-G	0.96 %	0.96 %	0.96 %	0.96 %	0.97 %
MIROC-ES2L	1.11 %	1.11 %	1.11 %	1.11 %	1.12 %
CESM2	1.36 %	1.36 %	1.36 %	1.36 %	1.37 %
NorESM2-LM	1.63 %	1.63 %	1.63 %	1.63 %	1.64 %

This table reports SCC results with the deterministic META model for all seven CMIP6-calibrated AMOC projections. The second columns report the SCC values as they are in the last column of Table 1, with the only difference being that they use the deterministic META model and not the mean of 10,000 Monte Carlo runs. The remaining four columns show the same quantity, but with modified pattern scaling. Given that AMOC weakening is expected to alter surface temperature patterns, we test the robustness of the carbon-caused SCC effect on the assumption of AMOC-induced temperature patterns. The second columns assumes that AMOC weakening doesn't influence the pattern scaling, whereas the other four columns overlay the AMOC-induced changes in surface temperature patterns used in Anthoff et al., 2016 and Dietz et al., 2021. Every prescribed temperature pattern change starts in 2015, is linearly phased in until the year 2050, and stays constant after that. As the results show, the SCC effect of the AMOC carbon feedback does not depend on the specific assumption on how pattern scaling develops in this century.

Table B5: Sensitivity analysis with respect to discounting and damage function parameters.

η	δ	φ	Damage function calibration	Additional damages (MPI-ESM | NorESM)	Absolute SCC (MPI-ESM | NorESM)	SCC change (MPI-ESM | NorESM)
0.8	0.1%	0.25	central	12.3 trillion $ | 27.8 trillion $	384.7 $ | 390.4 $	0.67 % | 2.19 %
0.8	0.5%	0.25	central	7.3 trillion $ | 16.0 trillion $	261.8 $ | 265.3 $	0.61 % | 1.97 %
0.8	1.0%	0.25	central	3.8 trillion $ | 8.2 trillion $	171.1 $ | 173.1 $	0.52 % | 1.70 %
1.05	0.1%	0.25	central	6.6 trillion $ | 14.6 trillion $	277.9 $ | 281.7 $	0.61 % | 1.98 %
1.05	0.5%	0.25	central	3.9 trillion $ | 8.5 trillion $	197.3 $ | 199.7 $	0.54 % | 1.75 %
1.05	1.0%	0.25	central	2.2 trillion $ | 4.5 trillion $	135.8 $ | 137.2 $	0.46 % | 1.48 %
1.5	0.1%	0.25	central	2.2 trillion $ | 4.8 trillion $	194.5 $ | 196.7 $	0.44 % | 1.58 %
1.5	0.5%	0.25	central	1.4 trillion $ | 2.9 trillion $	148.8 $ | 150.2 $	0.38 % | 1.34 %
1.5	1.0%	0.25	central	0.8 trillion $ | 1.6 trillion $	111.6 $ | 112.5 $	0.33 % | 1.13 %
1.05	0.5%	1.0	low	0.7 trillion $ | 1.5 trillion $	30.0 $ | 30.4 $	0.57 % | 1.83 %
1.05	0.5%	1.0	central	1.2 trillion $ | 2.7 trillion $	54.0 $ | 54.7 $	0.60 % | 1.91 %
1.05	0.5%	1.0	high	1.8 trillion $ | 3.9 trillion $	78.4 $ | 79.5 $	0.62 % | 1.95 %
1.05	0.5%	0.25	low	2.3 trillion $ | 5.0 trillion $	112.1 $ | 113.5 $	0.53 % | 1.72 %
1.05	0.5%	0.25	central	3.9 trillion $ | 8.5 trillion $	197.3 $ | 199.7 $	0.54 % | 1.75 %
1.05	0.5%	0.25	high	5.2 trillion $ | 11.5 trillion $	280.2 $ | 283.5 $	0.54 % | 1.75 %
1.05	0.5%	0.0	low	7.9 trillion $ | 14.9 trillion $	2142.2 $ | 2162.7 $	0.45 % | 1.41 %
1.05	0.5%	0.0	central	-1.0 trillion $ | -6.5 trillion $	4078.2 $ | 4119.2 $	0.49 % | 1.50 %
1.05	0.5%	0.0	high	-307.2 trillion $ | -772.0 trillion $	6136.8 $ | 6196.3 $	0.47 % | 1.45 %

η is the marginal elasticity of intertemporal substitution; δ is the rate of pure time preference; φ is the persistence parameter (0 corresponds to full persistence, 1 corresponds to no persistence); the damage function calibration is taken from Dietz et al., 2021 and represents the Burke-Hsiang-Miguel damage function (Burke et al., 2015) for "central" values, while "low" and "high" values refer to the boundaries of the 95% confidence interval of the coefficients from Burke et al., 2015. Additional damages and SCC change are obtained like the values in Table 1 of the paper. SCC values are calculated for the year 2020 along the SSP2-4.5 scenario and given in 2010 USD. The AMOC is calibrated to MPI-ESM and NorESM projections, accordingly, because these two calibrations bound our impact estimates and serve to show the most extreme possible effects of a sensitivity analysis.

C

EUROPEAN HEAT EXTREMES UNDER NET-ZERO EMISSIONS

The work in this chapter was published as:

Alastrué de Asenjo, E., King, A. D., & Ziehn, T. (2025). European heat extremes under net-zero emissions. *Environmental Research Letters*, *20*(7), 074029. https://doi.org/10.1088/1748-9326/addee4

Contributions: Together with A. D. King, I conceptualised the study and the methodology. T. Ziehn and I curated the data. I implemented the software, performed the analysis and investigation, visualised the results, and wrote the original draft. All authors participated in discussing the results and in revising the final manuscript.

Note: The version here included contains minor formatting changes with respect to the published version.

European heat extremes under net-zero emissions

Eduardo Alastrué de Asenjo[1,2], Andrew D King[3,4], Tilo Ziehn[5]

[1] Institute of Oceanography, Center for Earth System Research and Sustainability (CEN), University of Hamburg, Hamburg, Germany.
[2] Max Planck Institute for Meteorology, Hamburg, Germany.
[3] ARC Centre of Excellence for the Weather of the 21st Century.
[4] School of Geography, Earth and Atmospheric Sciences, University of Melbourne, Melbourne, Kulin nations, Australia.
[5] CSIRO Environment, Aspendale, Kulin nations, Australia.

ABSTRACT

Projections of European heat extremes have been widely explored in the context of continued global warming. However, analyses of recent Earth system model simulations point to substantial climatic changes over multi-centennial timescales in net-zero emissions futures. Focusing on Europe, we address the gap in characterising heat extremes in long-term net-zero stabilised climates. We quantify the long-term effects of delayed mitigation on annual maximum daily maximum temperatures (TXx) in European regions using 1000-year-long stabilised simulations with ACCESS-ESM-1.5, reaching net-zero CO_2 emissions at different times over the coming decades. We evaluate ACCESS-ESM-1.5 against the ERA5 reanalysis for European maximum temperatures using rank frequency analysis and compare present-day maximum temperatures to their long-term future likelihood. Across all European regions, any delay in achieving net-zero emissions shifts the distribution to higher annual maximum temperatures, remaining elevated at the same levels for centuries. European regions show two- to five-fold frequency increases for heat events as strong as current records, while the Mediterranean region could experience 30-fold increases if emissions cessation is delayed until 2060. When comparing extreme heat distributions at global warming levels, we find substantial differences between transient and net-zero emissions quasi-stable climate states, with larger differences at higher warming levels. We provide the first comprehensive assessment of European extreme hot temperatures in net-zero stabilised climates, paving the way for further investigations of other extreme event types or regions in net-zero futures.

C.1 INTRODUCTION

Although the goal of achieving net-zero emissions is among the core concepts surrounding climate science and policy, temperature responses to net-zero emissions are as yet largely uncertain, particularly regional and local changes (e.g., MacDougall et al., 2022). Regionally, mean temperatures vary under net-zero emissions, while extreme temperature changes have not been comprehensively analysed. Projected changes in temperature extremes under net-zero emissions are of particular interest for Europe, where heat extremes have increased faster than in any other mid-latitude region in recent years (e.g., Rousi et al., 2022; Vautard et al., 2023). Existing analyses of heat extremes in idealised net-zero simulations did not concentrate on European regions and focused on monthly extremes rather than daily timescales (Cassidy et al., 2024). Moreover, recent 1000-year-long net-zero Earth system model future simulations suggest long-term temperature changes not captured in shorter net-zero experiments (King et al., 2024). Thus, the long-term evolution of European heat extremes in stabilised net-zero futures remains an open question.

Several modelling frameworks have been used to improve understanding of post-net-zero changes. The main activity is currently the Zero Emissions Commitment Model Intercomparison Project (ZECMIP, Jones et al., 2019), focused on the committed amount of global mean temperature change after emissions cessation. The residual between warming from oceanic thermal inertia and cooling from the natural global carbon sink results in a small and uncertain committed global temperature change (MacDougall et al., 2020). Even though this global temperature change is expected to be small, it is significantly different from internal variability (Borowiak et al., 2024), with substantial changes occurring regionally (MacDougall et al., 2022).

Despite these efforts, existing net-zero emissions simulations performed as part of the Coupled Model Intercomparison Project Phase 6 (CMIP6, Eyring et al., 2016) are not long enough to address climate stabilisation around policy-relevant temperature targets (King et al., 2021b). Zero-emissions temperature commitments are often assessed 50-150 years after emissions cessation despite recognising additional long-term changes (Palazzo Corner et al., 2023). These long-term changes imply that mitigation and adaptation measures around temperature targets would be inconsequential beyond the end of the century if they do not adequately address the eventual impacts of cumulative emissions. A recent net-zero emissions modelling effort was conducted with longer simulations, but focused on ocean circulation responses (Sigmond et al., 2020). While there are long-term stabilisation frameworks for constant atmospheric carbon dioxide concentrations (e.g., LongRunMIP, Rugenstein et al., 2019), they can-

not be used to understand committed changes under net-zero emissions (Matthews & Weaver, 2010), and therefore a long-term net-zero-emissions modelling protocol is needed (King et al., 2021b).

King et al., 2024 bridge this gap by proposing extended net-zero emissions simulations explicitly constructed to understand long-term climate stabilisation and the effects of delayed mitigation. They introduce net-zero Earth system model simulations spanning 1000 years, a timescale proving crucial as significant changes continue after the initial centuries (King et al., 2025a). Each simulation represents a net-zero CO_2 emissions trajectory beginning at different points in the 21st century. All simulations result in a slow but significant global mean surface temperature increase (0.03-0.05°C/century), as Southern Ocean warming (slow response to CO_2 forcing, Chamberlain et al., 2024) continues, and most regions show weaker changes. Such changes occur also over Europe, both for annual and summer mean temperatures (King et al., 2024). Nonetheless, whether this extends to European temperature extremes is as yet unknown.

European heat extremes have been thoroughly investigated as a result of their rapidly increasing likelihoods, intensities, and impacts, particularly since the unprecedented 2003 European heatwave, which resulted in thousands of excess fatalities (e.g., Christidis et al., 2015; Rousi et al., 2022; Vautard et al., 2023). While European heat extremes for different global mean temperature targets or decarbonisation scenarios show substantial benefits from stronger mitigation, these results are limited to transient simulations before the end of the century (King & Karoly, 2017; Suarez-Gutierrez et al., 2018; Diffenbaugh et al., 2023). A recent study based on ZECMIP net-zero emissions simulations found frequencies of local continental heat extremes to globally remain constant or decrease by up to 40% (Cassidy et al., 2024). However, this study did not focus on the effects on Europe or its regions, and the ZECMIP simulations also have other limitations, such as starting from a highly idealised concentration-driven 1pctCO2 experiment (1% increase/year in CO_2 concentrations) or a relatively short simulation period of only about 100 years after emissions cessation.

Here, we study the long-term (multi-centennial) evolution of European heat extremes under net-zero emissions. We use the same framework and 1000-year-long simulations from King et al., 2024; which enable us to characterise heat extremes in European regions in quasi-stable climates, understanding not only how they might change, but also the consequences of delayed mitigation and the implications at relevant global mean temperature targets.

C.2 DATA AND METHODS

C.2.1 *Earth system model data*

This study focuses on multi-centennial timescales in net-zero climates, and therefore, we use the simulations introduced by King et al., 2024. These extended net-zero CO_2 emissions simulations are performed with the Australian Community Climate and Earth System Simulator (ACCESS) ESM version 1.5 (Ziehn et al., 2020). ACCESS-ESM-1.5, part of CMIP6, has an atmospheric resolution of 1.875° longitude and 1.25° latitude, 1° in the ocean, and 40 initial-condition ensemble members for the historical experiment (1850-2014) and several concentration-driven 21st-century scenarios (2015-2100). There are seven 1000-year net-zero experiments, branched respectively from 2030 to 2060 in five-year intervals. They are initialised from the same ensemble member of a transient, emissions-driven future scenario, specifically the fossil-fueled development and high-forcing SSP5-8.5 (O'Neill et al., 2016). CO_2 emissions are set to zero at the branching year, while other greenhouse gases and anthropogenic aerosols are reset to 1850 levels.

C.2.2 *Extreme heat and attribution metrics*

To characterise European heat extremes, we use the annual TXx index. Annual TXx is defined by the Expert Team on Climate Change Detection and Indices (ETCCDI, e.g., Sillmann et al., 2013) as the annual maximum of daily maximum temperatures (variable *tasmax* in CMIP6). This index is impact-relevant in multiple contexts (e.g., structural engineering), and it is more appropriate for large spatial comparisons than threshold-based indices (Zhang et al., 2011). We calculate this index for each grid cell and then average over a region when appropriate. All values shown are anomalies relative to the reference period 1961-1990.

Attributing likelihoods of occurrence involves calculating metrics such as risk ratios (RRs) and fractions of attributable risk (FARs). For the attribution of events, we define the counterfactual world as the period 1995-2024 in the historical and concentration-driven SSP5-8.5 concatenated 40-member ensemble. We adopt this 30-year period to stand for a representation of the perceived present-day climate conditions. This representation is largely scenario-independent, as scenarios show a similar global mean temperature trajectory before 2035. Other metrics or approaches could have been followed (i.e., causal counterfactual theory; Hannart et al., 2016), but RRs and FARs are more straightforward to interpret in an experimental setup not designed specifically for the causal attribution of drivers. We compute

$$\mathrm{RR} = \frac{P_{NZ}}{P_0} \quad \text{and} \quad \mathrm{FAR} = 1 - \frac{P_0}{P_{NZ}},$$

where P_{NZ} and P_0 are the probabilities above a given threshold in the full net-zero experiments and the 1995-2024 historical+SSP5-8.5 ensemble, respectively (e.g., Stott et al., 2016).

C.2.3 *Model evaluation with reanalysis data*

To test whether ACCESS-ESM-1.5 appropriately represents the historical frequency and intensity of European annual TXx, we evaluate it against the fifth generation of the European Centre for Medium-Range Weather Forecasts Retrospective Analysis (ERA5, Hersbach et al., 2020). We calculate annual TXx in ERA5 also from the maximum of daily maximum temperature (*mx2t* variable). Spatial resolutions differ between ERA5 and ACCESS-ESM1.5 (31 km grid for ERA5), but regridding ERA5 data (through bilinear interpolation) to the coarser ACCESS-ESM-1.5 grid did not alter the main conclusions presented here.

We evaluate ACCESS-ESM-1.5 in the rank frequency analysis framework (Suarez-Gutierrez et al., 2018, 2021). This framework utilises initial-condition large ensembles to assess whether both their forced and internal variability are compatible with observations (or the ERA5 reanalysis, in this study). If that is the case, no ordered position that ERA5 annual TXx values take each year in comparison to the ensemble values for that year (i.e., the rank) should be favoured. If the resulting histogram is fairly flat, the model adequately captures observations, while a tilted histogram signals a systematic bias. Therefore, ACCESS-ESM-1.5 can be evaluated based on the flatness of a rank histogram of annual TXx ERA5 values compared to the large ensemble. To assess flatness and establish some tolerance range, we follow previous studies by smoothing the histogram, calculating its slope with a 7-bin (one bin per rank) window rolling mean for each rank. The expected flatness range given internal variability is calculated by repeating the process but now substituting ERA5 for each ensemble member (known as perfect model approach), and using a 7-bin slope central 75% confidence range, i.e., the slope's 12.5th and 87.5th ensemble percentiles for each rank. If the resulting ERA5 slope lies within the perfect model range, the model can be considered to appropriately represent annual TXx variability in ERA5.

C.2.4 *Global warming levels definition*

We also follow King et al., 2024's approach to defining global warming levels (GWLs). It is based on time-slices around a particular global mean surface temperature level (Schleussner et al., 2016). GWLs of 1.5, 2, and 3°C are considered relative to the 1850-1900 historical mean, with a ±0.2°C tolerance around the target. Decadal global temperature values (10-year running means) are used to reduce the effects of

internal variability. We differentiate between transient (SSP5-8.5 ensemble), early stable (net-zero experiments, years 100-450), and late stable (net-zero experiments, years 650-1000) GWLs. These conditions result, for the net-zero experiments, in GWLs almost fully belonging to a single experiment in each case and, as in King et al., 2024, we restrict our definition of GWLs to those experiments.

C.3 RESULTS

Throughout the analysis, we consider both Europe as a whole and also differentiate among four European reference regions according to the AR6 WGI (Iturbide et al., 2020): Northern Europe (NEU), Western and Central Europe (WCE), Eastern Europe (EEU), and Mediterranean (MED). We mask out the ocean to focus solely on land extremes and refer to Europe as the combination of all four regions.

To better interpret the implications of region-aggregated TXx indices, we first characterise the spatial signal underlying ERA5 annual TXx records through rank plots (figure C1). Such spatial rank plots offer a better visual representation than temperatures for large regions, as temperatures can vary substantially for different locations. For every TXx region-mean record year, we calculate each grid cell rank against all preceding years. For the TXx records in smaller regions, the spatial signals show that records arise from one large particular regional heat extreme event (which we corroborate by calculating monthly TXx indices, figure C.S1), while for Europe it often results from a combination of heat episodes in several regions in a given summer (figure C1a). For Europe, the record year is 2021 (figure C1a), with some of the warmest maximum temperatures measured in both EEU (June, figure C.S1d) and MED (August, figure C.S1o), having no precedent in the number of summer extreme heat days (Lhotka & Kyselý, 2022). The record for NEU is in 2018 (figure C1b), as a result of a widespread event in July (figure C.S1g, Yiou et al., 2020). For WCE, the record is 2019 (figure C1c), from an unusually early event in the last week of June (figure C.S1c, Vautard et al., 2020). In EEU, the record largely corresponds to the 2010 Russian heatwave (figure C1d), spanning the end of July and early August (figure C.S1n), a record anomaly in peak, duration, and extent (Barriopedro et al., 2011; Russo & Domeisen, 2023), and representing the deadliest measured extreme weather event in the last 20 years (Otto et al., 2024). Lastly, 2023 is the record year in MED (figure C1e), driven by record-breaking temperatures in July (figure C.S1j, Sun et al., 2025). Having gained a clearer insight into what type of events annual regional TXx means encapsulate, we move on to examine the temporal evolution of these indices.

All resulting annual TXx time series for Europe and its regions show an overall similar behaviour (figure C2). In the early histor-

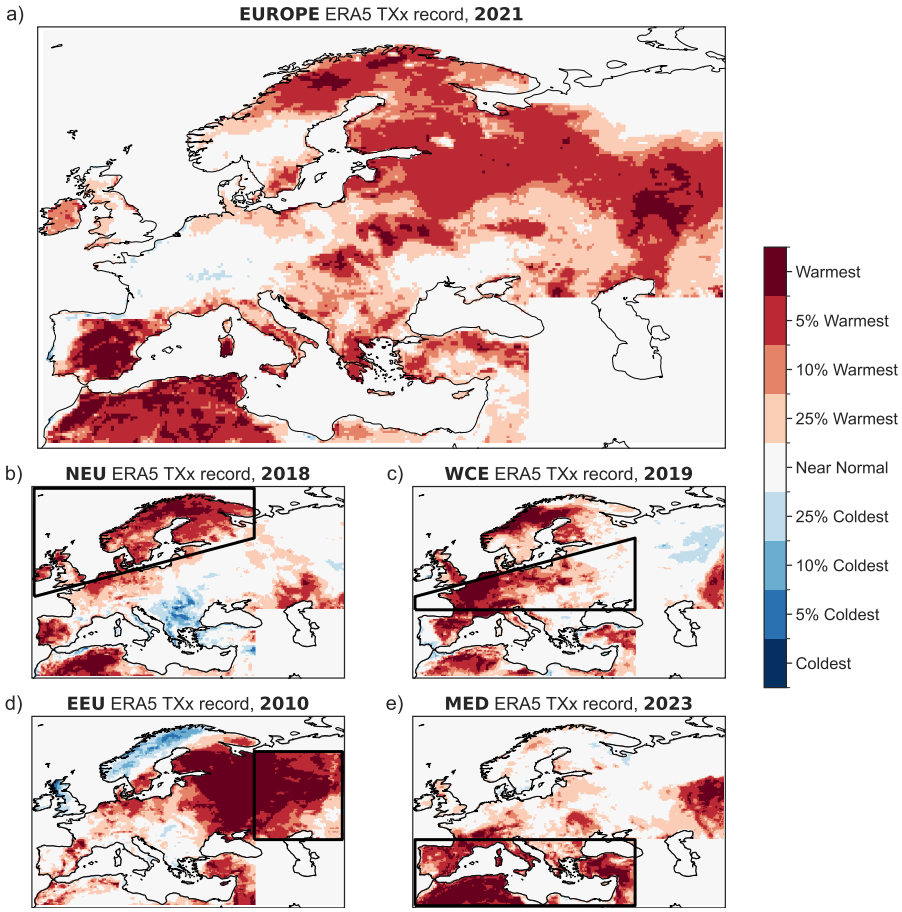

Figure C1: TXx ranks in ERA5 at every European grid cell for the year when the regional-averaged TXx is a record in a) Europe, b) Northern Europe, c) Western & Central Europe, d) Eastern Europe, and e) Mediterranean (regions are indicated by the black boxes). Ranks are calculated relative to the years preceding the event.

ical simulations, there is a slight declining trend (yielding about a 1°C cooling), likely driven by the mean cooling response to anthropogenic aerosols, quite prominent in ACCESS-ESM simulations (Rashid et al., 2022). Towards the end of the 20th century, as anthropogenic greenhouse gases continue to increase and aerosols decline, there is a strong TXx warming response in all regions. In current climate conditions (1995-2024), ERA5 has a positive 0.62°C/decade linear trend, well within the model spread (0.17 to 1.3 °C/decade in historical+SSP5-8.5, table C1). Until the end of the century, SSP5-8.5 projects a continued quasi-linear increase of TXx in all European regions, with the European ensemble mean almost reaching a 10°C anomaly by 2100 (figure C2a). In contrast, the net-zero experiments show a stationary behaviour for 1000 years in all regions, with no trend in any experiment being larger than 0.006°C/decade, table C1). However, each TXx stabilisation level is separated and increasingly higher for each five-year mitigation delay. Differences between sta-

bilisation levels increase for later emissions cessation years, with approximately 0.3°C differences between simulations branched earlier, and up to 0.5°C in those branched towards 2060. These differences account for 2.8-4.8°C total mean TXx increases in the European mean relative to the 1960-1990 baseline, with roughly similar values for all regions. This long-term stable TXx behaviour is accompanied by strong interannual variability. This variability does not depend much on the emissions cessation year and it is smaller in MED (0.6°C standard deviation, figure C2e) than in all other regions (1.5-2°C), as the Mediterranean Sea's influence moderates extreme changes. If instead of annual values we inspect 11-year averages to remove interannual variability, still some (multi-)decadal variability persists but the distinction between each simulation can be made much more clearly (figure C.S2).

To continue the interpretation of the resulting TXx values in the stabilisation experiments, we require a model evaluation step beyond the apparent agreement between the ERA5 trend and variability (1940-2024) and the historical ensemble. The evaluation through rank frequency analysis demonstrates a satisfactory performance of the ACCESS-ESM-1.5 European TXx values relative to ERA5 (figure C3). Histogram slopes fall within the range given by the perfect model approach in virtually all cases, except for one central range value for WCE, where the ERA5 slope is larger but almost overlaps with the model range. For Europe, WCE, and EEU, the very extreme ranks seem underrepresented in ERA5 relative to the model, with fewer cases for the two lowest or highest ranks. This could signal a slight model overestimation of TXx variability in these regions, but the slope values still fall within the model range at these edges. Overall, European TXx mean and variability are well captured by the model, which provides confidence in assessing extreme heat occurrence in the net-zero simulations.

Likelihoods of occurrence are visualised through probability density functions (PDFs, figure C4). PDFs are computed through non-parametric kernel density estimation and subsequently normalised. The resulting annual TXx PDFs exhibit a clear separation (approximately 1°C for Europe) between early historical (1850-1899) and current climates (1995-2024). This gap is most evident, in relative terms, in MED, where the recent past PDF has not just shifted but is also considerably wider, reflecting a variability increase and/or a strong recent trend (figure C4e). In the case of the net-zero experiments, the shift towards warmer TXx is large even relative to current climate distributions. The lack of a trend in Europe-wide and regional TXx means we can use all years in each net-zero emissions simulation to generate large samples for these PDFs. There is a significant warm shift for every five-year delay in emissions cessation (as obtained through pair-wise testing with an autocorrelation-adjusted KS test),

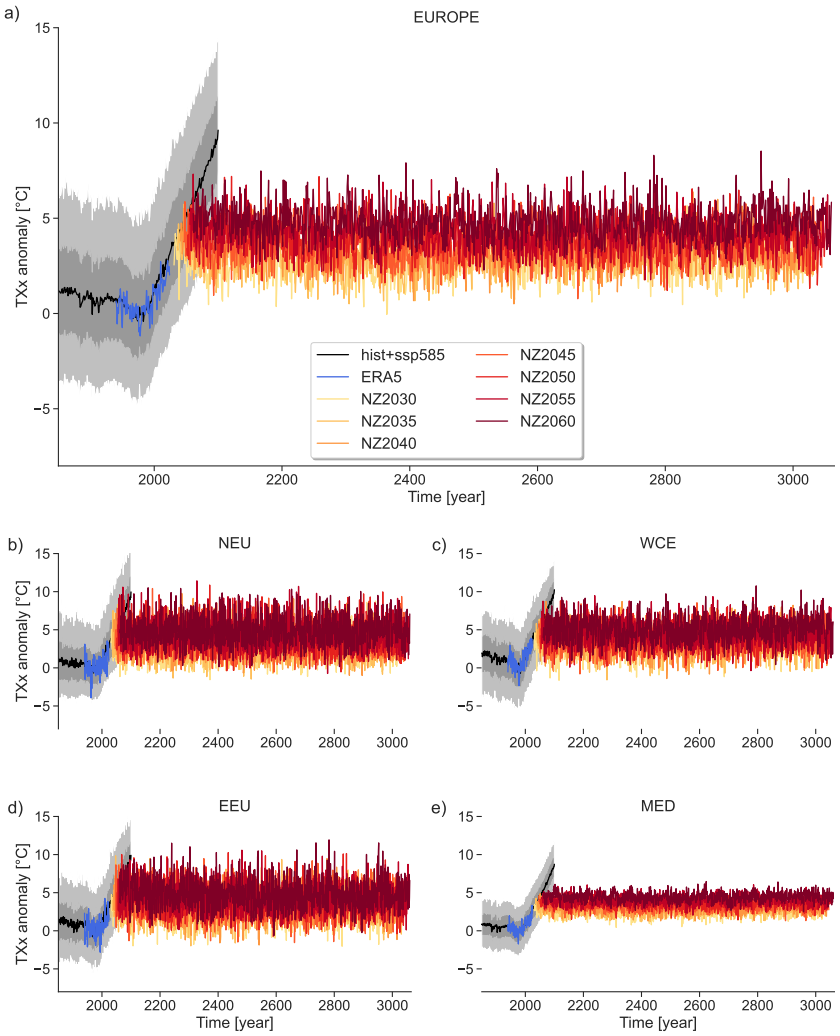

Figure C2: Annual TXx anomalies time series (relative to 1961-1990) averaged for a) Europe, b) Northern Europe, c) Western & Central Europe, d) Eastern Europe, and e) Mediterranean for ERA5 and ACCESS-ESM-1.5 simulations. For the historical+SSP5-8.5 ensemble, the black line is the ensemble mean, the dark grey shading the ensemble standard deviation, and the light grey shading the ensemble spread. Yellow to red lines are the net-zero emissions experiments, with each label's number representing the year of emissions cessation. Note that the net-zero experiments have been initialised from an emissions-driven realisation of the SSP5-8.5 scenario, which is within the range of the concentration-driven ensemble shown here.

but no clear change in variability. MED stands out again, as, despite having the smallest absolute changes and variability, this area exhibits the largest relative shifts between the past and current distributions (figure C4e). For all regions, we include the respective ERA5 annual TXx record (vertical blue lines in figure C4). Compared to current climate distributions, the ERA5 record is at the 79th percentile in Europe, 84th in NEU, 82nd in WCE, 88th in EEU, and 97th in MED.

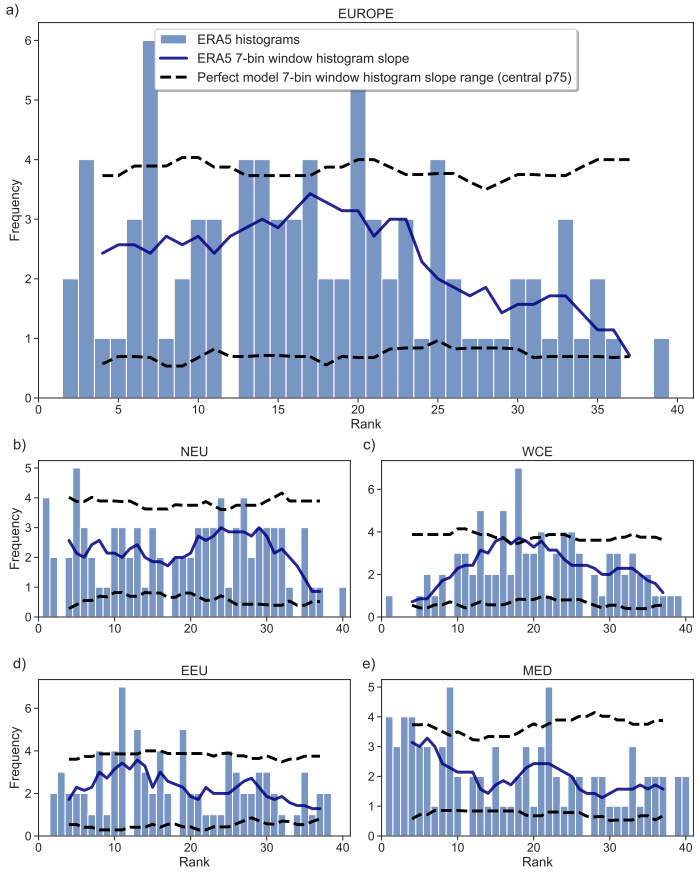

Figure C3: Rank histogram (one bin per rank) of the position of each ERA5 annual TXx value if compared to an ordered list of values from the ACCESS-ESM-1.5 ensemble (historical+SSP5-8.5) for the same year. The dark blue line represents the slope of the histogram, by calculating a 7-bin window rolling mean for each rank. Dashed black lines represent the 7-bin slope's perfect model central 75% confidence range, i.e., the slope's 12.5th and 87.5th percentiles of the ensemble when comparing each ensemble member against the rest of the ensemble. A flat histogram consistently within the model range indicates that ERA5 trend and variability are adequately captured, while a tilted histogram would signal a systematic bias.

Some of these percentiles are not particularly extreme. This may be due to a slight model variability overestimation or a lack of plausible hot extremes in the last few years given the limited ERA5 sample size and the strong underlying trend. All PDFs indicate that recent record TXx values, representing the upper tail of present-day distributions, become the average or colder than the average of net-zero futures for simulations with emissions cessation in 2050 or later.

We further extend the analysis of likelihoods by attributing the potential impacts of delays in emissions cessation through risk ratios (RRs, figure C5) and fractions of attributable risk (FARs, figure C.S3). These measures do not only represent likelihoods for a given TXx

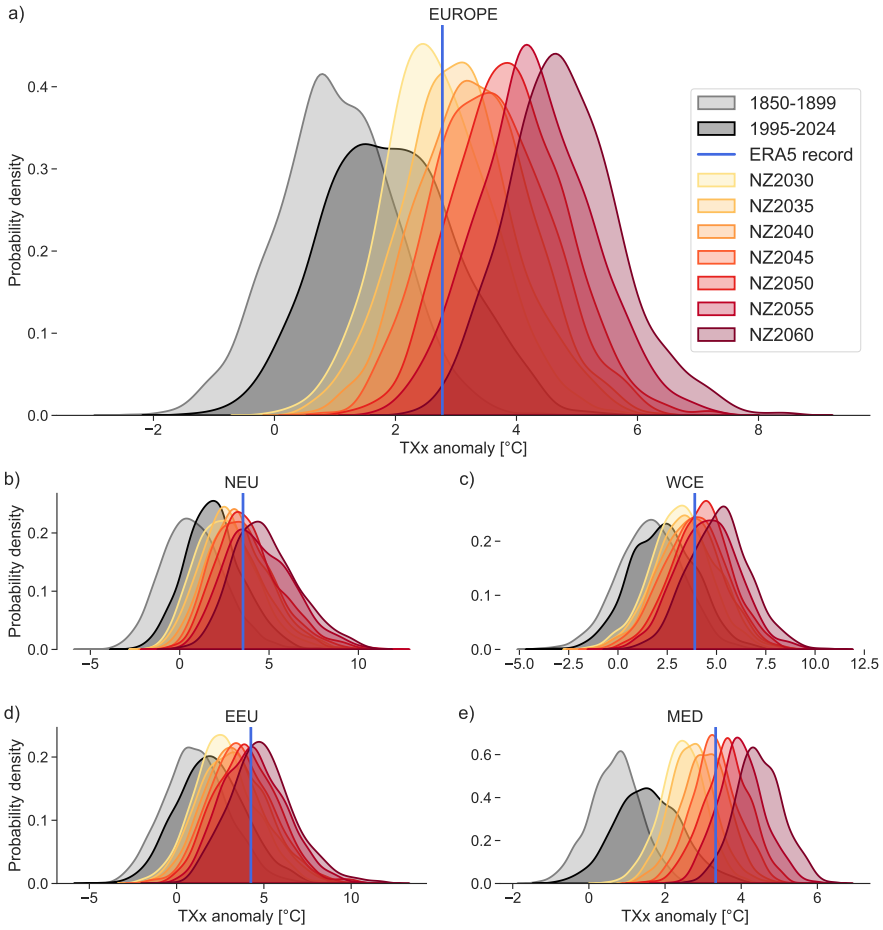

Figure C4: Probability distribution functions of annual TXx anomalies (relative to 1961-1990) averaged for a) Europe, b) Northern Europe, c) Western & Central Europe, d) Eastern Europe, and e) Mediterranean for ACCESS-ESM-1.5 simulations. Vertical blue lines indicate the maximum value of the TXx anomaly in ERA5 for the respective regions. The light and dark grey curves show the historical+SSP5-8.5 ensembles for an early and a recent period. Yellow to red lines are the net-zero stabilisation experiments, with the number of each label representing the year of emissions cessation.

value (as in the PDFs) but measure likelihoods above thresholds, potentially more meaningful when extrapolating the events' impacts. Relative to the present-day reference, risk ratios grow exponentially for increasing TXx thresholds. These increases result from distribution shifts towards warmer temperatures, with present-day TXx distribution tails representing values closer to the distribution means in the net-zero stabilised futures. Particularly, when assessing risk ratios for present-day ERA5 records (table C2), the values in most regions range from approximately 2 to 5, again with increasingly higher differences for later five-year mitigation delays. For MED, the increase is more substantial, with the likelihood of exceeding the ERA5 record

increasing up to 30-fold for the 2060 branched net-zero simulation relative to 1995-2024 (figure C5e). In the equivalent FARs (figure C.S3), the same general behaviour is shared by all regions; earlier cessation years are associated with lower FAR values than later cessation years. In fact, delays of just five years in mitigation make a measurable difference in the attributability of TXx changes relative to present-day values. Use of higher thresholds results in generally larger FARs, that often approach one for high enough thresholds. In MED, FARs are considerably larger and very close to one even for comparatively low thresholds (around 3°C, figure C.S3e). In some cases, particularly in EEU, FARs vary largely for high thresholds (figure C.S3d), changing from zero to one by small threshold increments. These large variations result from very few extreme cases at the end of the distributions' tails, also temporarily lowering the RRs below 1 (figure C5d). For thresholds at the ERA5 records, FARs generally increase from approximately 0.4 to 0.8 when delaying net-zero emissions until 2060, with a larger change (from 0.56 to 0.97) in MED (table C2). Overall, both RRs and FARs reveal increasingly hotter maximum temperatures in Europe with further delays in emissions cessation.

While European TXx values are stable but shift across net-zero emissions simulations, global temperatures slowly increase during these experiments (King et al., 2024). This suggests that TXx distributions would be different between transient climate states and at different times after emissions cessation even for a fixed global warming level (GWL). When differentiating between transient, early stable, and late stable TXx distributions and likelihoods of extreme values at GWLs, conclusions are different for different GWLs (figure C6 and figure C.S4). In all cases, there is a clear distinction between transient and quasi-stable distributions, with a substantial TXx warm shift in the transient PDFs. Between the early and late stable PDFs, both annual TXx distributions are very similar at the 1.5 and 2°C GWLs in all regions (e.g., figures C6a,b). However, at the 3°C GWL, there is a clear shift between both TXx distributions in all regions, with the early stable distribution mean being around 0.5°C warmer for Europe (figure C6c). We tested this difference for a possible bias in the selection of years at the 3°C GWL, as early stable years around 3°C are slightly warmer than the late stable, but this shift in European TXx persists. Hence, we conclude that European TXx distributions require careful examination at given GWLs, as they can be heavily path-dependent.

C.4 DISCUSSION AND CONCLUSIONS

This study comprises a European test case for characterising and attributing heat extremes in long-term net-zero climates. Key components of our analysis were the contrasting of simulated net-zero climates against present-day heat records, the characterisation of mitiga-

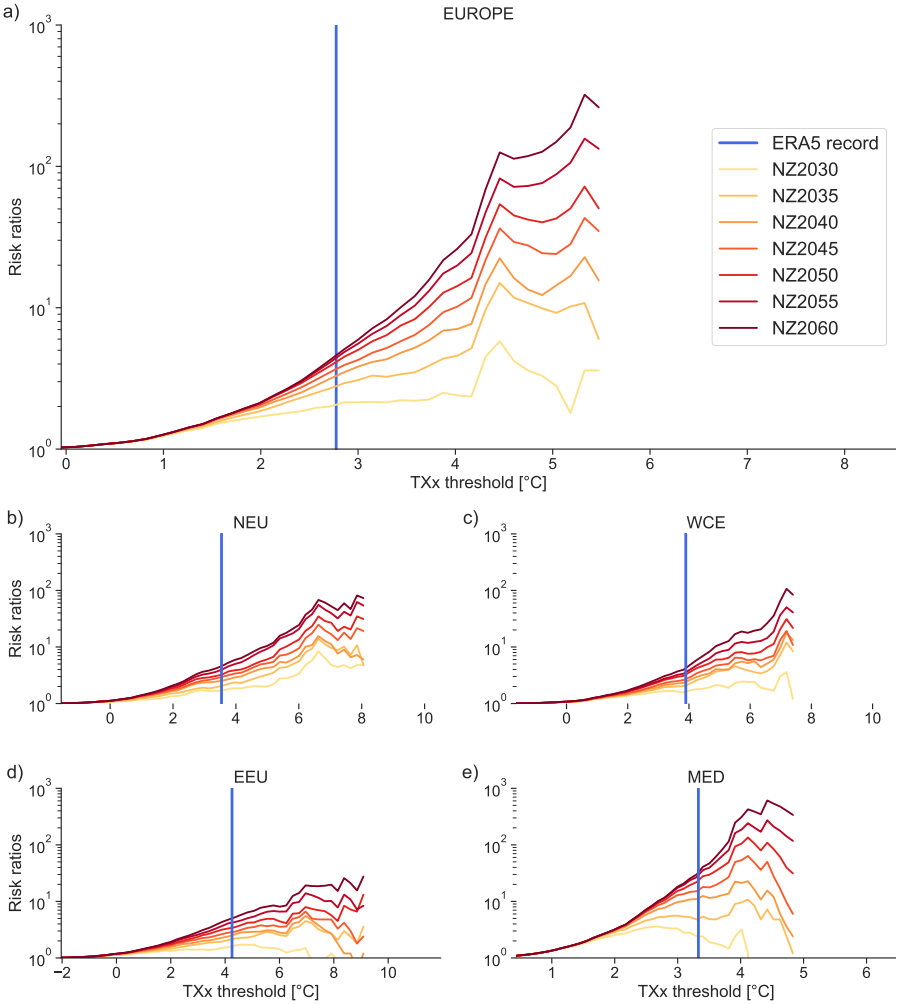

Figure C5: Risk ratios (logarithmic scale) of annual TXx anomaly thresholds averaged for a) Europe, b) Northern Europe, c) Western & Central Europe, d) Eastern Europe, and e) Mediterranean for the ACCESS-ESM-1.5 net-zero stabilisation simulations (label number indicates the year of emissions cessation), compared to the historical+SSP5-8.5 last 30 years (1995-2024). Vertical blue lines indicate the maximum value of the TXx anomaly in ERA5 for the respective regions.

tion delays, and the implications at equivalent global warming levels. This analysis was feasible due to a unique set of ACCESS-ESM-1.5 simulations, i.e., the 1000-year net-zero emissions experiments and the historical and SSP5-8.5 large ensembles.

The 1000-year net-zero emissions ACCESS-ESM-1.5 simulations (King et al., 2024), despite capturing ERA5 European TXx mean and variability, have a number of limitations. The simulations are constructed as idealised experiments and are not meant to represent plausible future scenarios. The changes are introduced too abruptly to be realistic, with CO_2 emissions set to zero and other greenhouse gases and aerosols concentrations set to preindustrial levels from one

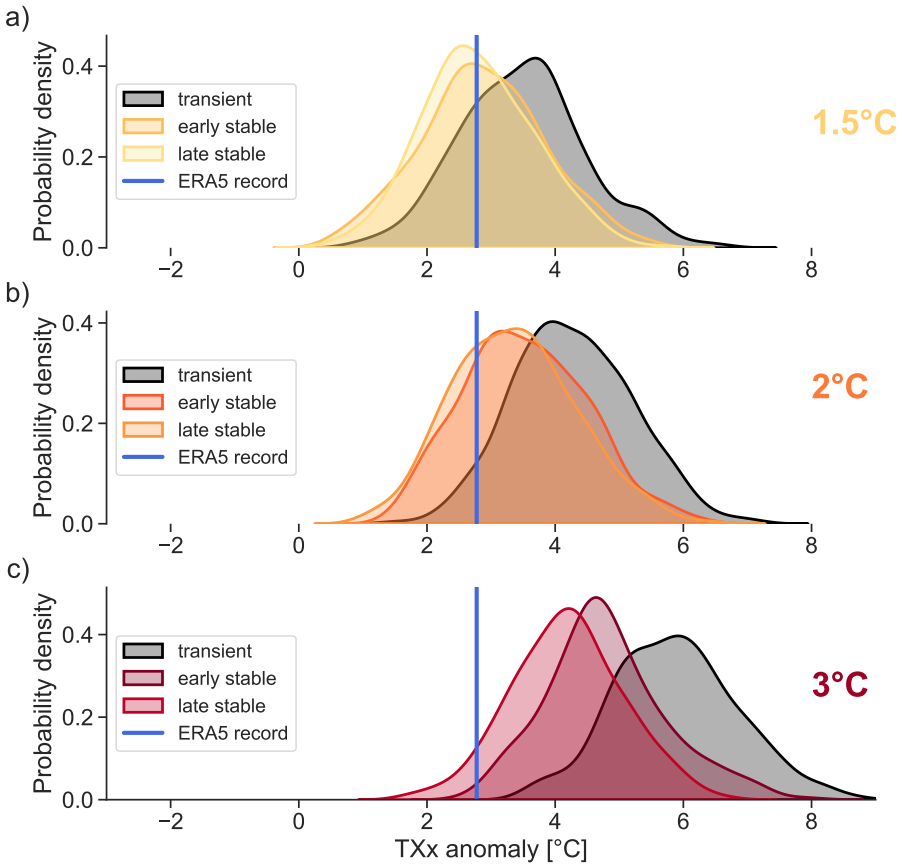

Figure C6: Probability distribution functions of European-averaged annual TXx anomalies (relative to 1961-1990) at global warming levels of a) 1.5°C, b) 2°C, and c) 3°C in ACCESS-ESM-1.5 simulations (within ±0.2°C of the level, baseline is 1850-1900). Black curves are transient anomalies (i.e., for the historical+SSP5-8.5 ensemble), light colours are early stable years (100-450), and dark colours are late stable years (650-1000) from the net-zero stabilisation experiments. Vertical blue lines indicate the maximum value of the TXx anomaly in ERA5 for each region.

time step to the next. In reality, having a more gradual reduction of emissions would entail larger cumulative emissions, further shifting the probability distribution function towards more intense heat extremes. Additionally, the simulations are branched from SSP5-8.5, a high emissions scenario now considered unlikely under current policies (Hausfather, 2025). Therefore, the estimates of five-year delays in emissions cessation are likely overestimated, as changes between net-zero simulations grow larger in this scenario. Nevertheless, scenarios do not differ much in their first years, so conclusions would not be expected to change substantially when assessing differences between early emissions cessation experiments. Additionally, part of the simulations' idealisation is the questionable prospect of staying at net-zero emissions once they are reached, instead of continuing into net-negative emissions. While a framework exists to address tempera-

ture target overshoots and reversibility under net-negative emissions (CDRMIP, Keller et al., 2018), it currently presents the same long-term limitations as the ZECMIP (Jones et al., 2019). Ultimately, even if multi-model simulations would be required to test our results' robustness, we assess the framework introduced by King et al., 2024 to be idealised but the best available and most appropriate set of experiments for understanding the long-term net-zero behaviour of the climate system.

One of our key findings highlights the stationarity of European heat extremes under net-zero emissions, and this stationarity motivates the clustering of all extreme events in each single simulation to calculate their statistics. However, a potential caveat is the slow background global mean warming, which leads to different climate background states being clustered together. To test whether this grouping ignores important discrepancies for different periods under slow global mean warming, we repeat the analysis separating the first and second 500 years of the net-zero experiments. This separation does not lead to substantial changes (figure C.S5, European PDFs). Ideally, if a single-model large ensemble of 1000-year-long net-zero experiments were available, extreme events could be studied in separate short time windows.

Although beyond the scope of our study, the stationarity of heat extremes under net-zero emissions in all European regions prompts an enquiry into the nature of this behaviour. With known potential dynamic mechanisms and local feedbacks driving changes in Europe, such as the jet stream, Arctic sea ice, North Atlantic surface temperature variability, or the Atlantic Meridional Overturning Circulation, further comprehensive analysis of the role and interaction of these mechanisms is needed.

Understanding the mechanisms underlying changes in heat extremes, as well as other climatic variables, would also help in identifying potential impacts. For instance, when driven by atmospheric blocking, heat extremes tend to co-occur with precipitation deficits (Horton et al., 2016). Co-occurrences of temperature and drought extremes in Europe are expected to rapidly increase (Suarez-Gutierrez et al., 2023) and may lead to major agricultural yield losses (Lesk et al., 2022). Considering temperature and humidity jointly is also fundamental for estimating heat-related mortality (Matthews et al., 2025). Analysing multiple variables will also be essential to calibrate the impacts of the main conclusions in our study, such as whether larger relative distribution shifts towards higher heat extremes (as found for the Mediterranean region) would be more impactful than larger absolute shifts.

All conclusions here obtained for European heat extremes are conditional on the choice of extreme index. TXx is a broadly used and easily interpretable index and, therefore, appropriate for the general

span of this study. The region-averaged annual TXx, as seen when representing its underlying spatial (figure C1) and monthly (figure C.S1) signals, is generally an aggregate measure of the hottest heat episode in each summer. Therefore, TXx encompasses both intensity and extent, but other indices are more suitable if the scope is to disentangle both or to include a temporal component, a characteristic only indirectly in TXx. To gauge the transferability of our conclusions to index choice, we contrast TXx against another widely used ETCCDI extreme index, TX90p. Yearly TX90p represents the number of days in a year with daily maximum temperatures surpassing the daily 90th percentile (calculated with a 5-day running window in the reference period). TX90p is a threshold-based index and therefore characterises the temporal dimension of extremes by focusing on changing frequencies above a reference intensity (rather than maximum intensities). We calculate equivalent European TX90p time series (figure C.S6), probability distribution functions (figure C.S7), and risk ratios (figure C.S8), and all qualitative results are the same as for TXx. Thus, our main conclusions on stationarity under net-zero emissions and on increased likelihoods with delays in cessation also apply to the frequency of extreme heat in Europe and its regions.

We found substantial differences in European temperature extremes at a given GWL related to whether the climate is transient or stable. These differences highlight that projections of climate extremes for GWLs should be explicit in their framing to avoid misinterpretation. Simply stating the change in likelihood or intensity of an extreme index at a GWL without such framing could lead to poorly informed decision-making. This path dependence is crucial for stakeholders and policymakers to design and implement robust and effective adaptation and mitigation strategies that neither consistently under- nor overestimate climate impacts. Even within the quasi-stable periods, we found two different pathways reaching a 3°C GWL resulting in two separate distributions of extreme heat. All these results emphasise the need for further understanding of how reaching temperature targets at different rates of CO_2 emissions may impact other climate system components (e.g., Hankel, 2025), particularly heat extremes.

We have shown that, even under net-zero emissions, the intensity of European hottest temperature extremes in any European region will not decrease for many centuries. Yet, delayed emissions cessation will translate into significantly more severe heat extremes, with the largest relative increases occurring over the Mediterranean region. Furthermore, we have found shifts at given global warming levels between transient, early and late stable climates, underpinning the need for long-term net-zero perspectives. Overall, even though European hottest extremes persist at elevated levels for centuries in net-zero futures, as short delays in emissions cessation result in more intense

extremes projected even centuries later, our results highlight the long-term value of promptly reducing emissions.

DATA AVAILABILITY STATEMENT

ERA5 data is available on the Climate Data Store of the Copernicus Climate Change Service at https://doi.org/10.24381/cds.adbb2d47. ACCESS-ESM-1.5 CMIP6 simulations are available on the Australian node of the Earth System Grid Federation: the historical ensemble is available at https://doi.org/10.22033/ESGF/CMIP6.2288, and the SSP5-8.5 scenario ensemble at https://doi.org/10.22033/ESGF/CMIP6.2291. Post-processed variables used in this study, particularly from the 1000-year-long net-zero emissions ACCESS-ESM-1.5 simulations from King et al., 2024, are available at https://doi.org/10.5281/zenodo.15433420. The code for processing the data and producing all figures is on the repository https://github.com/edualas/netzero_EuHeatExtremes.

ACKNOWLEDGMENTS

Authors' contribution statement: **E.A.dA** Conceptualisation; Data curation; Formal analysis; Funding acquisition; Investigation; Methodology; Software; Visualisation; Writing - original draft; Writing - Review & Editing. **A.D.K** Conceptualisation; Funding acquisition; Methodology; Resources; Supervision; Writing - Review & Editing. **T.Z** Data curation; Writing - Review & Editing.

E.A.dA acknowledges funding by the Deutsche Forschungsgemeinschaft (DFG, German Research Foundation) under Germany's Excellence Strategy – EXC 2037 'CLICCS- Climate, Climatic Change, and Society' – Project Number: 390683824, as well as a scholarship for research stays abroad from the MIN Graduate Center at the University of Hamburg. A.D.K. acknowledges support from the Australian Research Council through the Centre of Excellence for the Weather of the 21st Century (CE230100012). A.D.K. and T.Z. acknowledge the Australian Government National Environmental Science Program.

CONFLICT OF INTEREST

The authors declare no competing interests.

C.5 APPENDIX

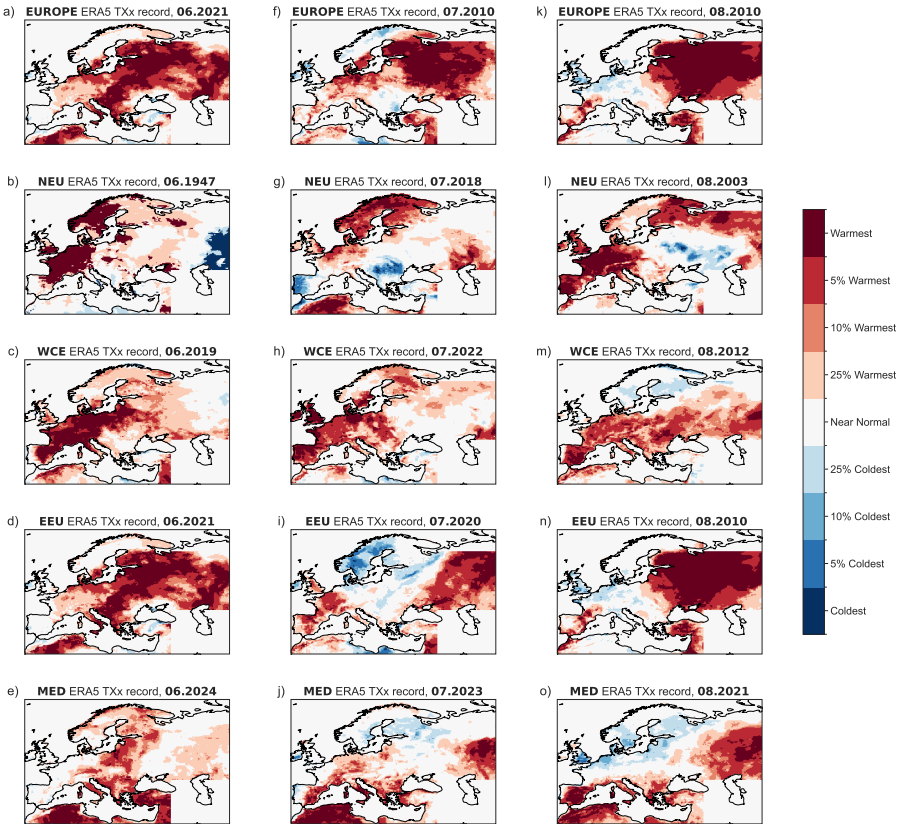

Figure C.S1: Equivalent to figure C1, but for monthly TXx in the month of June (first column), July (second column), and August (third column).

Table C1: Annual TXx statistics in Europe and its regions for ERA5 and ACCESS-ESM-1.5 experiments, as shown in the time series in figure C2.

REGION	DATA / EXPERIMENT	YEARS	MEAN [°C]	STD [°C]	TREND [°C / DEC]
EUROPE	ERA5	1995-2024	1.4	0.7	0.62
	hist+ssp585 (min, max)	1995-2024	(1.3, 2.5)	(0.8, 1.4)	(0.17, 1.3)
	NZ2030	2030-3030	2.7	0.9	0.003
	NZ2035	2035-3035	3.0	0.9	0.001
	NZ2040	2040-3040	3.3	0.9	-0.001
	NZ2045	2045-3045	3.6	0.9	0.000
	NZ2050	2050-3050	3.9	0.9	-0.002
	NZ2055	2055-3055	4.3	0.9	-0.003
	NZ2060	2060-3060	4.8	0.9	-0.001
NEU	ERA5	1995-2024	1.0	1.2	0.53
	hist+ssp585 (min, max)	1995-2024	(1.0, 3.1)	(1.0, 2.0)	(0.16, 1.45)
	NZ2030	2030-3030	2.6	1.7	0.003
	NZ2035	2035-3035	2.9	1.8	0.000
	NZ2040	2040-3040	3.3	1.7	-0.004
	NZ2045	2045-3045	3.6	1.8	-0.002
	NZ2050	2050-3050	3.9	1.8	-0.003
	NZ2055	2055-3055	4.4	1.9	-0.004
	NZ2060	2060-3060	4.8	1.8	0.000
WCE	ERA5	1995-2024	2.1	1.0	0.73
	hist+ssp585 (min, max)	1995-2024	(1.2, 3.2)	(1.2, 2.1)	(0.14, 1.5)
	NZ2030	2030-3030	3.1	1.5	0.005
	NZ2035	2035-3035	3.5	1.6	0.004
	NZ2040	2040-3040	3.7	1.6	0.004
	NZ2045	2045-3045	3.9	1.6	0.001
	NZ2050	2050-3050	4.2	1.5	0.000
	NZ2055	2055-3055	4.6	1.6	-0.002
	NZ2060	2060-3060	5.1	1.5	0.003
EEU	ERA5	1995-2024	1.3	1.2	0.65
	hist+ssp585 (min, max)	1995-2024	(1.1, 3.1)	(1.2, 2.5)	(-0.52, 1.85)
	NZ2030	2030-3030	2.8	1.7	0.002
	NZ2035	2035-3035	3.1	1.9	0.000
	NZ2040	2040-3040	3.4	1.8	-0.002
	NZ2045	2045-3045	3.7	1.8	-0.001
	NZ2050	2050-3050	4.0	1.8	-0.004
	NZ2055	2055-3055	4.4	1.8	-0.006
	NZ2060	2060-3060	4.9	1.9	-0.004
MED	ERA5	1995-2024	1.3	0.7	0.54
	hist+ssp585 (min, max)	1995-2024	(1.1, 2.0)	(0.5, 1.1)	(0.28, 0.93)
	NZ2030	2030-3030	2.5	0.6	0.001
	NZ2035	2035-3035	2.7	0.6	0.002
	NZ2040	2040-3040	3.0	0.6	0.000
	NZ2045	2045-3045	3.3	0.6	-0.001
	NZ2050	2050-3050	3.6	0.6	-0.001
	NZ2055	2055-3055	4.0	0.6	-0.001
	NZ2060	2060-3060	4.5	0.6	0.000

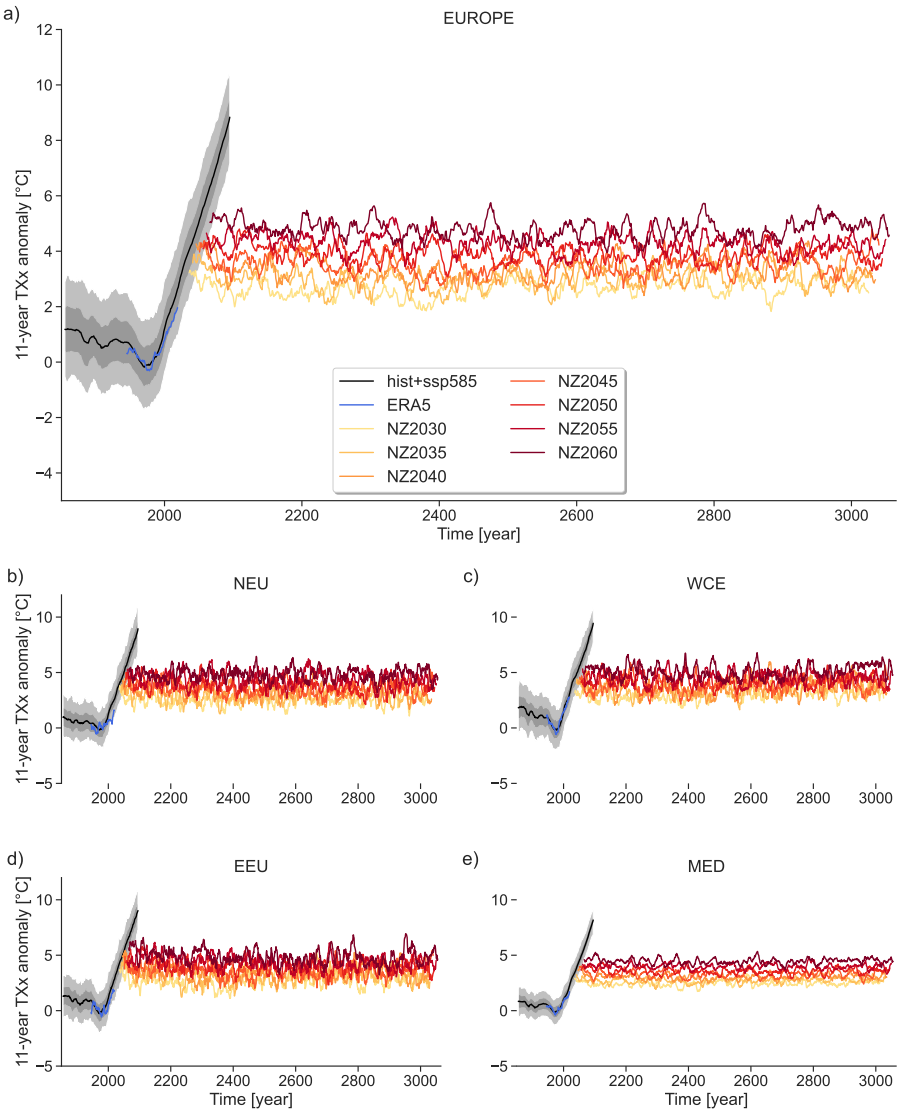

Figure C.S2: Equivalent to figure C2, but now an 11-year moving average is applied to the annual values of TXx.

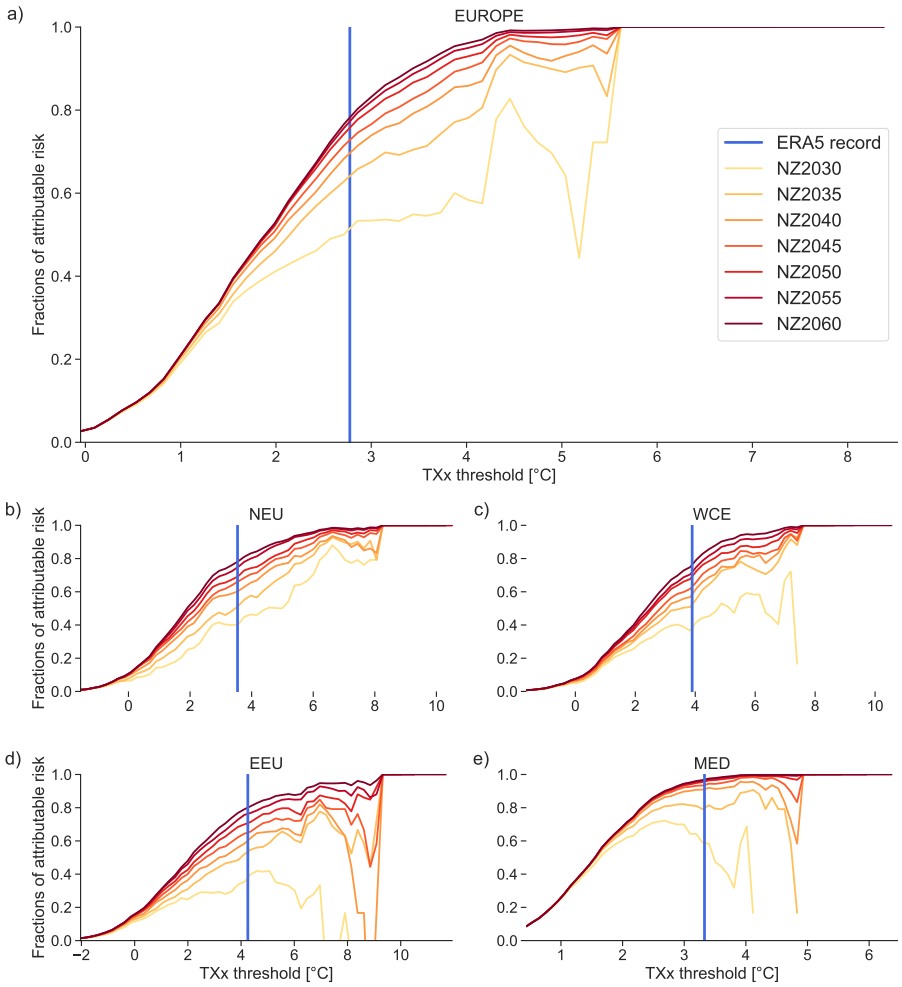

Figure C.S3: Equivalent to figure C5, but now for fractions of attributable risk.

Table C2: Risk ratios (RR) and fractions of attributable risk (FAR) for all net-zero ACCESS-ESM-1.5 experiments in Europe and its regions as in figure C5 and figure C.S3, but specifically calculated at the threshold given by the record in ERA5 for that particular region.

REGION	ERA5 RECORD [°C]	EXPERIMENT	RR	FAR
EUROPE	2.78	NZ2030	2.1	0.52
		NZ2035	2.9	0.65
		NZ2040	3.4	0.70
		NZ2045	3.8	0.73
		NZ2050	4.2	0.76
		NZ2055	4.5	0.78
		NZ2060	4.7	0.79
NEU	3.54	NZ2030	1.7	0.40
		NZ2035	2.0	0.51
		NZ2040	2.5	0.60
		NZ2045	3.0	0.66
		NZ2050	3.2	0.69
		NZ2055	3.9	0.75
		NZ2060	4.6	0.78
WCE	3.90	NZ2030	1.7	0.40
		NZ2035	2.1	0.53
		NZ2040	2.5	0.60
		NZ2045	2.8	0.64
		NZ2050	3.3	0.70
		NZ2055	3.6	0.72
		NZ2060	4.3	0.77
EEU	4.25	NZ2030	1.6	0.37
		NZ2035	2.1	0.53
		NZ2040	2.5	0.60
		NZ2045	2.9	0.65
		NZ2050	3.4	0.70
		NZ2055	4.2	0.76
		NZ2060	5.0	0.80
MED	3.33	NZ2030	2.3	0.56
		NZ2035	4.8	0.79
		NZ2040	10.8	0.91
		NZ2045	15.1	0.93
		NZ2050	22.5	0.96
		NZ2055	27.9	0.96
		NZ2060	31.4	0.97

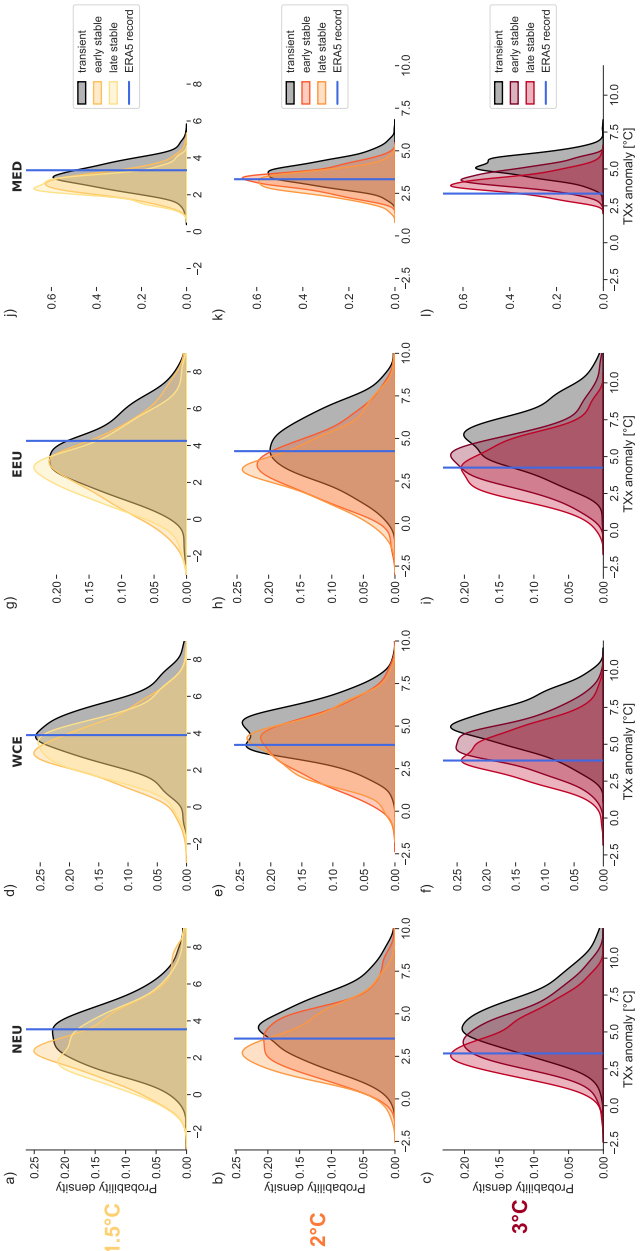

Figure C.S4: Equivalent to figure C6, but each column is one European region: Northern Europe (first column), Western & Central Europe (second column), Eastern Europe (third column), and Mediterranean (fourth column). Note that now the x-axis scales are different in different rows.

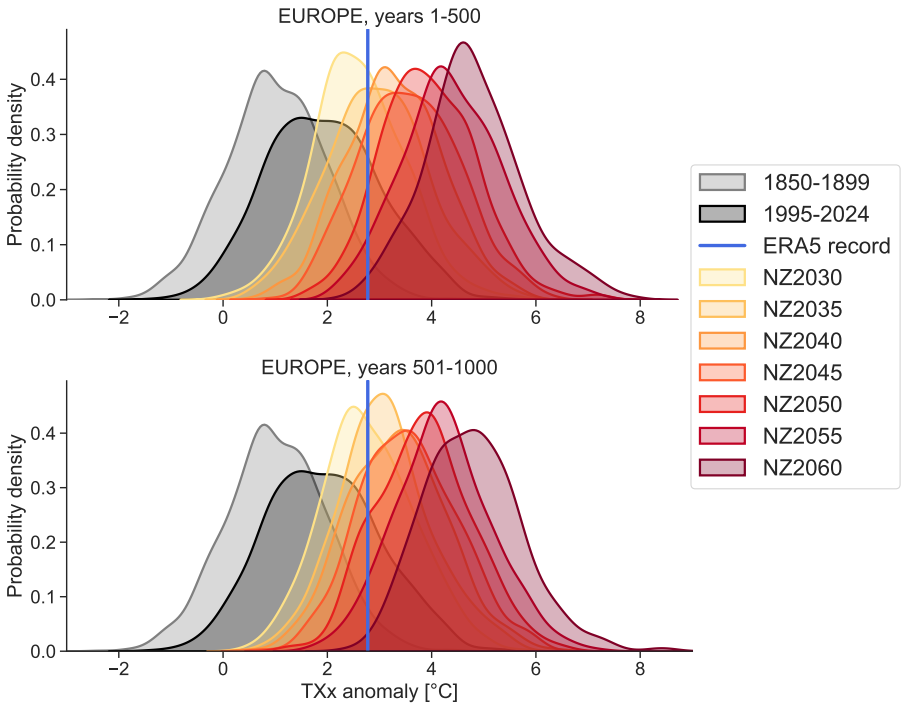

Figure C.S5: Equivalent plot to figure C4a, but now calculated separately for the first (top) and last (bottom) 500 years.

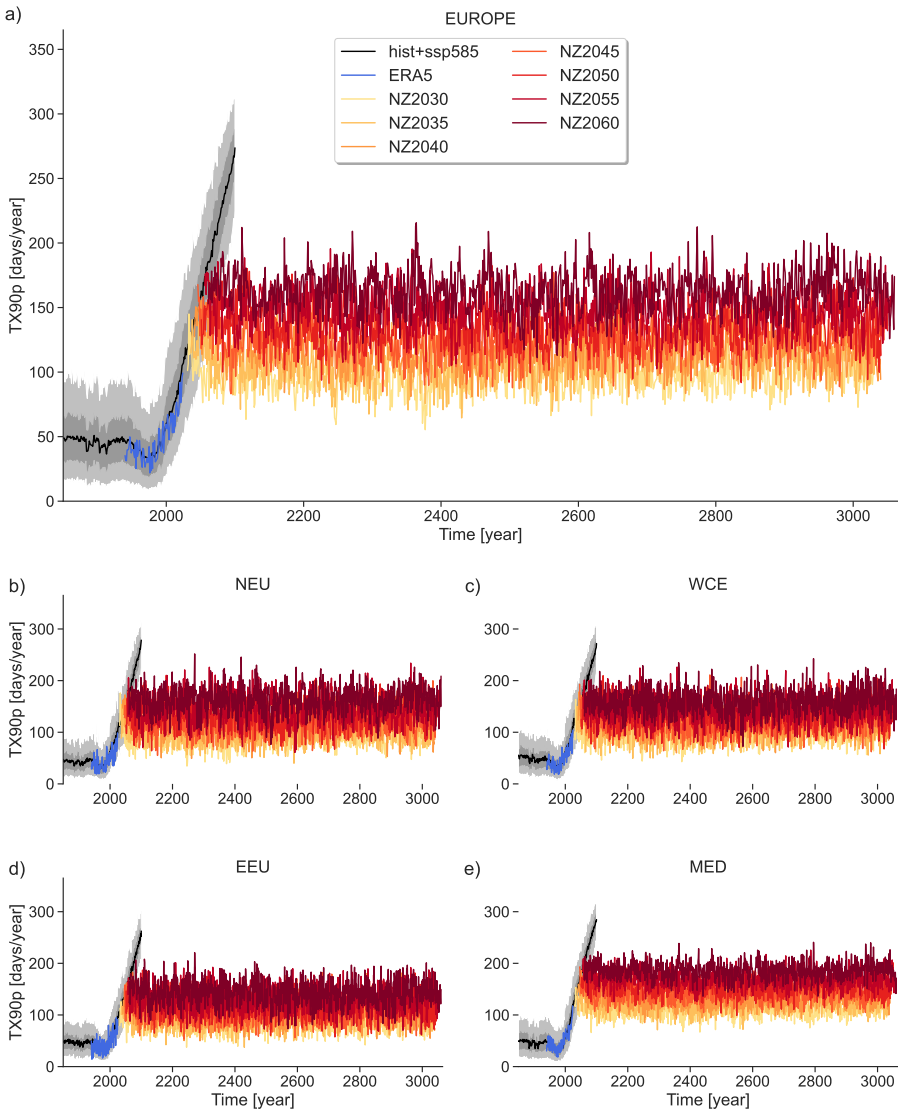

Figure C.S6: Equivalent to figure C2, but for the annual TX90p index. Percentiles are computed in the reference period (1961-1990) using a centred 5-day running window for each day of the year, and the spatial calculations and averages and performed as for TXx.

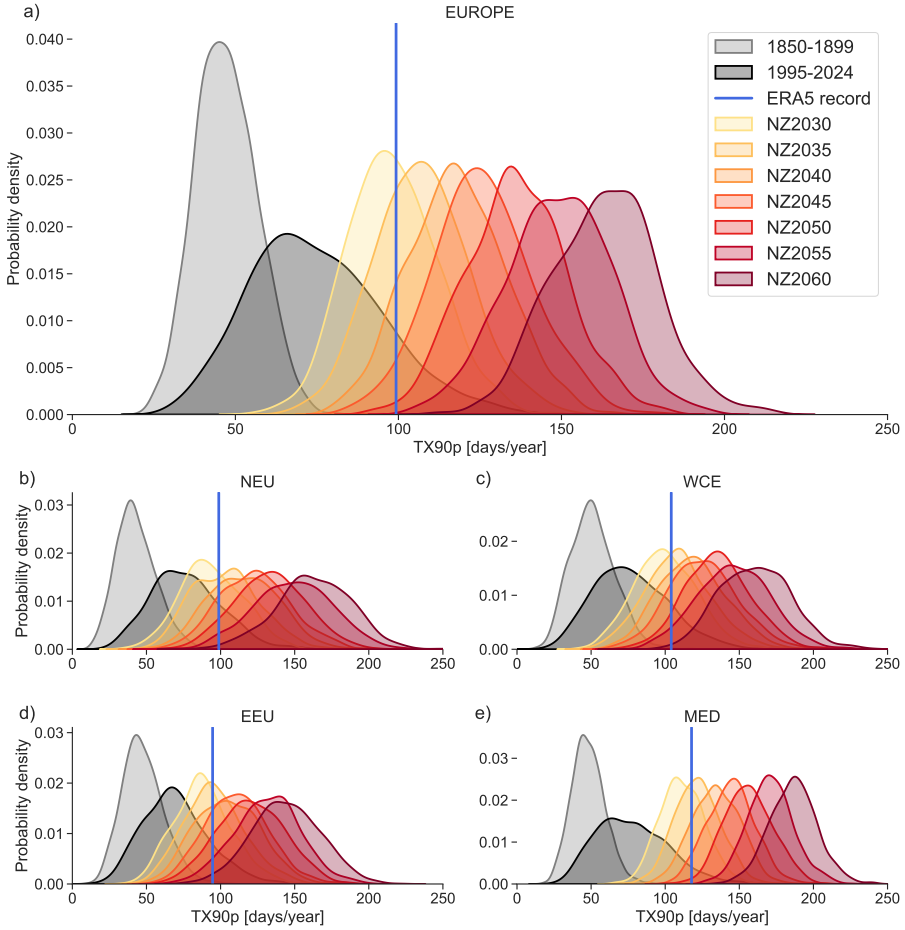

Figure C.S7: Equivalent to figure C4, but for the annual TX90p index. Percentiles are computed in the reference period (1961-1990) using a centred 5-day running window for each day of the year, and the spatial calculations and averages and performed as for TXx.

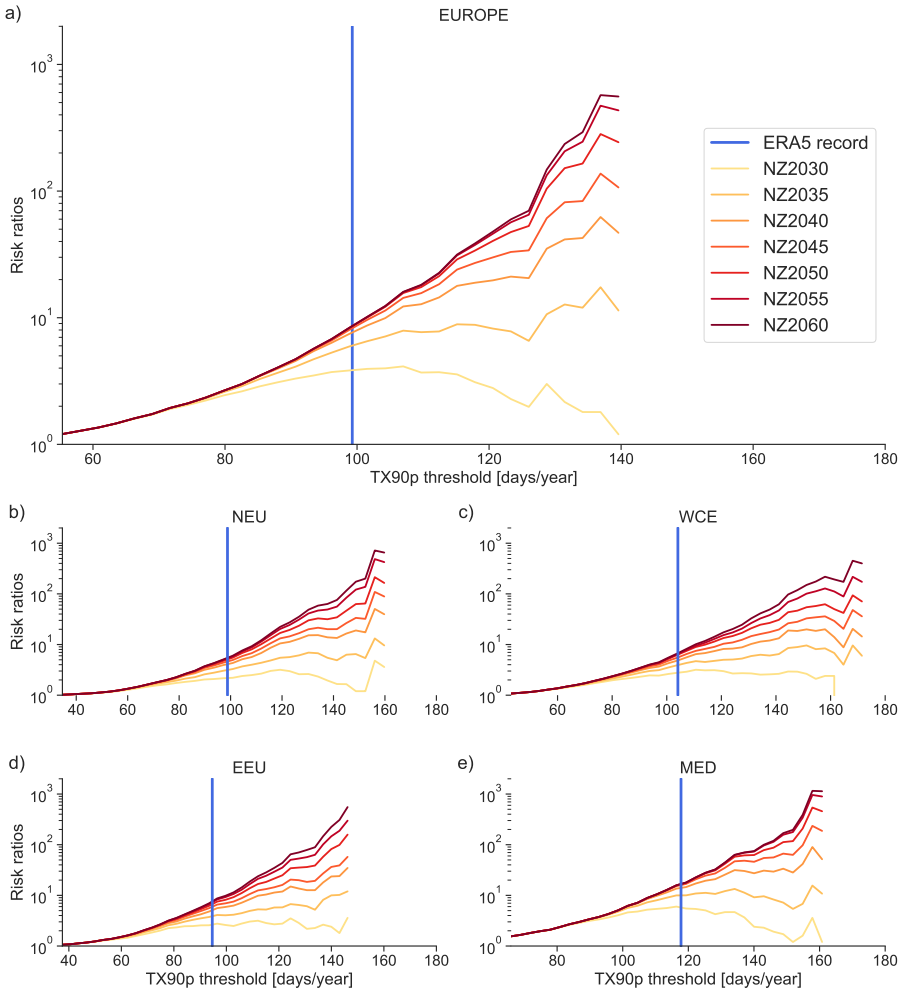

Figure C.S8: Equivalent to figure C5, but for the annual TX90p index. Percentiles are computed in the reference period (1961-1990) using a centred 5-day running window for each day of the year, and the spatial calculations and averages and performed as for TXx.

BIBLIOGRAPHY

Acosta Navarro, J. C., Varma, V., Riipinen, I., Seland, Ø., Kirkevåg, A., Struthers, H., Iversen, T., Hansson, H.-C., & Ekman, A. M. L. (2016). Amplification of Arctic warming by past air pollution reductions in Europe. *Nature Geoscience*, *9*(4), 277–281. https://doi.org/10.1038/ngeo2673

Alastrué de Asenjo, E., Baehr, J., & Barkhordarian, A. (in preparation). Anthropogenic greenhouse gases emerging as a necessary cause for interannual AMOC weakenings.

An, S.-I., Shin, J., Yeh, S.-W., Son, S.-W., Kug, J.-S., Min, S.-K., & Kim, H.-J. (2021). Global Cooling Hiatus Driven by an AMOC Overshoot in a Carbon Dioxide Removal Scenario. *Earth's Future*, *9*(7), e2021EF002165. https://doi.org/10.1029/2021EF002165

Anthoff, D., Estrada, F., & Tol, R. S. J. (2016). Shutting Down the Thermohaline Circulation. *American Economic Review*, *106*(5), 602–606. https://doi.org/10.1257/aer.p20161102

Armstrong McKay, D. I., & Loriani, S. (2023). Earth system tipping points. In T. M. Lenton, D. I. Armstrong McKay, S. Loriani, J. F. Abrams, S. J. Lade, J. F. Donges, M. Milkoreit, T. Powell, S. R. Smith, C. Zimm, J. E. Buxton, E. Bailey, L. Laybourn, A. Ghadiali, & J. Dyke (Eds.), *The Global Tipping Points Report*. University of Exeter, Exeter, UK.

Armstrong McKay, D. I., Staal, A., Abrams, J. F., Winkelmann, R., Sakschewski, B., Loriani, S., Fetzer, I., Cornell, S. E., Rockström, J., & Lenton, T. M. (2022). Exceeding 1.5°C global warming could trigger multiple climate tipping points. *Science*, *377*(6611), eabn7950. https://doi.org/10.1126/science.abn7950

Arora, V. K., Katavouta, A., Williams, R. G., Jones, C. D., Brovkin, V., Friedlingstein, P., Schwinger, J., Bopp, L., Boucher, O., Cadule, P., Chamberlain, M. A., Christian, J. R., Delire, C., Fisher, R. A., Hajima, T., Ilyina, T., Joetzjer, E., Kawamiya, M., Koven, C. D., … Ziehn, T. (2020). Carbon–concentration and carbon–climate feedbacks in CMIP6 models and their comparison to CMIP5 models. *Biogeosciences*, *17*(16), 4173–4222. https://doi.org/10.5194/bg-17-4173-2020

Årthun, M., Brakstad, A., Dörr, J., Johnson, H. L., Mans, C., Semper, S., & Våge, K. (2025). Atlantification drives recent strengthening of the Arctic overturning circulation. *Science Advances*, *11*(28), eadu1794. https://doi.org/10.1126/sciadv.adu1794

Baker, J. A., Bell, M. J., Jackson, L. C., Vallis, G. K., Watson, A. J., & Wood, R. A. (2025). Continued Atlantic overturning circula-

tion even under climate extremes. *Nature*, *638*(8052), 987–994. https://doi.org/10.1038/s41586-024-08544-0

Barriopedro, D., Fischer, E. M., Luterbacher, J., Trigo, R. M., & García-Herrera, R. (2011). The Hot Summer of 2010: Redrawing the Temperature Record Map of Europe. *Science*, *332*(6026), 220–224. https://doi.org/10.1126/science.1201224

Bellomo, K., Angeloni, M., Corti, S., & von Hardenberg, J. (2021). Future climate change shaped by inter-model differences in Atlantic meridional overturning circulation response. *Nature Communications*, *12*(1), 1–10. https://doi.org/10.1038/s41467-021-24015-w

Bellomo, K., Meccia, V. L., D'Agostino, R., Fabiano, F., Larson, S. M., Von Hardenberg, J., & Corti, S. (2023). Impacts of a weakened AMOC on precipitation over the Euro-Atlantic region in the EC-Earth3 climate model. *Climate Dynamics*, *61*(7-8), 3397–3416. https://doi.org/10.1007/s00382-023-06754-2

Bellomo, K., & Mehling, O. (2024). Impacts and State-Dependence of AMOC Weakening in a Warming Climate. *Geophysical Research Letters*, *51*(10), e2023GL107624. https://doi.org/10.1029/2023GL107624

Ben-Yami, M., Good, P., Jackson, L. C., Crucifix, M., Hu, A., Saenko, O., Swingedouw, D., & Boers, N. (2024a). Impacts of AMOC Collapse on Monsoon Rainfall: A Multi-Model Comparison. *Earth's Future*, *12*(9), e2023EF003959. https://doi.org/10.1029/2023EF003959

Ben-Yami, M., Morr, A., Bathiany, S., & Boers, N. (2024b). Uncertainties too large to predict tipping times of major Earth system components from historical data. *Science Advances*, *10*(31), eadl4841. https://doi.org/10.1126/sciadv.adl4841

Biesbroek, R., Haasnoot, M., Mach, K. J., & Petersen, A. C. (2025). Adaptation planning in the context of a weakening and possibly collapsing Atlantic Meridional Overturning Circulation (AMOC). *Regional Environmental Change*, *25*(3), 93. https://doi.org/10.1007/s10113-025-02434-5

Blackport, R., Sigmond, M., & Screen, J. A. (2024). Models and observations agree on fewer and milder midlatitude cold extremes even over recent decades of rapid Arctic warming. *Science Advances*, *10*(40), eadp1346. https://doi.org/10.1126/sciadv.adp1346

Boers, N. (2021). Observation-based early-warning signals for a collapse of the Atlantic Meridional Overturning Circulation. *Nature Climate Change*, *11*(8), 680–688. https://doi.org/10.1038/s41558-021-01097-4

Boot, A. A., Steenbeek, J., Coll, M., von der Heydt, A. S., & Dijkstra, H. A. (2025). Global Marine Ecosystem Response to a Strong AMOC Weakening Under Low and High Future Emission Sce-

narios. *Earth's Future*, *13*(1), e2024EF004741. https://doi.org/10.1029/2024EF004741

Boot, A. A., von der Heydt, A. S., & Dijkstra, H. A. (2024). Response of atmospheric pCO2 to a strong AMOC weakening under low and high emission scenarios. *Climate Dynamics*. https://doi.org/10.1007/s00382-024-07295-y

Borchert, L. F., Müller, W. A., & Baehr, J. (2018). Atlantic Ocean Heat Transport Influences Interannual-to-Decadal Surface Temperature Predictability in the North Atlantic Region. *Journal of Climate*, *31*(17), 6763–6782. https://doi.org/10.1175/JCLI-D-17-0734.1

Borowiak, A., King, A. D., Brown, J. R., Jones, C. D., Ziehn, T., Meinshausen, M., & Cassidy, L. (2024). Projected Global Temperature Changes After Net Zero Are Small But Significant. *Geophysical Research Letters*, *51*(8), e2024GL108654. https://doi.org/10.1029/2024GL108654

Borowiak, A., King, A. D., Brown, J. R., & Ziehn, T. (2025). Revised estimates of temperature changes under net zero CO2 emissions. *npj Climate and Atmospheric Science*, *8*(1), 275. https://doi.org/10.1038/s41612-025-01148-z

Brown, P. T., Ming, Y., Li, W., & Hill, S. A. (2017). Change in the magnitude and mechanisms of global temperature variability with warming. *Nature Climate Change*, *7*(10), 743–748. https://doi.org/10.1038/nclimate3381

Brown, P. J., McDonagh, E. L., Sanders, R., Watson, A. J., Wanninkhof, R., King, B. A., Smeed, D. A., Baringer, M. O., Meinen, C. S., Schuster, U., Yool, A., & Messias, M.-J. (2021). Circulation-driven variability of Atlantic anthropogenic carbon transports and uptake. *Nature Geoscience*, *14*(8), 571–577. https://doi.org/10.1038/s41561-021-00774-5

Brunner, L., Schaller, N., Anstey, J., Sillmann, J., & Steiner, A. K. (2018). Dependence of Present and Future European Temperature Extremes on the Location of Atmospheric Blocking. *Geophysical Research Letters*, *45*(12), 6311–6320. https://doi.org/10.1029/2018GL077837

Bryden, H. L., King, B. A., McCarthy, G. D., & McDonagh, E. L. (2014). Impact of a 30% reduction in Atlantic meridional overturning during 2009–2010. *Ocean Science*, *10*(4), 683–691. https://doi.org/10.5194/os-10-683-2014

Buckley, M. W., & Marshall, J. (2016). Observations, inferences, and mechanisms of the Atlantic Meridional Overturning Circulation: A review. *Reviews of Geophysics*, *54*(1), 5–63. https://doi.org/10.1002/2015RG000493

Budyko, M. I. (1969). The effect of solar radiation variations on the climate of the Earth. *Tellus*, *21*(5), 611–619. https://doi.org/10.1111/j.2153-3490.1969.tb00466.x

Burke, M., Hsiang, S. M., & Miguel, E. (2015). Global non-linear effect of temperature on economic production. *Nature*, *527*(7577), 235–239. https://doi.org/10.1038/nature15725

Caesar, L., Rahmstorf, S., Robinson, A., Feulner, G., & Saba, V. (2018). Observed fingerprint of a weakening Atlantic Ocean overturning circulation. *Nature*, *556*(7700), 191–196. https://doi.org/10.1038/s41586-018-0006-5

Cai, Y., Judd, K. L., Lenton, T. M., Lontzek, T. S., & Narita, D. (2015). Environmental tipping points significantly affect the cost-benefit assessment of climate policies. *Proceedings of the National Academy of Sciences*, *112*(15), 4606–4611. https://doi.org/10.1073/pnas.1503890112

Cai, Y., Lenton, T. M., & Lontzek, T. S. (2016). Risk of multiple interacting tipping points should encourage rapid CO2 emission reduction. *Nature Climate Change*, *6*(5), 520–525. https://doi.org/10.1038/nclimate2964

Callahan, C. W., Chen, C., Rugenstein, M., Bloch-Johnson, J., Yang, S., & Moyer, E. J. (2021). Robust decrease in El Niño/Southern Oscillation amplitude under long-term warming. *Nature Climate Change*, *11*(9), 752–757. https://doi.org/10.1038/s41558-021-01099-2

Carleton, T., & Greenstone, M. (2022). A Guide to Updating the US Government's Social Cost of Carbon. *Review of Environmental Economics and Policy*, *16*(2), 196–218. https://doi.org/10.1086/720988

Carson, R. (1962). *Silent Spring*. Houghton Mifflin.

Carvalho-Oliveira, J., Borchert, L. F., Duchez, A., Dobrynin, M., & Baehr, J. (2021). Subtle influence of the Atlantic Meridional Overturning Circulation (AMOC) on seasonal sea surface temperature (SST) hindcast skill in the North Atlantic. *Weather and Climate Dynamics*, *2*(3), 739–757. https://doi.org/10.5194/wcd-2-739-2021

Cassidy, L. J., King, A. D., Brown, J. R., MacDougall, A. H., Ziehn, T., Min, S.-K., & Jones, C. D. (2024). Regional temperature extremes and vulnerability under net zero CO2 emissions. *Environmental Research Letters*, *19*(1), 014051. https://doi.org/10.1088/1748-9326/ad114a

Chamberlain, M. A., Ziehn, T., & Law, R. M. (2024). The Southern Ocean as the climate's freight train – driving ongoing global warming under zero-emission scenarios with ACCESS-ESM1.5. *Biogeosciences*, *21*(12), 3053–3073. https://doi.org/10.5194/bg-21-3053-2024

Chen, C., Liu, W., & Wang, G. (2019). Understanding the Uncertainty in the 21st Century Dynamic Sea Level Projections: The Role of the AMOC. *Geophysical Research Letters*, *46*(1), 210–217. https://doi.org/10.1029/2018gl080676

Chen, X., & Tung, K. K. (2018). Global surface warming enhanced by weak Atlantic overturning circulation. *Nature*, *559*(7714), 387–391. https://doi.org/10.1038/s41586-018-0320-y

Cheng, J., Liu, Z., Zhang, S., Liu, W., Dong, L., Liu, P., & Li, H. (2016). Reduced interdecadal variability of Atlantic Meridional Overturning Circulation under global warming. *Proceedings of the National Academy of Sciences*, *113*(12), 3175–3178. https://doi.org/10.1073/pnas.1519827113

Christidis, N., Jones, G. S., & Stott, P. A. (2015). Dramatically increasing chance of extremely hot summers since the 2003 European heatwave. *Nature Climate Change*, *5*(1), 46–50. https://doi.org/10.1038/nclimate2468

Copernicus Climate Change Service (C3S) & World Meteorological Organization (WMO). (2025). European State of the Climate 2024. https://climate.copernicus.eu/ESOTC/2024

Corti, S., Molteni, F., & Palmer, T. N. (1999). Signature of recent climate change in frequencies of natural atmospheric circulation regimes. *Nature*, *398*(6730), 799–802. https://doi.org/10.1038/19745

Curry, J. A., Schramm, J. L., & Ebert, E. E. (1995). Sea Ice-Albedo Climate Feedback Mechanism. *Journal of Climate*, *8*(2), 240–247. https://doi.org/10.1175/1520-0442(1995)008<0240:SIACFM>2.0.CO;2

Deser, C., Lehner, F., Rodgers, K. B., Ault, T., Delworth, T. L., DiNezio, P. N., Fiore, A., Frankignoul, C., Fyfe, J. C., Horton, D. E., Kay, J. E., Knutti, R., Lovenduski, N. S., Marotzke, J., McKinnon, K. A., Minobe, S., Randerson, J., Screen, J. A., Simpson, I. R., & Ting, M. (2020). Insights from Earth system model initial-condition large ensembles and future prospects. *Nature Climate Change*, *10*(4), 277–286. https://doi.org/10.1038/s41558-020-0731-2

Deser, C., Phillips, A., Bourdette, V., & Teng, H. (2012). Uncertainty in climate change projections: The role of internal variability. *Climate Dynamics*, *38*(3-4), 527–546. https://doi.org/10.1007/s00382-010-0977-x

Deser, C., Walsh, J. E., & Timlin, M. S. (2000). Arctic Sea Ice Variability in the Context of Recent Atmospheric Circulation Trends. *Journal of Climate*, *13*(3), 617–633. https://doi.org/10.1175/1520-0442(2000)013<0617:asivit>2.0.co;2

DeVries, T., Holzer, M., & Primeau, F. (2017). Recent increase in oceanic carbon uptake driven by weaker upper-ocean overturning. *Nature*, *542*(7640), 215–218. https://doi.org/10.1038/nature21068

Diamond, R., Sime, L. C., Schroeder, D., Jackson, L. C., Holland, P. R., Alastrué de Asenjo, E., Bellomo, K., Danabasoglu, G., Hu, A., Jungclaus, J., Montoya, M., Meccia, V. L., Saenko,

O. A., & Swingedouw, D. (2025). A Weakened AMOC Could Cause Southern Ocean Temperature and Sea-Ice Change on Multidecadal Timescales. *Journal of Geophysical Research: Oceans*, *130*(7), e2024JC022027. https://doi.org/10.1029/2024JC022027

Dietz, S., & Koninx, F. (2022). Economic impacts of melting of the Antarctic Ice Sheet. *Nature Communications*, *13*(1), 5819. https://doi.org/10.1038/s41467-022-33406-6

Dietz, S., Rising, J., Stoerk, T., & Wagner, G. (2021). Economic impacts of tipping points in the climate system. *Proceedings of the National Academy of Sciences*, *118*(34). https://doi.org/10.1073/pnas.2103081118

Dietz, S., Rising, J., Stoerk, T., & Wagner, G. (2022). Reply to Keen et al.: Dietz et al. modeling of climate tipping points is informative even if estimates are a probable lower bound. *Proceedings of the National Academy of Sciences*, *119*(21), e2201191119. https://doi.org/10.1073/pnas.2201191119

Dietz, S., & Stern, N. (2015). Endogenous Growth, Convexity of Damage and Climate Risk: How Nordhaus' Framework Supports Deep Cuts in Carbon Emissions. *The Economic Journal*, *125*(583), 574–620. https://doi.org/10.1111/ecoj.12188

Diffenbaugh, N. S., Barnes, E. A., & Keys, P. W. (2023). Probability of continued local-scale warming and extreme events during and after decarbonization. *Environmental Research: Climate*, *2*(2), 021003. https://doi.org/10.1088/2752-5295/accf2f

Ditlevsen, P., & Ditlevsen, S. (2023). Warning of a forthcoming collapse of the Atlantic meridional overturning circulation. *Nature Communications*, *14*(1), 4254. https://doi.org/10.1038/s41467-023-39810-w

Drijfhout, S., Hazeleger, W., Selten, F., & Haarsma, R. (2008). Future changes in internal variability of the Atlantic Meridional Overturning Circulation. *Climate Dynamics*, *30*(4), 407–419. https://doi.org/10.1007/s00382-007-0297-y

Duarte, D., Liu, W., & Zhang, L. (2025). A weakened Atlantic Meridional Overturning Circulation will affect future heat waves by mostly attenuating their severity. *Climate Dynamics*, *63*(6), 238. https://doi.org/10.1007/s00382-025-07736-2

England, M. R., Eisenman, I., Lutsko, N. J., & Wagner, T. J. W. (2021). The Recent Emergence of Arctic Amplification. *Geophysical Research Letters*, *48*(15). https://doi.org/10.1029/2021gl094086

EPA. (2023, November). *Report on the social cost of greenhouse gases: Estimates incorporating recent scientific advances* (tech. rep.). U.S. Environmental Protection Agency.

Errickson, F., & Rennels, L. (2021, September). *MimiFAIRV2 large data file storage* (Version 0.1.0-DEV). Zenodo. https://doi.org/10.5281/zenodo.5513221

Eyring, V., Bony, S., Meehl, G. A., Senior, C. A., Stevens, B., Stouffer, R. J., & Taylor, K. E. (2016). Overview of the Coupled Model Intercomparison Project Phase 6 (CMIP6) experimental design and organization. *Geoscientific Model Development*, *9*(5), 1937–1958. https://doi.org/10.5194/gmd-9-1937-2016

Faranda, D., Messori, G., Jezequel, A., Vrac, M., & Yiou, P. (2023). Atmospheric circulation compounds anthropogenic warming and impacts of climate extremes in Europe. *Proceedings of the National Academy of Sciences*, *120*(13). https://doi.org/10.1073/pnas.2214525120

Ferster, B. S., Fedorov, A. V., Mignot, J., & Guilyardi, E. (2025). AMOC Variability in Climate Models and Its Dependence on the Mean State. *Geophysical Research Letters*, *52*(3), e2024GL110356. https://doi.org/10.1029/2024GL110356

Forster, P. M., Smith, C., Walsh, T., Lamb, W. F., Lamboll, R., Cassou, C., Hauser, M., Hausfather, Z., Lee, J.-Y., Palmer, M. D., von Schuckmann, K., Slangen, A. B. A., Szopa, S., Trewin, B., Yun, J., Gillett, N. P., Jenkins, S., Matthews, H. D., Raghavan, K., … Zhai, P. (2025). Indicators of Global Climate Change 2024: Annual update of key indicators of the state of the climate system and human influence. *Earth System Science Data*, *17*(6), 2641–2680. https://doi.org/10.5194/essd-17-2641-2025

Forster, P. M., Storelvmo, T., Armour, K., Collins, W., Dufresne, J.-L., Frame, D., Lunt, D., Mauritsen, T., Palmer, M., Watanabe, M., Wild, M., & Zhang, H. (2021). The Earth's Energy Budget, Climate Feedbacks, and Climate Sensitivity. In V. Masson-Delmotte, P. Zhai, A. Pirani, S. L. Connors, C. Péan, S. Berger, N. Caud, Y. Chen, L. Goldfarb, M. I. Gomis, M. Huang, K. Leitzell, E. Lonnoy, J. B. R. Matthews, T. K. Maycock, T. Waterfield, O. Yelekçi, R. Yu, & B. Zhou (Eds.), *Change 2021: The Physical Science Basis. Contribution of Working Group I to the Sixth Assessment Report of the Intergovernmental Panel on Climate Change* (pp. 923–1054). Cambridge University Press. https://doi.org/10.1017/9781009157896.009

Fox-Kemper, B., Hewitt, H., Xiao, C., Aðalgeirsdóttir, G., Drijfhout, S., Edwards, T., Golledge, N., Hemer, M., Kopp, R., Krinner, G., Mix, A., Notz, D., Nowicki, S., Nurhati, I., Ruiz, L., Sallée, J.-B., Slangen, A., & Yu, Y. (2021). Ocean, cryosphere and sea level change. In V. Masson-Delmotte, P. Zhai, A. Pirani, S. L. Connors, C. Péan, S. Berger, N. Caud, Y. Chen, L. Goldfarb, M. I. Gomis, M. Huang, K. Leitzell, E. Lonnoy, J. B. R. Matthews, T. K. Maycock, T. Waterfield, O. Yelekçi, R. Yu, & B. Zhou (Eds.), *Change 2021: The Physical Science Basis. Contribution of Working Group I to the Sixth Assessment Report of the Intergovernmental Panel on Climate Change* (pp. 1211–1361). Cambridge University Press. https://doi.org/10.1017/9781009157896.011

Frajka-Williams, E., Foukal, N., & Danabasoglu, G. (2023). Should AMOC observations continue: How and why? *Philosophical Transactions of the Royal Society A: Mathematical, Physical and Engineering Sciences*, *381*(2262), 20220195. https://doi.org/10.1098/rsta.2022.0195

Frajka-Williams, E., Ansorge, I. J., Baehr, J., Bryden, H. L., Chidichimo, M. P., Cunningham, S. A., Danabasoglu, G., Dong, S., Donohue, K. A., Elipot, S., Heimbach, P., Holliday, N. P., Hummels, R., Jackson, L. C., Karstensen, J., Lankhorst, M., Le Bras, I. A., Susan Lozier, M., McDonagh, E. L., … Wilson, C. (2019). Atlantic meridional overturning circulation: Observed transport and variability. *Frontiers in Marine Science*, *6*(JUN), 1–18. https://doi.org/10.3389/fmars.2019.00260

Frankcombe, L. M., England, M. H., Kajtar, J. B., Mann, M. E., & Steinman, B. A. (2018). On the Choice of Ensemble Mean for Estimating the Forced Signal in the Presence of Internal Variability. *Journal of Climate*, *31*(14), 5681–5693. https://doi.org/10.1175/JCLI-D-17-0662.1

Frankignoul, C., Gastineau, G., & Kwon, Y.-O. (2013). The Influence of the AMOC Variability on the Atmosphere in CCSM3. *Journal of Climate*, *26*(24), 9774–9790. https://doi.org/10.1175/JCLI-D-12-00862.1

Fricko, O., Havlik, P., Rogelj, J., Klimont, Z., Gusti, M., Johnson, N., Kolp, P., Strubegger, M., Valin, H., Amann, M., Ermolieva, T., Forsell, N., Herrero, M., Heyes, C., Kindermann, G., Krey, V., McCollum, D. L., Obersteiner, M., Pachauri, S., … Riahi, K. (2017). The marker quantification of the Shared Socioeconomic Pathway 2: A middle-of-the-road scenario for the 21st century. *Global Environmental Change*, *42*, 251–267. https://doi.org/10.1016/j.gloenvcha.2016.06.004

Friedlingstein, P., Cox, P., Betts, R., Bopp, L., Bloh, W. v., Brovkin, V., Cadule, P., Doney, S., Eby, M., Fung, I., Bala, G., John, J., Jones, C., Joos, F., Kato, T., Kawamiya, M., Knorr, W., Lindsay, K., Matthews, H. D., … Zeng, N. (2006). Climate–Carbon Cycle Feedback Analysis: Results from the C4MIP Model Intercomparison. *Journal of Climate*, *19*(14), 3337–3353. https://doi.org/10.1175/JCLI3800.1

Friedlingstein, P., O'Sullivan, M., Jones, M. W., Andrew, R. M., Bakker, D. C. E., Hauck, J., Landschützer, P., Le Quéré, C., Luijkx, I. T., Peters, G. P., Peters, W., Pongratz, J., Schwingshackl, C., Sitch, S., Canadell, J. G., Ciais, P., Jackson, R. B., Alin, S. R., Anthoni, P., … Zheng, B. (2023). Global Carbon Budget 2023. *Earth System Science Data*, *15*(12), 5301–5369. https://doi.org/10.5194/essd-15-5301-2023

Friedlingstein, P., O'Sullivan, M., Jones, M. W., Andrew, R. M., Hauck, J., Landschützer, P., Le Quéré, C., Li, H., Luijkx, I. T., Olsen,

A., Peters, G. P., Peters, W., Pongratz, J., Schwingshackl, C., Sitch, S., Canadell, J. G., Ciais, P., Jackson, R. B., Alin, S. R., ... Zeng, J. (2025). Global Carbon Budget 2024. *Earth System Science Data*, *17*(3), 965–1039. https://doi.org/10.5194/essd-17-965-2025

Fyke, J., Sergienko, O., Löfverström, M., Price, S., & Lenaerts, J. T. M. (2018). An Overview of Interactions and Feedbacks Between Ice Sheets and the Earth System. *Reviews of Geophysics*, *56*(2), 361–408. https://doi.org/10.1029/2018rg000600

Gastineau, G., & Frankignoul, C. (2012). Cold-season atmospheric response to the natural variability of the Atlantic meridional overturning circulation. *Climate Dynamics*, *39*(1), 37–57. https://doi.org/10.1007/s00382-011-1109-y

Gatti, L. V., Basso, L. S., Miller, J. B., Gloor, M., Gatti Domingues, L., Cassol, H. L. G., Tejada, G., Aragão, L. E. O. C., Nobre, C., Peters, W., Marani, L., Arai, E., Sanches, A. H., Corrêa, S. M., Anderson, L., Von Randow, C., Correia, C. S. C., Crispim, S. P., & Neves, R. A. L. (2021). Amazonia as a carbon source linked to deforestation and climate change. *Nature*, *595*(7867), 388–393. https://doi.org/10.1038/s41586-021-03629-6

Ghil, M., & Lucarini, V. (2020). The physics of climate variability and climate change. *Reviews of Modern Physics*, *92*(3). https://doi.org/10.1103/revmodphys.92.035002

Goodwin, P., & Lenton, T. M. (2009). Quantifying the feedback between ocean heating and CO2 solubility as an equivalent carbon emission. *Geophysical Research Letters*, *36*(15). https://doi.org/10.1029/2009GL039247

Goosse, H., Kay, J. E., Armour, K. C., Bodas-Salcedo, A., Chepfer, H., Docquier, D., Jonko, A., Kushner, P. J., Lecomte, O., Massonnet, F., Park, H.-S., Pithan, F., Svensson, G., & Vancoppenolle, M. (2018). Quantifying climate feedbacks in polar regions. *Nature Communications*, *9*(1). https://doi.org/10.1038/s41467-018-04173-0

Gruber, N., Clement, D., Carter, B. R., Feely, R. A., van Heuven, S., Hoppema, M., Ishii, M., Key, R. M., Kozyr, A., Lauvset, S. K., Lo Monaco, C., Mathis, J. T., Murata, A., Olsen, A., Perez, F. F., Sabine, C. L., Tanhua, T., & Wanninkhof, R. (2019). The oceanic sink for anthropogenic CO_2 from 1994 to 2007. *Science*, *363*(6432), 1193–1199. https://doi.org/10.1126/science.aau5153

Gu, Q., Gervais, M., Danabasoglu, G., Kim, W. M., Castruccio, F., Maroon, E., & Xie, S.-P. (2024). Wide range of possible trajectories of North Atlantic climate in a warming world. *Nature Communications*, *15*(1), 4221. https://doi.org/10.1038/s41467-024-48401-2

Hankel, C. (2025). The effect of CO2 ramping rate on the transient weakening of the Atlantic Meridional Overturning Circulation. *Proceedings of the National Academy of Sciences*, *122*(1), e2411357121. https://doi.org/10.1073/pnas.2411357121

Hannart, A., Pearl, J., Otto, F. E., Naveau, P., & Ghil, M. (2016). Causal counterfactual theory for the attribution of weather and climate-related events. *Bulletin of the American Meteorological Society*, *97*(1), 99–110. https://doi.org/10.1175/BAMS-D-14-00034.1

Hänsel, M., Drupp, M. A., Johannson, D., Nesje, F., Azar, C. A., Freeman, M., Groom, B., & Sterner, T. (2020). Climate economics support for the UN climate targets. *Nature Climate Change*, *10*. https://doi.org/10.1038/s41558-020-0833-x

Hasselmann, K. (1976). Stochastic climate models Part I. Theory. *Tellus*, *28*(6), 473–485. https://doi.org/10.1111/j.2153-3490.1976.tb00696.x

Hausfather, Z. (2025). An assessment of current policy scenarios over the 21st century and the reduced plausibility of high-emissions pathways. *Dialogues on Climate Change*, 29768659241304854. https://doi.org/10.1177/29768659241304854

Hausfather, Z., & Peters, G. P. (2020). Emissions – the 'business as usual' story is misleading. *Nature*, *577*(7792), 618–620. https://doi.org/10.1038/d41586-020-00177-3

Hawkins, E., Smith, R. S., Gregory, J. M., & Stainforth, D. A. (2016). Irreducible uncertainty in near-term climate projections. *Climate Dynamics*, *46*(11-12), 3807–3819. https://doi.org/10.1007/s00382-015-2806-8

Hawkins, E., & Sutton, R. (2009). The Potential to Narrow Uncertainty in Regional Climate Predictions. *Bulletin of the American Meteorological Society*, *90*(8), 1095–1108. https://doi.org/10.1175/2009BAMS2607.1

Hersbach, H., Bell, B., Berrisford, P., Hirahara, S., Horányi, A., Muñoz-Sabater, J., Nicolas, J., Peubey, C., Radu, R., Schepers, D., Simmons, A., Soci, C., Abdalla, S., Abellan, X., Balsamo, G., Bechtold, P., Biavati, G., Bidlot, J., Bonavita, M., … Thépaut, J.-N. (2020). The ERA5 global reanalysis. *Quarterly Journal of the Royal Meteorological Society*, *146*(730), 1999–2049. https://doi.org/10.1002/qj.3803

Hirschi, J., Baehr, J., Marotzke, J., Stark, J., Cunningham, S., & Beismann, J. O. (2003). A monitoring design for the Atlantic meridional overturning circulation. *Geophysical Research Letters*, *30*(7), 7–10. https://doi.org/10.1029/2002GL016776

Hirschi, J. J.-M., Killworth, P. D., & Blundell, J. R. (2007). Subannual, Seasonal, and Interannual Variability of the North Atlantic Meridional Overturning Circulation. *Journal of Physical*

Oceanography, *37*(5), 1246–1265. https://doi.org/10.1175/JPO3049.1

Horton, R. M., Mankin, J. S., Lesk, C., Coffel, E., & Raymond, C. (2016). A Review of Recent Advances in Research on Extreme Heat Events. *Current Climate Change Reports*, *2*(4), 242–259. https://doi.org/10.1007/s40641-016-0042-x

Howard, P. H., & Sterner, T. (2017). Few and not so far between: A meta-analysis of climate damage estimates. *Environmental & Resource Economics*, *68*(1, SI), 197–225. https://doi.org/10.1007/s10640-017-0166-z

Huntingford, C., Jones, P. D., Livina, V. N., Lenton, T. M., & Cox, P. M. (2013). No increase in global temperature variability despite changing regional patterns. *Nature*, *500*(7462), 327–330. https://doi.org/10.1038/nature12310

Hurrell, J. W. (1995). Decadal Trends in the North Atlantic Oscillation: Regional Temperatures and Precipitation. *Science*, *269*(5224), 676–679. https://doi.org/10.1126/science.269.5224.676

Hurrell, J. W., & Deser, C. (2010). North Atlantic climate variability: The role of the North Atlantic Oscillation. *Impact of climate variability on marine ecosystems: A comparative approach*, *79*(3), 231–244. https://doi.org/10.1016/j.jmarsys.2009.11.002

Hurrell, J., Kushnir, Y., Ottersen, G., & Visbeck, M. (2003, January). *The North Atlantic Oscillation: Climatic Significance and Environmental Impact* (Vol. 134). https://doi.org/10.1029/GM134

Iturbide, M., Gutiérrez, J. M., Alves, L. M., Bedia, J., Cerezo-Mota, R., Cimadevilla, E., Cofiño, A. S., Di Luca, A., Faria, S. H., Gorodetskaya, I. V., Hauser, M., Herrera, S., Hennessy, K., Hewitt, H. T., Jones, R. G., Krakovska, S., Manzanas, R., Martínez-Castro, D., Narisma, G. T., … Vera, C. S. (2020). An update of IPCC climate reference regions for subcontinental analysis of climate model data: Definition and aggregated datasets. *Earth System Science Data*, *12*(4), 2959–2970. https://doi.org/10.5194/essd-12-2959-2020

Jackson, L. C., Kahana, R., Graham, T., Ringer, M. A., Woollings, T., Mecking, J. V., & Wood, R. A. (2015). Global and European climate impacts of a slowdown of the AMOC in a high resolution GCM. *Climate Dynamics*, *45*(11-12), 3299–3316. https://doi.org/10.1007/s00382-015-2540-2

Jackson, L. C., Alastrué de Asenjo, E., Bellomo, K., Danabasoglu, G., Haak, H., Hu, A., Jungclaus, J., Lee, W., Meccia, V. L., Saenko, O., Shao, A., & Swingedouw, D. (2023a). Understanding AMOC stability: The North Atlantic Hosing Model Intercomparison Project. *Geoscientific Model Development*, *16*(7), 1975–1995. https://doi.org/10.5194/gmd-16-1975-2023

Jackson, L. C., Biastoch, A., Buckley, M. W., Desbruyères, D. G., Williams, E. F., Moat, B., & Robson, J. (2022). The evolution of

the North Atlantic Meridional Overturning Circulation since 1980. *Nature Reviews Earth & Environment*, *0123456789*. https://doi.org/10.1038/s43017-022-00263-2

Jackson, L. C., Hewitt, H. T., Bruciaferri, D., Calvert, D., Graham, T., Guiavarc'h, C., Menary, M. B., New, A. L., Roberts, M., & Storkey, D. (2023b). Challenges simulating the AMOC in climate models. *Philosophical Transactions of the Royal Society A: Mathematical, Physical and Engineering Sciences*, *381*(2262), 20220187. https://doi.org/10.1098/rsta.2022.0187

Jacob, D., Goettel, H., Jungclaus, J., Muskulus, M., Podzun, R., & Marotzke, J. (2005). Slowdown of the thermohaline circulation causes enhanced maritime climate influence and snow cover over Europe. *Geophysical Research Letters*, *32*(21), 1–5. https://doi.org/10.1029/2005GL023286

Johnson, H. L., Cessi, P., Marshall, D. P., Schloesser, F., & Spall, M. A. (2019). Recent Contributions of Theory to Our Understanding of the Atlantic Meridional Overturning Circulation. *Journal of Geophysical Research: Oceans*, *124*(8), 5376–5399. https://doi.org/10.1029/2019JC015330

Jones, C. D., Arora, V., Friedlingstein, P., Bopp, L., Brovkin, V., Dunne, J., Graven, H., Hoffman, F., Ilyina, T., John, J. G., Jung, M., Kawamiya, M., Koven, C., Pongratz, J., Raddatz, T., Randerson, J. T., & Zaehle, S. (2016). C4MIP – The Coupled Climate–Carbon Cycle Model Intercomparison Project:experimental protocol for CMIP6. *Geoscientific Model Development*, *9*(8), 2853–2880. https://doi.org/10.5194/gmd-9-2853-2016

Jones, C. D., Frölicher, T. L., Koven, C., MacDougall, A. H., Matthews, H. D., Zickfeld, K., Rogelj, J., Tokarska, K. B., Gillett, N. P., Ilyina, T., Meinshausen, M., Mengis, N., Séférian, R., Eby, M., & Burger, F. A. (2019). The Zero Emissions Commitment Model Intercomparison Project (ZECMIP) contribution to C4MIP: Quantifying committed climate changes following zero carbon emissions. *Geoscientific Model Development*, *12*(10), 4375–4385. https://doi.org/10.5194/gmd-12-4375-2019

Jungclaus, J. H., Fischer, N., Haak, H., Lohmann, K., Marotzke, J., Matei, D., Mikolajewicz, U., Notz, D., & Von Storch, J. S. (2013). Characteristics of the ocean simulations in the Max Planck Institute Ocean Model (MPIOM) the ocean component of the MPI-Earth system model. *Journal of Advances in Modeling Earth Systems*, *5*(2), 422–446. https://doi.org/10.1002/jame.20023

Katavouta, A., & Williams, R. G. (2021). Ocean carbon cycle feedbacks in CMIP6 models: Contributions from different basins. *Biogeosciences*, *18*(10), 3189–3218. https://doi.org/10.5194/bg-18-3189-2021

Keen, S., Lenton, T. M., Garrett, T. J., Rae, J. W. B., Hanley, B. P., & Grasselli, M. (2022). Estimates of economic and environmen-

tal damages from tipping points cannot be reconciled with the scientific literature. *Proceedings of the National Academy of Sciences*, *119*(21), e2117308119. https://doi.org/10.1073/pnas.2117308119

Keller, D. P., Lenton, A., Scott, V., Vaughan, N. E., Bauer, N., Ji, D., Jones, C. D., Kravitz, B., Muri, H., & Zickfeld, K. (2018). The Carbon Dioxide Removal Model Intercomparison Project (CDRMIP): Rationale and experimental protocol for CMIP6. *Geoscientific Model Development*, *11*(3), 1133–1160. https://doi.org/10.5194/gmd-11-1133-2018

Khatiwala, S., Tanhua, T., Mikaloff Fletcher, S., Gerber, M., Doney, S. C., Graven, H. D., Gruber, N., McKinley, G. A., Murata, A., Ríos, A. F., & Sabine, C. L. (2013). Global ocean storage of anthropogenic carbon. *Biogeosciences*, *10*(4), 2169–2191. https://doi.org/10.5194/bg-10-2169-2013

King, A. D., Abram, N. J., Alastrué De Asenjo, E., & Ziehn, T. (2025a, March). ESD Ideas: Extended net zero simulations are critical for informed decision making. https://doi.org/10.5194/egusphere-2025-903

King, A. D., Borowiak, A. R., Brown, J. R., Frame, D. J., Harrington, L. J., Min, S.-K., Pendergrass, A., Rugenstein, M., Sniderman, J. M. K., & Stone, D. A. (2021a). Transient and Quasi-Equilibrium Climate States at 1.5°C and 2°C Global Warming. *Earth's Future*, *9*(11), e2021EF002274. https://doi.org/10.1029/2021EF002274

King, A. D., & Karoly, D. J. (2017). Climate extremes in Europe at 1.5 and 2 degrees of global warming. *Environmental Research Letters*, *12*(11), 114031. https://doi.org/10.1088/1748-9326/aa8e2c

King, A. D., Lane, T. P., Henley, B. J., & Brown, J. R. (2020). Global and regional impacts differ between transient and equilibrium warmer worlds. *Nature Climate Change*, *10*(1), 42–47. https://doi.org/10.1038/s41558-019-0658-7

King, A. D., Sniderman, J. M. K., Dittus, A. J., Brown, J. R., Hawkins, E., & Ziehn, T. (2021b). Studying climate stabilization at Paris Agreement levels. *Nature Climate Change*, *11*(12), 1010–1013. https://doi.org/10.1038/s41558-021-01225-0

King, A. D., Ziehn, T., Chamberlain, M., Borowiak, A. R., Brown, J. R., Cassidy, L., Dittus, A. J., Grose, M., Maher, N., Paik, S., Perkins-Kirkpatrick, S. E., & Sengupta, A. (2024). Exploring climate stabilisation at different global warming levels in ACCESS-ESM-1.5. *Earth System Dynamics*, *15*(5), 1353–1383. https://doi.org/10.5194/esd-15-1353-2024

King, A. D., Alastrué de Asenjo, E., Maycock, A., Ziehn, T., Borowiak, A. R., Clark, S., & Maher, N. (2025b). Detectability of post-net zero climate changes and the effects of delay in emissions

cessation. https://doi.org/10.22541/au.173930365.54563852/v1

Kodra, E., Steinhaeuser, K., & Ganguly, A. R. (2011). Persisting cold extremes under 21st-century warming scenarios. *Geophysical Research Letters*, *38*(8), n/a–n/a. https://doi.org/10.1029/2011gl047103

Kopp, R. E., Shwom, R. L., Wagner, G., & Yuan, J. (2016). Tipping elements and climate–economic shocks: Pathways toward integrated assessment. *Earth's Future*, *4*(8), 346–372. https://doi.org/10.1002/2016EF000362

Kuhlbrodt, T., Rahmstorf, S., Zickfeld, K., Vikebø, F. B., Sundby, S., Hofmann, M., Link, P. M., Bondeau, A., Cramer, W., & Jaeger, C. (2009). An integrated assessment of changes in the thermohaline circulation. *Climatic Change*, *96*(4), 489–537. https://doi.org/10.1007/s10584-009-9561-y

Latif, M., & Keenlyside, N. S. (2009). El Niño/Southern Oscillation response to global warming. *Proceedings of the National Academy of Sciences*, *106*(49), 20578–20583. https://doi.org/10.1073/pnas.0710860105

Latif, M., Sun, J., Visbeck, M., & Hadi Bordbar, M. (2022). Natural variability has dominated Atlantic Meridional Overturning Circulation since 1900. *Nature Climate Change*. https://doi.org/10.1038/s41558-022-01342-4

Laurian, A., Drijfhout, S. S., Hazeleger, W., & van den Hurk, B. (2010). Response of the Western European climate to a collapse of the thermohaline circulation. *Climate Dynamics*, *34*(5), 689–697. https://doi.org/10.1007/s00382-008-0513-4

Leach, N. J., Jenkins, S., Nicholls, Z., Smith, C. J., Lynch, J., Cain, M., Walsh, T., Wu, B., Tsutsui, J., & Allen, M. R. (2021). Fairv2.0.0: A generalized impulse response model for climate uncertainty and future scenario exploration. *Geoscientific Model Development*, *14*(5), 3007–3036. https://doi.org/10.5194/gmd-14-3007-2021

Lee, J.-Y., Marotzke, J., Bala, G., Cao, L., Corti, S., Dunne, J., Engelbrecht, F., Fischer, E., Fyfe, J., Jones, C., Maycock, A., Mutemi, J., Ndiaye, O., Panickal, S., & Zhou, T. (2021). Future Global Climate: Scenario-Based Projections and Near-Term Information. In V. Masson-Delmotte, P. Zhai, A. Pirani, S. L. Connors, C. Péan, S. Berger, N. Caud, Y. Chen, L. Goldfarb, M. I. Gomis, M. Huang, K. Leitzell, E. Lonnoy, J. B. R. Matthews, T. K. Maycock, T. Waterfield, O. Yelekçi, R. Yu, & B. Zhou (Eds.), *Change 2021: The Physical Science Basis. Contribution of Working Group I to the Sixth Assessment Report of the Intergovernmental Panel on Climate Change* (pp. 553–672). Cambridge University Press. https://doi.org/10.1017/9781009157896.006

Lee, Y.-H., Yeh, S.-W., Wang, G., An, S.-I., Song, H., Son, S.-W., & Yang, Y.-M. (2025). Early or delayed Northern Hemisphere warming driven by the AMOC in a net-zero CO2 world. *npj Climate and Atmospheric Science*, *8*(1), 291. https://doi.org/10.1038/s41612-025-01165-y

Lehner, F., & Deser, C. (2023). Origin, importance, and predictive limits of internal climate variability. *Environmental Research: Climate*, *2*(2), 023001. https://doi.org/10.1088/2752-5295/accf30

Lenton, T. M., Held, H., Kriegler, E., Hall, J. W., Lucht, W., Rahmstorf, S., & Schellnhuber, H. J. (2009). Tipping elements in the Earth System. *Proceedings of the National Academy of Sciences of the United States of America*, *106*(49), 20561–20563. https://doi.org/10.1073/pnas.0911106106

Lesk, C., Anderson, W., Rigden, A., Coast, O., Jägermeyr, J., McDermid, S., Davis, K. F., & Konar, M. (2022). Compound heat and moisture extreme impacts on global crop yields under climate change. *Nature Reviews Earth & Environment*, *3*(12), 872–889. https://doi.org/10.1038/s43017-022-00368-8

Levermann, A., Griesel, A., Hofmann, M., Montoya, M., & Rahmstorf, S. (2005). Dynamic sea level changes following changes in the thermohaline circulation. *Climate Dynamics*, *24*(4), 347–354. https://doi.org/10.1007/s00382-004-0505-y

Lhotka, O., & Kyselý, J. (2022). The 2021 European Heat Wave in the Context of Past Major Heat Waves. *Earth and Space Science*, *9*(11), e2022EA002567. https://doi.org/10.1029/2022EA002567

Li, C., Zwiers, F., Zhang, X., Li, G., Sun, Y., & Wehner, M. (2021). Changes in Annual Extremes of Daily Temperature and Precipitation in CMIP6 Models. *Journal of Climate*, *34*(9), 3441–3460. https://doi.org/10.1175/JCLI-D-19-1013.1

Little, C. M., Hu, A., Hughes, C. W., McCarthy, G. D., Piecuch, C. G., Ponte, R. M., & Thomas, M. D. (2019). The Relationship Between U.S. East Coast Sea Level and the Atlantic Meridional Overturning Circulation: A Review. *Journal of Geophysical Research: Oceans*, *124*(9), 6435–6458. https://doi.org/10.1029/2019jc015152

Liu, Q., Bader, J., Jungclaus, J. H., & Matei, D. (2025). More extreme summertime North Atlantic Oscillation under climate change. *Communications Earth & Environment*, *6*(1), 474. https://doi.org/10.1038/s43247-025-02422-x

Liu, W., Duarte Cavalcante Pinto, D., Fedorov, A., & Zhu, J. (2023a). The Impacts of a Weakened Atlantic Meridional Overturning Circulation on ENSO in a Warmer Climate. *Geophysical Research Letters*, *50*(8). https://doi.org/10.1029/2023gl103025

Liu, W., & Fedorov, A. (2022). Interaction between Arctic sea ice and the Atlantic meridional overturning circulation in a warming

climate. *Climate Dynamics*, *58*(5), 1811–1827. https://doi.org/10.1007/s00382-021-05993-5

Liu, W., Fedorov, A. V., Xie, S. P., & Hu, S. (2020). Climate impacts of a weakened Atlantic meridional overturning circulation in a warming climate. *Science Advances*, *6*(26), 1–8. https://doi.org/10.1126/sciadv.aaz4876

Liu, W., Xie, S.-P., Liu, Z., & Zhu, J. (2017). Overlooked possibility of a collapsed Atlantic Meridional Overturning Circulation in warming climate. *Science Advances*, *3*(1), e1601666. https://doi.org/10.1126/sciadv.1601666

Liu, Y., Moore, J. K., Primeau, F., & Wang, W. L. (2023b). Reduced CO2 uptake and growing nutrient sequestration from slowing overturning circulation. *Nature Climate Change*, *13*(1), 83–90. https://doi.org/10.1038/s41558-022-01555-7

Lorenz, E. N. (1963). Deterministic Nonperiodic Flow. *Journal of the Atmospheric Sciences*, *20*(2), 130–141. https://doi.org/10.1175/1520-0469(1963)020<0130:DNF>2.0.CO;2

Ma, Q., Shi, X., Scholz, P., Sidorenko, D., Lohmann, G., & Ionita, M. (2024). Revisiting climate impacts of an AMOC slowdown: Dependence on freshwater locations in the North Atlantic. *Science Advances*, *10*(47), eadr3243. https://doi.org/10.1126/sciadv.adr3243

MacDougall, A. H., Frölicher, T. L., Jones, C. D., Rogelj, J., Matthews, H. D., Zickfeld, K., Arora, V. K., Barrett, N. J., Brovkin, V., Burger, F. A., Eby, M., Eliseev, A. V., Hajima, T., Holden, P. B., Jeltsch-Thömmes, A., Koven, C., Mengis, N., Menviel, L., Michou, M., … Ziehn, T. (2020). Is there warming in the pipeline? A multi-model analysis of the Zero Emissions Commitment from CO_2. *Biogeosciences*, *17*(11), 2987–3016. https://doi.org/10.5194/bg-17-2987-2020

MacDougall, A. H., Mallett, J., Hohn, D., & Mengis, N. (2022). Substantial regional climate change expected following cessation of CO2 emissions. *Environmental Research Letters*, *17*(11), 114046. https://doi.org/10.1088/1748-9326/ac9f59

Mahajan, S., Zhang, R., & Delworth, T. L. (2011). Impact of the Atlantic Meridional Overturning Circulation (AMOC) on Arctic Surface Air Temperature and Sea Ice Variability. *Journal of Climate*, *24*(24), 6573–6581. https://doi.org/10.1175/2011jcli4002.1

Maher, N., Milinski, S., & Ludwig, R. (2021). Large ensemble climate model simulations: Introduction, overview, and future prospects for utilising multiple types of large ensemble. *Earth System Dynamics*, *12*(2), 401–418. https://doi.org/10.5194/esd-12-401-2021

Maher, N., Milinski, S., Suarez-Gutierrez, L., Botzet, M., Dobrynin, M., Kornblueh, L., Kröger, J., Takano, Y., Ghosh, R., Hede-

mann, C., Li, C., Li, H., Manzini, E., Notz, D., Putrasahan, D., Boysen, L., Claussen, M., Ilyina, T., Olonscheck, D., … Marotzke, J. (2019). The Max Planck Institute Grand Ensemble: Enabling the Exploration of Climate System Variability. *Journal of Advances in Modeling Earth Systems*, *11*(7), 2050–2069. https://doi.org/10.1029/2019MS001639

Marotzke, J. (2023). From theory to RAPID AMOC observations: A personal voyage of discovery. *Philosophical Transactions of the Royal Society A: Mathematical, Physical and Engineering Sciences*, *381*(2262), 20220192. https://doi.org/10.1098/rsta.2022.0192

Marotzke, J., & Forster, P. M. (2015). Forcing, feedback and internal variability in global temperature trends. *Nature*, *517*(7536), 565–570. https://doi.org/10.1038/nature14117

Marshall, J., Johnson, H., & Goodman, J. (2001a). A Study of the Interaction of the North Atlantic Oscillation with Ocean Circulation. *Journal of Climate*, *14*(7), 1399–1421. https://doi.org/10.1175/1520-0442(2001)014<1399:asotio>2.0.co;2

Marshall, J., Kushnir, Y., Battisti, D., Chang, P., Czaja, A., Dickson, R., Hurrell, J., McCartney, M., Saravanan, R., & Visbeck, M. (2001b). North Atlantic climate variability: Phenomena, impacts and mechanisms. *International Journal of Climatology*, *21*(15), 1863–1898. https://doi.org/10.1002/joc.693

Mastrandrea, M. D., Field, C. B., Stocker, T. F., Edenhofer, O., Ebi, K. L., Frame, D. J., Held, H., Kriegler, E., Mach, K. J., Matschoss, P. R., Plattner, G.-K., Yohe, G. W., & Zwiers, F. W. (2010). Guidance Note for Lead Authors of the IPCC Fifth Assessment Report on Consistent Treatment of Uncertainties. http://www.ipcc.ch

Matthews, H. D., & Weaver, A. J. (2010). Committed climate warming. *Nature Geoscience*, *3*(3), 142–143. https://doi.org/10.1038/ngeo813

Matthews, T., Raymond, C., Foster, J., Baldwin, J. W., Ivanovich, C., Kong, Q., Kinney, P., & Horton, R. M. (2025). Mortality impacts of the most extreme heat events. *Nature Reviews Earth & Environment*, *6*(3), 193–210. https://doi.org/10.1038/s43017-024-00635-w

Mauritsen, T., Bader, J., Becker, T., Behrens, J., Bittner, M., Brokopf, R., Brovkin, V., Claussen, M., Crueger, T., Esch, M., Fast, I., Fiedler, S., Fläschner, D., Gayler, V., Giorgetta, M., Goll, D. S., Haak, H., Hagemann, S., Hedemann, C., … Roeckner, E. (2019). Developments in the MPI-M Earth System Model version 1.2 (MPI-ESM1.2) and Its Response to Increasing CO2. *Journal of Advances in Modeling Earth Systems*, *11*(4), 998–1038. https://doi.org/10.1029/2018MS001400

McCarthy, G., Frajka-Williams, E., Johns, W. E., Baringer, M. O., Meinen, C. S., Bryden, H. L., Rayner, D., Duchez, A., Roberts,

C., & Cunningham, S. A. (2012). Observed interannual variability of the Atlantic meridional overturning circulation at 26.5°N. *Geophysical Research Letters*, *39*(19). https://doi.org/10.1029/2012GL052933

Meccia, V. L., & Blázquez, J. (2025). Impacts of a Reduced AMOC on the South America Mean Climate and Extremes. *Journal of Geophysical Research: Atmospheres*, *130*(18), e2025JD044103. https://doi.org/10.1029/2025JD044103

Meccia, V. L., Simolo, C., Bellomo, K., & Corti, S. (2024). Extreme cold events in Europe under a reduced AMOC. *Environmental Research Letters*, *19*(1), 014054. https://doi.org/10.1088/1748-9326/ad14b0

Meccia, V. L., Simolo, C., Bellomo, K., & Corti, S. (2025). The impact of a weakened AMOC on European heatwaves. *Environmental Research Letters*, *20*(2), 024005. https://doi.org/10.1088/1748-9326/ada3e7

Mecking, J. V., & Drijfhout, S. S. (2023). The decrease in ocean heat transport in response to global warming. *Nature Climate Change*, *13*(11), 1229–1236. https://doi.org/10.1038/s41558-023-01829-8

Mecking, J. V., Keenlyside, N. S., & Greatbatch, R. J. (2015). Multiple timescales of stochastically forced North Atlantic Ocean variability: A model study. *Ocean Dynamics*, *65*(9-10), 1367–1381. https://doi.org/10.1007/s10236-015-0868-0

Mitchell, J. M. (1976). An Overview of Climatic Variability and its Causal Mechanisms. *Quaternary Research*, *6*(4), 481–493. https://doi.org/10.1016/0033-5894(76)90021-1

Mitevski, I., Lee, S. H., Vecchi, G., Orbe, C., & Polvani, L. M. (2025). More positive and less variable North Atlantic Oscillation at high CO2 forcing. *npj Climate and Atmospheric Science*, *8*(1), 1–9. https://doi.org/10.1038/s41612-025-01051-7

Moat, B. I., Smeed, D., Rayner, D., Johns, W. E., Smith, R. H., Volkov, Denis L, Volkov, D. L., Elipot, S., Petit, T., Katjar, J. B., Baringer, M. O., & Collins, J. (2025). Atlantic meridional overturning circulation observed by the RAPID-MOCHA-WBTS (RAPID-Meridional Overturning Circulation and Heatflux Array-Western Boundary Time Series) array at 26N from 2004 to 2023 (v2023.1a). https://doi.org/10.5285/33826D6E-801C-B0A7-E063-7086ABC0B9DB

Monteiro, P., Sallée, J., P., F., Fox-Kemper, B., Hewitt, H., Ishii, M., Rogelj, J., & Zickfeld, K. (2021). The ocean carbon-heat nexus and climate change commitment. In V. Masson-Delmotte, P. Zhai, A. Pirani, S. Connors, C. Péan, S. Berger, N. Caud, Y. Chen, L. Goldfarb, M. Gomis, M. Huang, K. Leitzell, E. Lonnoy, J. Matthews, T. Maycock, T. Waterfield, O. Yelekçi, R. Yu, & B. Zhou (Eds.), *Climate Change 2021: The Physical Science Basis.*

Contribution of Working Group I to the Sixth Assessment Report of the Intergovernmental Panel on Climate Change (pp. 743–746). Cambridge University Press.

Moore, F. C., Drupp, M. A., Rising, J., Dietz, S., Rudik, I., & Wagner, G. (2024). Synthesis of evidence yields high social cost of carbon due to structural model variation and uncertainties. *Proceedings of the National Academy of Sciences*, *121*(52), e2410733121. https://doi.org/10.1073/pnas.2410733121

Nath, I. B., Ramey, V. A., & Klenow, P. J. (2024, July). *How Much Will Global Warming Cool Global Growth?* (Working Paper No. 32761). National Bureau of Economic Research. https://doi.org/10.3386/w32761

Nesje, F., Drupp, M. A., Freeman, M. C., & Groom, B. (2023). Philosophers and economists agree on climate policy paths but for different reasons. *Nature Climate Change*, *13*(6), 515–522. https://doi.org/10.1038/s41558-023-01681-w

Nielsen, S. B., Jochum, M., Pedro, J. B., Eden, C., & Nuterman, R. (2019). Two-Timescale Carbon Cycle Response to an AMOC Collapse. *Paleoceanography and Paleoclimatology*, *34*(4), 511–523. https://doi.org/10.1029/2018PA003481

Nordhaus, W. (2014). Estimates of the Social Cost of Carbon: Concepts and Results from the DICE-2013R Model and Alternative Approaches. *Journal of the Association of Environmental and Resource Economists*, *1*(1/2), 273–312. https://doi.org/10.1086/676035

Nordhaus, W. (2019). Economics of the disintegration of the Greenland ice sheet. *Proceedings of the National Academy of Sciences*, *116*(25), 12261–12269. https://doi.org/10.1073/pnas.1814990116

Nordhaus, W. D. (2017). Revisiting the social cost of carbon. *Proceedings of the National Academy of Sciences*, *114*(7), 1518–1523. https://doi.org/10.1073/pnas.1609244114

Notz, D., & SIMIP Community. (2020). Arctic Sea Ice in CMIP6. *Geophysical Research Letters*, *47*(10), e2019GL086749. https://doi.org/10.1029/2019GL086749

Obata, A. (2007). Climate–Carbon Cycle Model Response to Freshwater Discharge into the North Atlantic. *Journal of Climate*, *20*(24), 5962–5976. https://doi.org/10.1175/2007jcli1808.1

Oelsmann, J., Borchert, L., Hand, R., Baehr, J., & Jungclaus, J. H. (2020). Linking Ocean Forcing and Atmospheric Interactions to Atlantic Multidecadal Variability in MPI-ESM1.2. *Geophysical Research Letters*, *47*(10). https://doi.org/10.1029/2020GL087259

Olonscheck, D., Mauritsen, T., & Notz, D. (2019). Arctic sea-ice variability is primarily driven by atmospheric temperature fluctu-

ations. *Nature Geoscience*, *12*(6), 430–434. https://doi.org/10.1038/s41561-019-0363-1

Olonscheck, D., Suarez-Gutierrez, L., Milinski, S., Beobide-Arsuaga, G., Baehr, J., Fröb, F., Ilyina, T., Kadow, C., Krieger, D., Li, H., Marotzke, J., Plésiat, É., Schupfner, M., Wachsmann, F., Wallberg, L., Wieners, K.-H., & Brune, S. (2023). The New Max Planck Institute Grand Ensemble With CMIP6 Forcing and High-Frequency Model Output. *Journal of Advances in Modeling Earth Systems*, *15*(10), e2023MS003790. https://doi.org/10.1029/2023MS003790

O'Neill, B. C., Tebaldi, C., Van Vuuren, D. P., Eyring, V., Friedlingstein, P., Hurtt, G., Knutti, R., Kriegler, E., Lamarque, J. F., Lowe, J., Meehl, G. A., Moss, R., Riahi, K., & Sanderson, B. M. (2016). The Scenario Model Intercomparison Project (ScenarioMIP) for CMIP6. *Geoscientific Model Development*, *9*(9), 3461–3482. https://doi.org/10.5194/gmd-9-3461-2016

Open Letter by Climate Scientists to the Nordic Council of Ministers. (2024, October). https://en.vedur.is/media/ads_in_header/AMOC-letter_Final.pdf

Orihuela-Pinto, B., England, M. H., & Taschetto, A. S. (2022). Interbasin and interhemispheric impacts of a collapsed Atlantic Overturning Circulation. *Nature Climate Change*, *12*(6), 558–565. https://doi.org/10.1038/s41558-022-01380-y

Otto, F., Clarke, B., Barnes, C., Kimutai, J., Zachariah, M., Merz, N., Vrkic, D., Sjoukje, P., Kew, S., Pinto, I., Vahlberg, M., Singh, R., Horne, Z., Arrighi, J., Sparks, N., Guiguere, J., & Gilford, D. (2024, October). 10 years of rapidly disentangling drivers of extreme weather disasters. https://doi.org/10.25561/115431

Palazzo Corner, S., Siegert, M., Ceppi, P., Fox-Kemper, B., Frölicher, T. L., Gallego-Sala, A., Haigh, J., Hegerl, G. C., Jones, C. D., Knutti, R., Koven, C. D., MacDougall, A. H., Meinshausen, M., Nicholls, Z., Sallée, J. B., Sanderson, B. M., Séférian, R., Turetsky, M., Williams, R. G., … Rogelj, J. (2023). The Zero Emissions Commitment and climate stabilization. *Frontiers in Science*, *1*. https://doi.org/10.3389/fsci.2023.1170744

Parsons, L. A., Yin, J., Overpeck, J. T., Stouffer, R. J., & Malyshev, S. (2014). Influence of the Atlantic Meridional Overturning Circulation on the monsoon rainfall and carbon balance of the American tropics. *Geophysical Research Letters*, *41*(1), 146–151. https://doi.org/10.1002/2013gl058454

Patterson, M. (2023). North-West Europe Hottest Days Are Warming Twice as Fast as Mean Summer Days. *Geophysical Research Letters*, *50*(10), e2023GL102757. https://doi.org/10.1029/2023GL102757

Pérez, F. F., Mercier, H., Vázquez-Rodríguez, M., Lherminier, P., Velo, A., Pardo, P. C., Rosón, G., & Ríos, A. F. (2013). Atlantic Ocean

CO_2 uptake reduced by weakening of the meridional overturning circulation. *Nature Geoscience*, *6*(2), 146–152. https://doi.org/10.1038/ngeo1680

Pohlmann, H., Sienz, F., & Latif, M. (2006). Influence of the multidecadal Atlantic meridional overturning circulation variability on European climate. *Journal of Climate*, *19*(23), 6062–6067. https://doi.org/10.1175/JCLI3941.1

Polo, I., Robson, J., Sutton, R., & Balmaseda, M. A. (2014). The Importance of Wind and Buoyancy Forcing for the Boundary Density Variations and the Geostrophic Component of the AMOC at 26°N. *Journal of Physical Oceanography*, *44*(9), 2387–2408. https://doi.org/10.1175/JPO-D-13-0264.1

Quesada, B., Vautard, R., & Yiou, P. (2023). Cold waves still matter: Characteristics and associated climatic signals in Europe. *Climatic Change*, *176*(6), 70. https://doi.org/10.1007/s10584-023-03533-0

Rantanen, M., Karpechko, A. Y., Lipponen, A., Nordling, K., Hyvärinen, O., Ruosteenoja, K., Vihma, T., & Laaksonen, A. (2022). The Arctic has warmed nearly four times faster than the globe since 1979. *Communications Earth & Environment*, *3*(1), 168. https://doi.org/10.1038/s43247-022-00498-3

Rashid, H. A., Sullivan, A., Dix, M., Bi, D., Mackallah, C., Ziehn, T., Dobrohotoff, P., O'Farrell, S., Harman, I. N., Bodman, R., & Marsland, S. (2022). Evaluation of climate variability and change in ACCESS historical simulations for CMIP6. *Journal of Southern Hemisphere Earth Systems Science*, *72*(2), 73–92. https://doi.org/10.1071/ES21028

Rennert, K., Errickson, F., Prest, B. C., Rennels, L., Newell, R. G., Pizer, W., Kingdon, C., Wingenroth, J., Cooke, R., Parthum, B., Smith, D., Cromar, K., Diaz, D., Moore, F. C., Müller, U. K., Plevin, R. J., Raftery, A. E., Ševčíková, H., Sheets, H., … Anthoff, D. (2022). Comprehensive Evidence Implies a Higher Social Cost of CO_2. *Nature*, *610*, 1–3. https://doi.org/10.1038/s41586-022-05224-9

Riebold, J., Richling, A., Ulbrich, U., Rust, H., Semmler, T., & Handorf, D. (2023). On the linkage between future Arctic sea ice retreat, Euro-Atlantic circulation regimes and temperature extremes over Europe. *Weather and Climate Dynamics*, *4*(3), 663–682. https://doi.org/10.5194/wcd-4-663-2023

Ritchie, P. D. L., Smith, G. S., Davis, K. J., Fezzi, C., Halleck-Vega, S., Harper, A. B., Boulton, C. A., Binner, A. R., Day, B. H., Gallego-Sala, A. V., Mecking, J. V., Sitch, S. A., Lenton, T. M., & Bateman, I. J. (2020). Shifts in national land use and food production in Great Britain after a climate tipping point. *Nature Food*, *1*(1), 76–83. https://doi.org/10.1038/s43016-019-0011-3

Robson, J., Sutton, R., & Smith, D. (2014). Decadal predictions of the cooling and freshening of the North Atlantic in the 1960s and the role of ocean circulation. *Climate Dynamics*, *42*(9-10), 2353–2365. https://doi.org/10.1007/s00382-014-2115-7

Rodgers, K. B., Lee, S.-S., Rosenbloom, N., Timmermann, A., Danabasoglu, G., Deser, C., Edwards, J., Kim, J.-E., Simpson, I. R., Stein, K., Stuecker, M. F., Yamaguchi, R., Bódai, T., Chung, E.-S., Huang, L., Kim, W. M., Lamarque, J.-F., Lombardozzi, D. L., Wieder, W. R., & Yeager, S. G. (2021). Ubiquity of human-induced changes in climate variability. *Earth System Dynamics*, *12*(4), 1393–1411. https://doi.org/10.5194/esd-12-1393-2021

Rousi, E., Kornhuber, K., Beobide-Arsuaga, G., Luo, F., & Coumou, D. (2022). Accelerated western European heatwave trends linked to more-persistent double jets over Eurasia. *Nature Communications*, *13*(1), 3851. https://doi.org/10.1038/s41467-022-31432-y

Rugenstein, M., Bloch-Johnson, J., Abe-Ouchi, A., Andrews, T., Beyerle, U., Cao, L., Chadha, T., Danabasoglu, G., Dufresne, J.-L., Duan, L., Foujols, M.-A., Frölicher, T., Geoffroy, O., Gregory, J., Knutti, R., Li, C., Marzocchi, A., Mauritsen, T., Menary, M., … Yang, S. (2019). LongRunMIP: Motivation and Design for a Large Collection of Millennial-Length AOGCM Simulations. *Bulletin of the American Meteorological Society*, *100*(12), 2551–2570. https://doi.org/10.1175/BAMS-D-19-0068.1

Russo, E., & Domeisen, D. I. V. (2023). Increasing Intensity of Extreme Heatwaves: The Crucial Role of Metrics. *Geophysical Research Letters*, *50*(14), e2023GL103540. https://doi.org/10.1029/2023GL103540

Sandeep, N., Swapna, P., Krishnan, R., Farneti, R., Prajeesh, A. G., Ayantika, D. C., & Manmeet, S. (2020). South Asian monsoon response to weakening of Atlantic meridional overturning circulation in a warming climate. *Climate Dynamics*, *54*(7-8), 3507–3524. https://doi.org/10.1007/s00382-020-05180-y

Sanderson, B. M., Booth, B. B. B., Dunne, J., Eyring, V., Fisher, R. A., Friedlingstein, P., Gidden, M. J., Hajima, T., Jones, C. D., Jones, C. G., King, A., Koven, C. D., Lawrence, D. M., Lowe, J., Mengis, N., Peters, G. P., Rogelj, J., Smith, C., Snyder, A. C., … Zaehle, S. (2024). The need for carbon-emissions-driven climate projections in CMIP7. *Geoscientific Model Development*, *17*(22), 8141–8172. https://doi.org/10.5194/gmd-17-8141-2024

Sarmiento, J. L., & Le Quéré, C. (1996). Oceanic Carbon Dioxide Uptake in a Model of Century-Scale Global Warming. *Science*, *274*(5291), 1346–1350. https://doi.org/10.1126/science.274.5291.1346

Scaife, A. A., Folland, C. K., Alexander, L. V., Moberg, A., & Knight, J. R. (2008). European Climate Extremes and the North Atlantic Oscillation. *Journal of Climate*, *21*(1), 72–83. https://doi.org/10.1175/2007jcli1631.1

Schädel, C., Rogers, B. M., Lawrence, D. M., Koven, C. D., Brovkin, V., Burke, E. J., Genet, H., Huntzinger, D. N., Jafarov, E., McGuire, A. D., Riley, W. J., & Natali, S. M. (2024). Earth system models must include permafrost carbon processes. *Nature Climate Change*, *14*(2), 114–116. https://doi.org/10.1038/s41558-023-01909-9

Schaeffer, M., Hare, W., Rahmstorf, S., & Vermeer, M. (2012). Long-term sea-level rise implied by 1.5 °C and 2 °C warming levels. *Nature Climate Change*, *2*(12), 867–870. https://doi.org/10.1038/nclimate1584

Schleussner, C.-F., Lissner, T. K., Fischer, E. M., Wohland, J., Perrette, M., Golly, A., Rogelj, J., Childers, K., Schewe, J., Frieler, K., Mengel, M., Hare, W., & Schaeffer, M. (2016). Differential climate impacts for policy-relevant limits to global warming: The case of 1.5 °C and 2 °C. *Earth System Dynamics*. https://doi.org/10.5194/esd-7-327-2016

Schuur, E. A. G., McGuire, A. D., Schädel, C., Grosse, G., Harden, J. W., Hayes, D. J., Hugelius, G., Koven, C. D., Kuhry, P., Lawrence, D. M., Natali, S. M., Olefeldt, D., Romanovsky, V. E., Schaefer, K., Turetsky, M. R., Treat, C. C., & Vonk, J. E. (2015). Climate change and the permafrost carbon feedback. *Nature*, *520*(7546), 171–179. https://doi.org/10.1038/nature14338

Schwarzwald, K., & Lenssen, N. (2022). The importance of internal climate variability in climate impact projections. *Proceedings of the National Academy of Sciences*, *119*(42), e2208095119. https://doi.org/10.1073/pnas.2208095119

Schwinger, J., Asaadi, A., Goris, N., & Lee, H. (2022a). Possibility for strong northern hemisphere high-latitude cooling under negative emissions. *Nature Communications*, *13*(1), 1095. https://doi.org/10.1038/s41467-022-28573-5

Schwinger, J., Asaadi, A., Steinert, N. J., & Lee, H. (2022b). Emit now, mitigate later? Earth system reversibility under overshoots of different magnitudes and durations. *Earth System Dynamics*, *13*(4), 1641–1665. https://doi.org/10.5194/esd-13-1641-2022

Sigmond, M., Fyfe, J. C., Saenko, O. A., & Swart, N. C. (2020). Ongoing AMOC and related sea-level and temperature changes after achieving the Paris targets. *Nature Climate Change*, *10*(7), 672–677. https://doi.org/10.1038/s41558-020-0786-0

Sillmann, J., Kharin, V. V., Zhang, X., Zwiers, F. W., & Bronaugh, D. (2013). Climate extremes indices in the CMIP5 multimodel ensemble: Part 1. Model evaluation in the present climate.

Journal of Geophysical Research Atmospheres, *118*(4), 1716–1733. https://doi.org/10.1002/jgrd.50203

Sillmann, J., & Roeckner, E. (2008). Indices for extreme events in projections of anthropogenic climate change. *Climatic Change*, *86*(1), 83–104. https://doi.org/10.1007/s10584-007-9308-6

Sillmann, J., Croci-Maspoli, M., Kallache, M., & Katz, R. W. (2011). Extreme Cold Winter Temperatures in Europe under the Influence of North Atlantic Atmospheric Blocking. *Journal of Climate*, *24*(22), 5899–5913. https://doi.org/10.1175/2011JCLI4075.1

Srokosz, M. A., & Bryden, H. L. (2015). Observing the Atlantic Meridional Overturning Circulation yields a decade of inevitable surprises. *Science*, *348*(6241). https://doi.org/10.1126/science.1255575

Stern, N. (2006). *The Economics of Climate Change: The Stern Review*. Cambridge University Press.

Stommel, H. (1961). Thermohaline Convection with Two Stable Regimes of Flow. *Tellus*, *13*(2), 224–230. https://doi.org/10.1111/j.2153-3490.1961.tb00079.x

Stott, P. A., Christidis, N., Otto, F. E., Sun, Y., Vanderlinden, J. P., van Oldenborgh, G. J., Vautard, R., von Storch, H., Walton, P., Yiou, P., & Zwiers, F. W. (2016). Attribution of extreme weather and climate-related events. *Wiley Interdisciplinary Reviews: Climate Change*, *7*(1), 23–41. https://doi.org/10.1002/wcc.380

Stott, P. A., Stone, D. A., & Allen, M. R. (2004). Human contribution to the European heatwave of 2003. *Nature*, *432*, 610–614. https://doi.org/10.1038/nature03089

Stouffer, R. J., Yin, J., Gregory, J. M., Dixon, K. W., Spelman, M. J., Hurlin, W., Weaver, A. J., Eby, M., Flato, G. M., Hasumi, H., Hu, A., Jungclaus, J. H., Kamenkovich, I. V., Levermann, A., Montoya, M., Murakami, S., Nawrath, S., Oka, A., Peltier, W. R., … Weber, S. L. (2006). Investigating the Causes of the Response of the Thermohaline Circulation to Past and Future Climate Changes. *Journal of Climate*, *19*(8), 1365–1387. https://doi.org/10.1175/JCLI3689.1

Straus, D. M., Molteni, F., & Corti, S. (2016, December). Atmospheric Regimes: The Link between Weather and the Large-Scale Circulation. In C. L. E. Franzke & T. J. O'Kane (Eds.), *Nonlinear and Stochastic Climate Dynamics* (1st ed., pp. 105–135). Cambridge University Press. https://doi.org/10.1017/9781316339251.005

Suarez-Gutierrez, L., Li, C., Müller, W. A., & Marotzke, J. (2018). Internal variability in European summer temperatures at 1.5 °C and 2 °C of global warming. *Environmental Research Letters*, *13*(6), 064026. https://doi.org/10.1088/1748-9326/aaba58

Suarez-Gutierrez, L., Milinski, S., & Maher, N. (2021). Exploiting large ensembles for a better yet simpler climate model evaluation. *Climate Dynamics*, *57*(9), 2557–2580. https://doi.org/10.1007/s00382-021-05821-w

Suarez-Gutierrez, L., Müller, W. A., & Marotzke, J. (2023). Extreme heat and drought typical of an end-of-century climate could occur over Europe soon and repeatedly. *Communications Earth & Environment*, *4*(1), 415. https://doi.org/10.1038/s43247-023-01075-y

Sun, Y., Jia, G., & Xu, X. (2025). Extreme high temperatures and heatwave events across Europe in 2023. *Environmental Research Communications*, *7*(2), 021001. https://doi.org/10.1088/2515-7620/adae60

Svendsen, L., Kvamstø, N. G., & Keenlyside, N. (2014). Weakening AMOC connects Equatorial Atlantic and Pacific interannual variability. *Climate Dynamics*, *43*(11), 2931–2941. https://doi.org/10.1007/s00382-013-1904-8

Swingedouw, D., Bopp, L., Matras, A., & Braconnot, P. (2007a). Effect of land-ice melting and associated changes in the AMOC result in little overall impact on oceanic CO2 uptake. *Geophysical Research Letters*, *34*(23). https://doi.org/10.1029/2007GL031990

Swingedouw, D., Braconnot, P., Delecluse, P., Guilyardi, E., & Marti, O. (2007b). Quantifying the AMOC feedbacks during a 2×CO2 stabilization experiment with land-ice melting. *Climate Dynamics*, *29*(5), 521–534. https://doi.org/10.1007/s00382-007-0250-0

Swingedouw, D., Houssais, M.-N., Herbaut, C., Blaizot, A.-C., Devilliers, M., & Deshayes, J. (2022). AMOC Recent and Future Trends: A Crucial Role for Oceanic Resolution and Greenland Melting? *Frontiers in Climate*, *4*. https://doi.org/10.3389/fclim.2022.838310

Swingedouw, D., Rodehacke, C. B., Behrens, E., Menary, M., Olsen, S. M., Gao, Y., Mikolajewicz, U., Mignot, J., & Biastoch, A. (2013). Decadal fingerprints of freshwater discharge around Greenland in a multi-model ensemble. *Climate Dynamics*, *41*(3-4), 695–720. https://doi.org/10.1007/s00382-012-1479-9

Tandon, N. F., & Kushner, P. J. (2015). Does External Forcing Interfere with the AMOC's Influence on North Atlantic Sea Surface Temperature? *Journal of Climate*, *28*(16), 6309–6323. https://doi.org/10.1175/JCLI-D-14-00664.1

Tebaldi, C., & Wehner, M. F. (2018). Benefits of mitigation for future heat extremes under RCP4.5 compared to RCP8.5. *Climatic Change*, *146*(3-4), 349–361. https://doi.org/10.1007/s10584-016-1605-5

Terhaar, J., Vogt, L., & Foukal, N. P. (2025). Atlantic overturning inferred from air-sea heat fluxes indicates no decline since the 1960s. *Nature Communications*, *16*(1), 222. https://doi.org/10.1038/s41467-024-55297-5

Thompson, D. W. J., Barnes, E. A., Deser, C., Foust, W. E., & Phillips, A. S. (2015). Quantifying the Role of Internal Climate Variability in Future Climate Trends. *Journal of Climate*, *28*(16), 6443–6456. https://doi.org/10.1175/JCLI-D-14-00830.1

Trenberth, K. E., & Caron, J. M. (2001). Estimates of Meridional Atmosphere and Ocean Heat Transports. *Journal of Climate*, *14*(16), 3433–3443. https://doi.org/10.1175/1520-0442(2001)014<3433:eomaao>2.0.co;2

UK Parliament. (2024, September). Climate Change: Atlantic Ocean. Question for Department for Energy Security and Net Zero. Written question HL634 by Baroness Jones of Moulsecoomb. https://questions-statements.parliament.uk/written-questions/detail/2024-09-02/hl634

Valdes, P. (2011). Built for stability. *Nature Geoscience*, *4*(7), 414–416. https://doi.org/10.1038/ngeo1200

van Westen, R. M., Kliphuis, M., & Dijkstra, H. A. (2024a). Physics-based early warning signal shows that AMOC is on tipping course. *Science Advances*, *10*(6), eadk1189. https://doi.org/10.1126/sciadv.adk1189

van Westen, R. M., & Baatsen, M. L. J. (2025). European Temperature Extremes Under Different AMOC Scenarios in the Community Earth System Model. *Geophysical Research Letters*, *52*(12), e2025GL114611. https://doi.org/10.1029/2025GL114611

van Westen, R. M., Kliphuis, M., & Dijkstra, H. A. (2024b). Physics-based early warning signal shows that AMOC is on tipping course. *Science Advances*, *10*(6), eadk1189. https://doi.org/10.1126/sciadv.adk1189

Vautard, R., Cattiaux, J., Happé, T., Singh, J., Bonnet, R., Cassou, C., Coumou, D., D'Andrea, F., Faranda, D., Fischer, E., Ribes, A., Sippel, S., & Yiou, P. (2023). Heat extremes in Western Europe increasing faster than simulated due to atmospheric circulation trends. *Nature Communications*, *14*(1), 6803. https://doi.org/10.1038/s41467-023-42143-3

Vautard, R., van Aalst, M., Boucher, O., Drouin, A., Haustein, K., Kreienkamp, F., van Oldenborgh, G. J., Otto, F. E. L., Ribes, A., Robin, Y., Schneider, M., Soubeyroux, J.-M., Stott, P., Seneviratne, S. I., Vogel, M. M., & Wehner, M. (2020). Human contribution to the record-breaking June and July 2019 heatwaves in Western Europe. *Environmental Research Letters*, *15*(9), 094077. https://doi.org/10.1088/1748-9326/aba3d4

Vellinga, M., & Wood, R. A. (2002). Global Climatic Impacts of a Collapse of the Atlantic Thermohaline Circulation. *Climatic*

Change, *54*(3), 251–267. https://doi.org/10.1023/A:1016168827653

Vellinga, M., & Wood, R. A. (2008). Impacts of thermohaline circulation shutdown in the twenty-first century. *Climatic Change*, *91*(1-2), 43–63. https://doi.org/10.1007/s10584-006-9146-y

Visbeck, M. H., Hurrell, J. W., Polvani, L., & Cullen, H. M. (2001). The North Atlantic Oscillation: Past, present, and future. *Proceedings of the National Academy of Sciences*, *98*(23), 12876–12877. https://doi.org/10.1073/pnas.231391598

Volkov, D. L., Smith, R. H., Garcia, R. F., Smeed, D. A., Moat, B. I., Johns, W. E., & Baringer, M. O. (2024). Florida Current transport observations reveal four decades of steady state. *Nature Communications*, *15*(1), 7780. https://doi.org/10.1038/s41467-024-51879-5

Wang, H., Zuo, Z., Qiao, L., Zhang, K., Sun, C., Xiao, D., Lin, Z., Bu, L., & Zhang, R. (2022). Frequency of the winter temperature extremes over Siberia dominated by the Atlantic Meridional Overturning Circulation. *npj Climate and Atmospheric Science*, *5*(1), 1–10. https://doi.org/10.1038/s41612-022-00307-w

Weijer, W., Cheng, W., Drijfhout, S. S., Fedorov, A. V., Hu, A., Jackson, L. C., Liu, W., McDonagh, E. L., Mecking, J. V., & Zhang, J. (2019). Stability of the Atlantic Meridional Overturning Circulation: A Review and Synthesis. *Journal of Geophysical Research: Oceans*, *124*(8), 5336–5375. https://doi.org/10.1029/2019JC015083

Weijer, W., Cheng, W., Garuba, O. A., Hu, A., & Nadiga, B. T. (2020). CMIP6 Models Predict Significant 21st Century Decline of the Atlantic Meridional Overturning Circulation. *Geophysical Research Letters*, *47*(12). https://doi.org/10.1029/2019GL086075

Williamson, M. S., Collins, M., Drijfhout, S. S., Kahana, R., Mecking, J. V., & Lenton, T. M. (2018). Effect of AMOC collapse on ENSO in a high resolution general circulation model. *Climate Dynamics*, *50*(7-8), 2537–2552. https://doi.org/10.1007/s00382-017-3756-0

Woollings, T. (2010). Dynamical influences on European climate: An uncertain future. *Philosophical Transactions of the Royal Society A: Mathematical, Physical and Engineering Sciences*, *368*(1924), 3733–3756. https://doi.org/10.1098/rsta.2010.0040

Yin, J., & Zhao, M. (2021). Influence of the Atlantic meridional overturning circulation on the U.S. extreme cold weather. *Communications Earth & Environment*, *2*(1), 1–10. https://doi.org/10.1038/s43247-021-00290-9

Yiou, P., Cattiaux, J., Faranda, D., Kadygrov, N., Jézéquel, A., Naveau, P., Ribes, A., Robin, Y., Thao, S., van Oldenborgh, G. J., & Vrac, M. (2020). Analyses of the Northern European Summer Heatwave of 2018. *Bulletin of the American Meteorological Soci-*

ety, *101*(1), S35–S40. Retrieved January 28, 2025, from https://www.jstor.org/stable/27032741

Zhang, J., & Zhang, R. (2015). On the evolution of Atlantic Meridional Overturning Circulation Fingerprint and implications for decadal predictability in the North Atlantic. *Geophysical Research Letters*, *42*(13), 5419–5426. https://doi.org/10.1002/2015gl064596

Zhang, L., & Wang, C. (2013). Multidecadal North Atlantic sea surface temperature and Atlantic meridional overturning circulation variability in CMIP5 historical simulations. *Journal of Geophysical Research: Oceans*, *118*(10), 5772–5791. https://doi.org/10.1002/jgrc.20390

Zhang, R., & Delworth, T. L. (2005). Simulated Tropical Response to a Substantial Weakening of the Atlantic Thermohaline Circulation. *Journal of Climate*, *18*(12), 1853–1860. https://doi.org/10.1175/JCLI3460.1

Zhang, R., Sutton, R., Danabasoglu, G., Kwon, Y.-O., Marsh, R., Yeager, S. G., Amrhein, D. E., & Little, C. M. (2019). A Review of the Role of the Atlantic Meridional Overturning Circulation in Atlantic Multidecadal Variability and Associated Climate Impacts. *Reviews of Geophysics*, *57*(2), 316–375. https://doi.org/10.1029/2019RG000644

Zhang, X., Alexander, L., Hegerl, G. C., Jones, P., Tank, A. K., Peterson, T. C., Trewin, B., & Zwiers, F. W. (2011). Indices for monitoring changes in extremes based on daily temperature and precipitation data. *WIREs Climate Change*, *2*(6), 851–870. https://doi.org/10.1002/wcc.147

Zickfeld, K., Eby, M., & Weaver, A. J. (2008). Carbon-cycle feedbacks of changes in the Atlantic meridional overturning circulation under future atmospheric CO2. *Global Biogeochemical Cycles*, *22*(3), n/a–n/a. https://doi.org/10.1029/2007GB003118

Zickfeld, K., Eby, M., Weaver, A. J., Alexander, K., Crespin, E., Edwards, N. R., Eliseev, A. V., Feulner, G., Fichefet, T., Forest, C. E., Friedlingstein, P., Goosse, H., Holden, P. B., Joos, F., Kawamiya, M., Kicklighter, D., Kienert, H., Matsumoto, K., Mokhov, I. I., … Zhao, F. (2013). Long-Term Climate Change Commitment and Reversibility: An EMIC Intercomparison. *Journal of Climate*, *26*(16), 5782–5809. https://doi.org/10.1175/JCLI-D-12-00584.1

Ziehn, T., Chamberlain, M. A., Law, R. M., Lenton, A., Bodman, R. W., Dix, M., Stevens, L., Wang, Y.-P., & Srbinovsky, J. (2020). The Australian Earth System Model: ACCESS-ESM1.5. *Journal of Southern Hemisphere Earth Systems Science*, *70*(1), 193–214. https://doi.org/10.1071/ES19035

DECLARATION ON OATH
EIDESSTATTLICHE VERSICHERUNG

I hereby declare and affirm that this doctoral dissertation is my own work and that I have not used any aids and sources other than those indicated.

If electronic resources based on generative artificial intelligence (gAI) were used in the course of writing this dissertation, I confirm that my own work was the main and value-adding contribution and that complete documentation of all resources used is available in accordance with good scientific practice. I am responsible for any erroneous or distorted content, incorrect references, violations of data protection and copyright law or plagiarism that may have been generated by the gAI.

Hiermit erkläre ich an Eides statt, dass ich die vorliegende Dissertationsschrift selbst verfasst und keine anderen als die angegebenen Quellen und Hilfsmittel benutzt habe.

Sofern im Zuge der Erstellung der vorliegenden Dissertationsschrift generative Künstliche Intelligenz (gKI) basierte elektronische Hilfsmittel verwendet wurden, versichere ich, dass meine eigene Leistung im Vordergrund stand und dass eine vollständige Dokumentation aller verwendeten Hilfsmittel gemäß der Guten wissenschaftlichen Praxis vorliegt. Ich trage die Verantwortung für eventuell durch die gKI generierte fehlerhafte oder verzerrte Inhalte, fehlerhafte Referenzen, Verstöße gegen das Datenschutz- und Urheberrecht oder Plagiate.

Hamburg, September 25, 2025

Eduardo Alastrué de Asenjo

Hinweis / Reference

Die gesamten Veröffentlichungen in der Publikationsreihe des MPI-M
„Berichte zur Erdsystemforschung / Reports on Earth System Science“,
ISSN 1614-1199

sind über die Internetseiten des Max-Planck-Instituts für Meteorologie erhältlich:
https://mpimet.mpg.de/forschung/publikationen

All the publications in the series of the MPI -M
„Berichte zur Erdsystemforschung / Reports on Earth System Science“,
ISSN 1614-1199

are available on the website of the Max Planck Institute for Meteorology:
https://mpimet.mpg.de/en/research/publications